Thin-Film Deposition of Polymers by Vacuum Degradation

Konstantin P. Gritsenko*,† and Anatoly M. Krasovsky‡

Department of Optoelectronics of Semiconductor Molecular Systems, Institute of Semiconductor Physics of National Academy of Sciences of Ukraine, 45 Nauki pr., Kyiv, 03028, Ukraine, and Thin Film Physics and Technology Department, Metal–Polymer Institute of the National Academy of Sciences of Belarus, 32a Kirova str., Gomel, 246652, Belarus

Received March 12, 2002

Contents

1. Introduction

Polymer films continue to find a variety of novel uses in electronic, optical, medical, and chemical devices as both passive and active components. Different deposition techniques are used: dipping, spin-coating, Langmuir−Blodgett, and several methods of deposition from a gas phase. Most stable polymers without restrictions imposed by solubility can be deposited from a gas phase only. Furthermore, increased interest has been shown in vacuum-deposited polymers, dye films, and composites for information recording, light beam splitters, modulators, wave mixers, second and third harmonic generation, optical sensors, etc. For most of these uses, thickness ranges from nanometers up to a few micrometers.

The subject of this review is the sequence of elementary physical and chemical processes which together result in the deposition of polymer films starting from a bulk polymer. These include the stages of initial polymer decomposition and evaporation as well as the transfer of the polymer degradation products to the surface where condensation and film formation occur.

Early work on these topics dates back at least to the mid-1950s.[1−3] The approach subsequently attracted the attention of scientists in the USSR. Judging from their scientific publications, a good deal of this sort of work was carried out in the former USSR. Many of their articles are in the Russian language and therefore are not easily accessible by much of the scientific community worldwide. The main purpose of our paper is to review these former Soviet Union results for the benefit of the worldwide scientific community, including also results obtained by other researchers for the sake of completeness. It should be noted that, since the mid-1990s, Japanese efforts, especially in the area of complex functional polymer film deposition using advanced methods, have dominated.

The method of thin-film production starting with polymer vacuum evaporation to some extent (by the film's functional designation) overlaps the more conventional methods of plasma synthesis from gaseous low-molecular-weight organic and organometallic compounds and plasma sputtering of polymer targets. There are many publications both in Russian and in English in that domain, such as the books by Tkachuk and Kolotyrkin,[4] Yasuda,[5] and Biederman and Osada.[6] But we think that these methods are not in direct competition, but instead complement each other in both process characteristics and film properties. Some other methods of polymer film deposition

† National Academy of Sciences of Ukraine.
‡ National Academy of Sciences of Belarus.

10.1021/cr010449q CCC: $44.00
Published on Web 07/22/2003

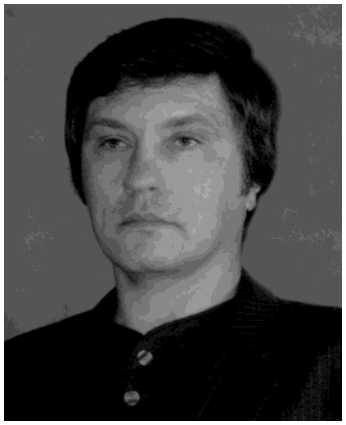

Konstantin P. Gritsenko graduated from the Kyiv Polytechnic Institute with a M.Sc. degree in physics of metals in 1981, and from the Metal–Polymer Research Institute of the Belarus Academy of Sciences with a Ph.D. degree in material sciences in 1997. His research activity started in 1980 in the Kyiv Polytechnic Institute with his M.S. project. His next research was concerned with multicomponent Te-based film deposition in a vacuum. It was done in the Optical Carrier Department of the Institute for Problems of Information Recording of the National Academy of Sciences of Ukraine (NASU). The Institute was the head organization in the USSR to design optical storage drivers. He then developed vacuum deposition methods for polymer and dye films for optical media. He was the head of a group to design materials and technologies for write once read many media. After the dissolution of the USSR, he became a postgraduate student in the Metal–Polymer Research Institute, Republic of Belarus, where he carried out the plasma and laser deposition of polymer films. Later he expanded his experience to include complex compounds that can be used as active layers. The general approach for deposition of complex organic solid films in a vacuum was elaborated. In November 1999 he was invited to the Department of Optoelectronics of Semiconductor Molecular Systems, Institute of Semiconductor Physics, NASU. He created a new research direction in the Institute the deposition of organic films from the gas phase for applications in optoelectronics. In 2000 he was awarded a 3-month Fellowship to the German Academy of Sciences. He was invited to deliver a lecture about organic film deposition in Germany, Canada, The Netherlands, and the UK. His current research activity is concerned with dye structure design and modification as related to deposition technology and structural and optoelectronic properties of dyes, polymers, and composite films.

Anatoly M. Krasovsky was born in 1935 in Russia. In 1958 he finished studies at the Belarussian Institute of Railways Transport. In 1963 he became a postgraduate student and Research Fellow, Head of Laboratory, Head of Department, Metal–Polymer Institute named after V. A. Belyi of the National Academy of Sciences of Belarus. In 1969 he defended his Dissertation of Candidate of Technical Sciences on "Formation and studies of thin polymer and metal–polymer coatings in vacuum"; in 1982 he defended his Dissertation of Doctor of Technical Sciences on "Research on the processes of formation of thin polymer and metal–polymer films in vacuum". He is the founder of the Thin Film Physics and Technology Department. His scientific interests are related with the studies of processes under laser, electron, and ion irradiation of polymers in a vacuum as the tool to deposit thin polymer films, and polymer film growth and structure studies. He has also used low-temperature plasma processes for thin polymer film deposition and surface modification. He found plasma of fluorocompounds and di-*p*-xylylene to be most useful. He has also studied thin polymer and metal–polymer films for use as active and passive layers in various devices, and developed laser processing of PTFE wastes into fibrous–porous materials and filters. Professor Krasovsky is the author or coauthor more than 150 papers, including two books and nearby 50 inventions. He has supervised 10 Ph.D. students.

from a gas phase, but not related with original polymer decomposition, like co-condensation of two evaporated compounds,[7−9] hot-wire-assisted deposition,[10] and monomer evaporation with UV curing,[11] are described in reviews and also are important for science and industry. It is worth mentioning a complete database for poly(*p*-xylylene) film deposition (www.wfbeach.com).

Before we start this review, a point regarding the terminology of the polymer film deposition process should be addressed. In English, as well as in Russian, there is no satisfactory term which describes the subject process in a word. Different terms have been used, even in different papers from the same author: "sputtering",[12] "emission",[13,14] "dispersioning".[15] Lately, the term "ablation" has been used for the process of laser beam film deposition. But no one has yet identified the distinctive process features which would make them worthy of the different names. The term "evaporation", still widely used in English articles, is not strictly correct with respect to polymers, since polymer evaporation, i.e., the transition of the whole polymer molecule from the condensed phase into the gaseous phase, is usually not possible without its concurrent degradation (unless special conditions are used to achieve evaporation of a separate molecule).

We will use the word "degradation" or "decomposition" for the general description of the vaporization process, and will use "deposition" to refer to film growth processes. In some cases, we shall continue to use the broadly accepted descriptor "evaporation" in this review.

2. Energy-Induced Physicochemical Processes in Polymers

2.1. Polymer Degradation during Thermal Heating in Vacuum

For the sake of convenience, most polymer thermal degradation studies employ air or an inert gas at pressures close to atmospheric as their means of delivering heat. Along with the desired degradation, secondary reactions also occur: reactions of the degradation products with air, as well as reactions among the degradation products themselves. To establish the identity of the primary products of polymer degradation, in vacuo polymer sample heating is preferred. Both types of secondary reactions are mitigated in this way. Vacuum, however, introduces difficulties of its own, not the least of which is that of obtaining adequate temperature uniformity across the polymer specimen.

Primary polymer degradation products are generated by the scission of the molecular chain at various

sites and/or the cleavage of side groups or atoms.[16,17] Depending on the nature of its structure, the scission of a polymer chain can occur either randomly or in an orderly depolymerization mechanism (i.e., unzipping). The array of degradation products is often rather complex. Both split-off atoms and side groups as well as fragments of the molecular chain are represented, often with modified structure. But in general, most primary degradation products collected are smaller than the original monomer unit. Increasing the temperature of polymer degradation widens the range of degradation products, giving more products of greater mass.[17] It has been pointed out[18,19] that the ratio of the thermal dissociation rates of two chemical bonds of differing strength may be estimated by

$$\frac{V_1}{V_2} = \exp\left(\frac{U_2 - U_1}{kT}\right) \tag{1}$$

where V is the dissociation rate and U the bond strength or energy. This formula, supplemented by an evaporation rate equation for low-molecular-weight substances having differing mass and chemical structure, describes the liberation rates for products of polymer degradation:

$$\frac{V_1^{ev}}{V_2^{ev}} = \exp\left(\frac{U_2 - U_1}{kT}\right)\exp\left(\frac{U_2^{ev} - U_1^{ev}}{kT}\right) = \exp\left[\frac{(U_2 + U_2^{ev}) - (U_1 + U_1^{ev})}{kT}\right] \tag{2}$$

where U_i^{ev} is the energy of evaporation for the ith fragment from the specimen's surface. This expression shows that, when the polymer is heated to a high temperature before an equilibrium of degradation and evaporation of the products can be established, the liberation of the larger, higher molecular weight products is favored. This is a distinctive feature of polymer degradation, in contrast to the evaporation of pure low-molecular-weight substances, for which temperature and chemical composition of the vapor are invariant.

However, the mass of the heavier volatile fragments cannot increase without limit. Limitations are imposed by the evaporation process rather than by polymer degradation. Kuzmina and Zaev[20] estimated that the maximum molecular weight of an evaporating fragment is about 1000 Da. They reason that, in order to evaporate a molecule, it is necessary to overcome the energy binding it to its neighbors. Since the impulse of thermal fluctuation is not distributed over the whole fragment, but rather localized at an individual atom and subsequently transmitted along the chain, the maximum impulse energy transmitted cannot be much in excess of the macromolecular backbone bond energy, E_f. It is this consideration that determines the maximum size of the evaporated fragment. If we assume that the evaporation energy for an oligomer fragment in the midst of its neighboring molecules is proportional to its chain length (i.e., its molecular weight), it can be estimated, using reference data on evaporation heat and strength of the chain bonds for known compounds with a similar chemical structure, that

$$Q = Q_0\frac{M}{M_0} \tag{3}$$

where Q and Q_0 are the heats of evaporation of the fragment and the reference compound, respectively, and M and M_0 are their molecular weights.

Proceeding from the requirement $E_f > Q = Q_0M/M_0$, we obtain $M_{max} < E_fM_0/Q_0$. For paraffins we have $E_f \approx 75-78$ kcal/mol,[15] and $Q_0/M_0 \approx 48-50$ cal/g.[21] Therefore, the largest evaporable PE chain fragments should be about $M_{max} = (76 \times 10^3)/49 \approx 1550$ amu. If the mechanistic representation of a heat fluctuation impulse transfer along the molecular chain is correct, we can assume the impulse to be applied to the fragment center. Thus, the M_{max} value estimated above ought to be doubled, viz., $M_{max} \approx 3100$ amu. Such fragments should be scarce, so we favor an M_{max} estimate for paraffins of perhaps $\sim$1500−2000 amu.

It should be emphasized that this is a description of a classic equilibrium evaporation process, which consists of applying a kinetic energy impulse to a molecular fragment in excess of the energy of the interaction of the fragment with its neighbors. Using special methods and nonequilibrium processes, it may be possible to evaporate still larger molecules, but this is not a classic evaporation process. Experimentally, the maximum molecular weight of a PE chain fragment, found by Madorsky,[17] was about 1200 amu, consistent with the above-determined limit. Yet there are other published results that disagree with our theoretical estimate. Kruglyak et al.[23] reported an average molecular weight of PE degradation products from 1200 to 7000. They report that an average molecular fragment of PE degradation contains more than 120 repeat units (i.e., over 3300 Da).[24] Reactions of the evaporated fragments with gaseous low-molecular-weight substances can take place during transit from the evaporator to the condensation surface. However, this cannot be expected to raise the molecular weight significantly.

The molecular weight of evaporated fragments for other polymers cannot significantly exceed those calculated for PE, at least to the extent that the energy of C−C bonds and heats of evaporation for most polymers are similar. The minimum molecular weight fragments observed correspond to the mass of the lightest atom, viz., hydrogen or carbon.

Discrepancies in the compositions of degradation products result to some extent from the lack of reliable methods for in situ analysis. The disadvantages of mass spectrometry in particular are the result of the uncertainty of the instrumental response to each component of the gaseous mixture. Nevertheless, mass spectrometric analyses of polymer degradation products are useful despite this response function uncertainty. When analyzing degradation products, it is necessary to remember that, in addition to chemically inactive components, they also contain reactive components, which can react within the analyzing instrument and thus affect the results. To analyze the composition of degradation products

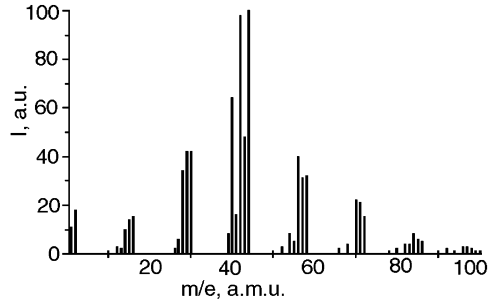

Figure 1. Mass spectrum of PP degradation products.

Table 1. Composition of the PP Degradation Products

m/e, amu	fragment	*I*, au	*m/e*, amu	fragment	*I*, au
1	H	11	57	C_4H_9	31
2	H_2	18	58	C_4H_{10}	32
12	C	3	66	C_5H_6	2
13	CH	2	68	C_5H_8	4
14	CH_2	10	70	C_5H_{10}	22
15	CH_3	14	71	C_5H_{11}	21
16	CH_4	15	72	C_5H_{12}	15
26	C_2H_2	2	78	C_6H_6	1
27	C_2H_3	6	80	C_6H_8	2
28	C_2H_4	34	82	C_6H_{10}	4
29	C_2H_5	42	83	C_6H_{11}	4
30	C_2H_6	42	84	C_6H_{12}	8
39	C_3H_3	8	85	C_6H_{13}	6
40	C_3H_4	64	86	C_6H_{14}	5
41	C_3H_5	16	92	C_7H_8	2
42	C_3H_6	98	94	C_7H_{10}	1
43	C_3H_7	48	96	C_7H_{12}	3
44	C_3H_8	100	97	C_7H_{13}	3
52	C_4H_4	3	98	C_7H_{14}	2
54	C_4H_6	8	99	C_7H_{15}	1
55	C_4H_7	5	100	C_7H_{16}	1
56	C_4H_8	40			

accurately, it is necessary to compare results from distinctly different analytical tools.

An analysis of PE degradation products by mass spectrometry was carried out by Luff and White.[25] The most abundant degradation products are those that generate a series of fragments at 26−30, 39−44, and 52−58 amu. The 12−16, 70−73, 80−86, and 96−100 amu series are considerably less abundant. Those of more than 100 amu are present in trace quantities only. Similar results were obtained later by Gritsenko and co-workers using both an open crucible and a crucible covered by a porous metal filter.[26] The mass spectrum of PP degradation products had a similar distribution, as shown in Figure 1 and Table 1. It should be mentioned that both saturated and unsaturated species were found. The unsaturated species include the following:

(i) *monoradicals* − CH_3, C_2H_5, C_3H_7, C_4H_9, C_5H_{11}, etc. in lower concentration;
(ii) *diradicals* − C_2H_4, C_3H_6, C_4H_8, C_5H_{10}, etc.; and
(iii) *triradicals* (more likely, monoradicals with double bonds) − C_2H_3, C_3H_5, C_4H_7.

Deeper products of destruction such as carbon and hydrogen are present but in small quantities.

A porous metal filter was used to mitigate the intrusion of droplets into the working chamber. Droplets are ejected from the polymer surface. There is little difference in mass spectral results from an open crucible and a crucible covered by porous filter.

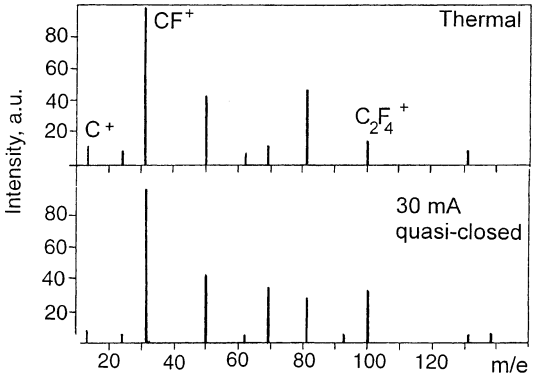

Figure 2. Mass spectra of PTFE degradation products: (a) open crucible and (b) quasi-closed crucible.

A similar filter was also used[27−29] in studies of PCA, PVDF, PCTFE, PET, and PC.

Belyi et al.[30] used a molecular discriminator and found that PCA degradation products consisted of two types: monomer and still smaller fragments. Khimchenko et al.[27] investigated the degradation products of PCA by mass spectroscopy. They showed that, during the first cycle of PCA in vacuo heating, water, ammonia, carbon, and oxides of nitrogen were liberated. The authors explain these facts by intra- and intermolecular reactions in PCA. Peaks corresponding to the PCA monomeric unit are negligible up to 673 K but grow in relative intensity as temperature is further elevated. The authors conclude that, regardless of pyrolysis conditions, products above 200 amu are present only in small quantities. This conclusion is supported by the similarities between the mass spectra of the degradation products collected either directly from the evaporation surface or after having passed through a porous filter heated 50−100 °C above the evaporator temperature.

The thermal degradation of PTFE was studied by Luff and White[25] and also by Collins and his coauthors.[31] There is a marked difference between PTFE degradation products in a vacuum and in an inert gas. Later, Gritsenko[29] obtained nearly identical mass spectra for PTFE thermal degradation products in a vacuum. These data are presented in Figure 2. The distribution of fragments is quite different than that for PE or PP. The mass spectrum of the PFEP vacuum degradation products contains the same species as found in the spectrum from PTFE itself, but with a different distribution.[32] Species within the 60−150 amu range are much more abundant, similar to results from the electron activation of PTFE degradation (see section 2.3).

There is a marked difference between mass spectra of PTFE and PCTFE pyrolysis products taken from an open crucible and from a porous filter.[29] Products with a higher molecular weight were observed from porous filter PCTFE treatment. In contrast, a great contribution from monomer and fragments with low molecular weight were observed for PTFE. The mass spectrum of PTFE degradation products from a quasi-closed crucible is presented in Figure 2. This observation supports the contribution of secondary reactions resulting from the destruction of fragments on the heated walls of the filter. Gritsenko considers that all components of the gases generated during

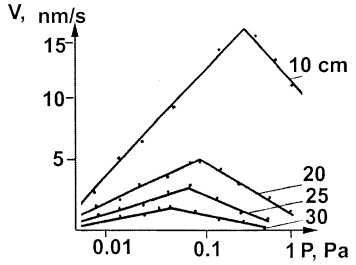

Figure 3. PE film deposition rate vs pressure at different distances from the evaporator: (1) 100, (2) 200, (3) 250, and (4) 300 mm.

PTFE degradation, including monomer, are products of interaction among the primary products of pyrolysis.[28] Interactions occur both in the gas phase and in the heated bulk, provided its dimensions exceed 0.1−0.3 mm. At least two factors depress the heavy fragments in the above studies:

(i) the filter itself, the heated surface of which intensifies degradation; and
(ii) the higher adsorptivity of the heavier fragments, which facilitates their deposition en route to the mass spectrometer source.

The mass spectrum of PTFE degradation products obtained without a filter[33] contains heavier fragments: *m*/*e* 166, 193, 341, 533, and 725.

Figure 3 shows PE film growth rate as a function of the pressure of decomposition products in the chamber, at various distances from the evaporator. Other polymers behave similarly. This experiment tells us something about the nature of the polymer degradation products which are responsible for film growth. The experimental chamber pressure is a balance between the rate of emission of gaseous products from the evaporator and the rate of exhaust pumping. At the start of a run, the increasing polymer temperature in the evaporator causes increases in both pressure and deposition rate. But at a certain pressure, higher when the evaporator is closer to the substrate, the deposition rate drops despite further increases in evaporator temperature.[21,23] Fragments seem to be colliding with each other before reaching the substrate, losing their chemical reactivity, and forming stabler species which tend not to be incorporated into the substrate deposit. Assuming that this critical evaporator−substrate distance corresponds to the mean free path of the active fragments, their estimated mass is 50−150 amu. Thus, most of the polymer degradation products that contribute to film growth are small fragments, although the participation of larger ones of lower chemical reactivity should also be taken into account.

Zadorozhny[33] studied the degradation products of several polymers. His data are summarized in Tables 2 and 3. The mass spectra of all polymers contain heavy fragments up to about 1000 amu. Gritsenko[28] found that the mass spectrum of PC (Figure 4 and Table 4) and PET evaporated through a porous filter contained no heavy fragments. Moreover, the IR spectrum of the film obtained by such method of PC decomposition showed that it was pure PE! It was suggested that the benzene rings were cleaved in the filter, but that seems improbable. This unexplained point shows that one who would use complex polymers for film deposition can anticipate difficulties.

Table 2. Mass Spectra of Thermally Evaporated Products

PE		PVDF		PCTFE		PC		PET	
m/*e*	*I*, au	*m*/*e*	*I*, au	*m*/*e*	*I*, au	*m*/*e*	*I*, au	*m*/*e*	*I*, au
16	15	2	6	31	3	125	35	16	4
32	17	57	7	85	5	213	41	44	5
44	22	84	8	97	8	268	16	97	20
56	17	118	5	166	36	341	36	144	44
100	15	161	5	257	19	390	39	166	13
156	19	460	4	356	8	567	32	193	19
170	17	683	6	432	6	622	41	341	25
198	18	938	4	645	13	695	10	537	20
250	10	950	3	680	13	750	6	725	15
282	7	966	3	790	17	917	11		
632	7	977	5			1109	8		

Table 3. Mass Spectra of PTFE-Evaporated Products

		m/*e*								
		12	50	81	100	150	382	900	924	1012
I, au	EBE[a]	8	21	15	39	15	10	10	10	10
	TE	6	22	16	36	13	7			

[a] EBE, electron beam evaporation; TE, thermal evaporation.

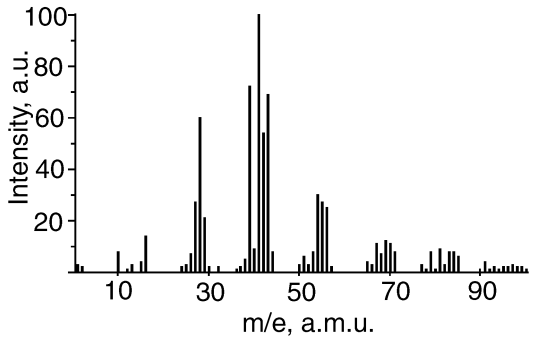

Figure 4. Mass spectrum of PC degradation products from a crucible covered with a porous metal filter.

To boost the yield of the heavier fragments, one needs to reduce the thermal treatment time at temperatures above the point where thermal degradation becomes appreciable. This can be achieved by intense impulse heating using a fast-rising pulse front. Several methods have been used to achieve this sort of heating. Krasovsky[14,15] heated a thin layer of polymer powder with a strip heater. Royh et al.[34] fed small portions of polymer powder onto a heated surface (673, 693, and 733 K for PE, PCA, and PCTFE, respectively). But ultimately the heating rate is limited in each case by the low heat conductivity of the gaseous interlayer between a polymer particle and the heater surface (a vapor-jacket evaporation regime).

Skripov et al.[35] used a poly(ethylene oxide) layer that was deposited on a thin metal wire and heated by a pulse of electric current. Although the heating rate approached 5×10^5 K/s, the volume of polymer evaporated is about 10^{-4} mm^3, and the method has little use beyond research studies.

Akashi et al.[36] used a similar technique in which a polymer applied onto a ribbon-like substrate was fed under vacuum into a heated zone at a speed of about

Table 4. Mass Spectra of PC-Evaporated Products

M, amu	fragment	*I*, au	*M*, amu	fragment	*I*, au
1	H	3	56	C_4H_8	25
2	H_2	2	57	C_4H_9	2
12	C	1	58	C_4H_{10}	1
13	CH	3	65	C_5H_5	4
14	CH_2	8	66	C_5H_6	3
15	CH_3	4	67	C_5H_7	11
16	CH_4	14	68	C_5H_8	7
24	C_2	2	69	C_5H_9	12
25	C_2H	3	70	C_5H_{10}	11
26	C_2H_2	7	71	C_5H_{11}	8
27	C_2H_3	27	77	C_6H_5	3
28	C_2H_4, CO	60	78	C_6H_6	1
29	C_2H_5	21	79	C_6H_7	8
30	C_2H_6	2	80	C_6H_8	1
32	O_2	2	81	C_6H_9	9
36	C_3	1	82	C_6H_{10}	3
37	C_3H	2	83	C_6H_{11}	8
38	C_3H_2	5	84	C_6H_{12}	8
39	C_3H_3	72	85	C_6H_{13}	6
40	C_3H_4	9	91	$C_6H_5CH_2$	4
41	C_3H_5	100	92	$C_6H_5CH_3$	1
42	C_3H_6	54	93	C_7H_9	2
43	C_3H_7	69	94	C_7H_{10}	1
44	C_3H_8 CO_2	8	95	C_7H_{11}	2
50	C_4H_2	3	96	C_7H_{12}	2
51	C_4H_3	6	97	C_7H_{13}	3
52	C_4H_4	3	98	C_7H_{14}	2
53	C_4H_5	8	99		2
54	C_4H_6	30	100		1
55	C_4H_7	27	101		1

1 mm/s. This method permitted a wider range of evaporated polymers, but the concept was not developed further. Gritsenko and co-workers[37] used a 50-μm tantalum foil coated with a 0.5−1-μm layer of PTFE deposited by thermal evaporation. This PTFE evaporation from Ta foil was carried out at 580−900 K within 0.5−2 s. The mass spectrum of the PTFE film degradation products showed an enhanced quantity of CF_3 and C_3F_5 fragments at the same temperature and pressure. A higher condensed fraction was found. This is explainable by the fact that the PTFE on the Ta foil had previously been thermally degraded in its initial evaporation, and hence was already of lower molecular weight.

Agabekov and co-workers[38,39] studied the thermal degradation products of polycyclohexadiene (PCHD) powder, Br-PCHD, cross-linked PCHD (CPCHD), and oxidized PCHD. Volatile fragment emission began at 135 °C. The mass spectra of PCHD contained species from 15 to 560 amu. The oxidized PCHD, however, produced species up to 900 amu, although the peaks $m/e > 200$ appeared only after 275 °C and at low intensity. These mass spectra are presented in Figure 5. Mass spectrometry also showed that H_2 and HBr were emitted during evaporation.

2.2. Electron and Ion-Beam Destruction of Polymers

Accelerated electron and ion beams enjoy much attention among the thin-film community, since these techniques are inherently restricted to a thin surface layer. The energy transmitted to a backbone atom can greatly exceed that injected thermally, and this can be a decisive factor affecting the features of degradation. Experience has shown that polymer

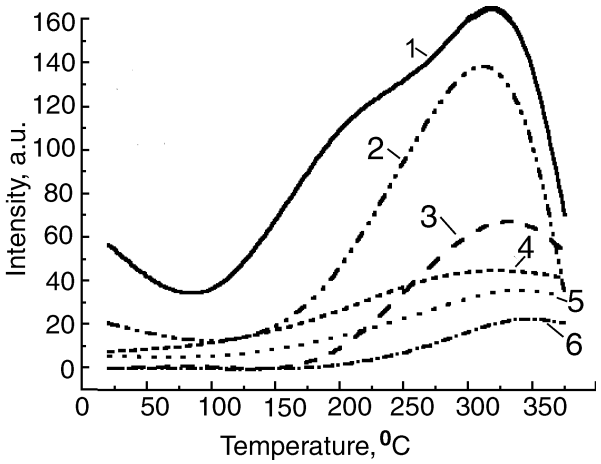

Figure 5. Composition of PCHD degradation products vs evaporation temperature: *m/e* (1) 18, (2) 44, (3) 81, (4) 105, (5) 28, and (6) 160.

degradation under the action of energetic charged particles takes place irrespective of the nature of the polymer or the treatment time. It has been established that three processes contribute to this effect:

(i) the scattering of primary particles after energy is transmitted to the target;
(ii) the emission of secondary charged particles knocked out by the primary particles; and
(iii) the removal of charge with the target evaporation products.

Rogachev and Kharitonov[40] proposed a model of electrical processes occurring during electron beam evaporation of polymer, and Krasovsky and Tolstopyatov[12] have offered refinements. Both models predict that the process of electrical equilibration takes tens to hundreds of microseconds, while thermal equilibrium takes much longer, perhaps several tens of seconds. So, these models can be valid for each kind of heating, but with different characteristics determined by functional parameters.

Fainstein and Silantiev[41] proposed another model based on two modes of polymer degradation:

(i) radiation-induced degradation, i.e., scission of chemical bonds by the energy transferred directly to macromolecule atoms; and
(ii) thermal degradation.

They determined that the size of a fragment liberated during radiation degradation was governed by the average distance between electrons in the beam. An analytical expression was derived for the dependence of fragment size distribution, including both radiation and pyrolysis factors. These models[12,40] are useful in that they allow us to predict the operating parameters of the electron beam required for film deposition. The accelerating voltage, however, is limited to the 1−10 kV range due to electrical breakdown in the gaseous medium.

Since the main mechanism of electron beam degradation of polymers is thermal, the degradation products' composition depends on the electron beam parameters as well as the thermal and physical characteristics of the target polymer. An increase in irradiation intensity gives a higher abundance of heavier fragments in PTFE degradation, but the

increased yield of heavies is attained much more easily than by pyrolysis.

The dependence of the rate of polymer degradation on its thermal conductivity has also been explored. Silaniev[42] found that the decomposition threshold for block PTFE was 0.5−0.7 MW/m^2. Krasovsky and Tolstopyatov,[43] using a compacted PTFE powder target, found that the decomposition power density threshold was an order of magnitude less due to the poorer thermal conductivity of the compacted material. It should be noted that this phenomenon is unique to PTFE, which has an extremely high viscosity as a melt. Powders of conventional thermoplastic polymers fuse more readily under radiant energy flux, forming a molten layer in good contact with the target surface.[44] Such fusion renders them the equivalent of a solid polymer from the standpoint of heat transfer.

Although the mechanism of polymer degradation by accelerated electrons is in essence thermal, the electron beam ensures a markedly faster heating of the surface layer than would conduction heating by physical contact between solid bodies. Table 3 shows a comparison between mass spectral data from the thermal and electron beam degradation of PTFE.[33] Note the differences between the heavier fragments.

We note that, in the case of PTFE electron beam decomposition, certain results which are common to contact heating process are not encountered, regardless of beam power. For example, the thermal regime at 680−1000 K, where the room-temperature condensables are for all practical purposes absent, was not encountered during electron beam evaporation.[44] This regime probably exists, but in a narrow power range determined by competition between the elementary processes of target electrical discharge, heating, and the evaporation of the decomposition products. At a low beam power, target charge accumulates because a steady state can be achieved only via secondary electron emission. As a result, the effective energy of electrons arriving at the target is lower than expected, since the electron energy upon arrival at the target is determined by the potential difference between the accelerator and the floating or biased potential of the target, which in turn is directly affected by charge accumulation. Nevertheless, when target degradation begins, a second mechanism of the target charge removal is switched on, i.e., charge removal by the evaporation products. Then, a new, lower equilibrium charge state is established within tens of microseconds. This results in an abrupt increase in target power dissipation. Thus, the overall system is characterized by a strong positive feedback. Such behavior was not seen in other polymers.

Many publications are dedicated to various aspects of the irradiation of polymers using different sources: UV, electron, ion, X-ray, and nuclear. The irradiation of polymers is widely used for a variety of scientific and industrial applications, among the most useful being surface modification. But not much has been reported for thin-film deposition. At this point, we briefly consider some of the main positions that might help in the understanding of the following sections dedicated to thin polymer film growth and their properties.

There are two modes of polymer degradation by ion irradiation:

(i) thermal; and
(ii) sputtering (i.e., chemical bond scission and the knocking out of molecular fragments by direct transfer of ion momentum to the fragment).

The ratio between sputtering and thermal evaporation under ion bombardment depends on the irradiation conditions. To increase the sputtering at the expense of the thermal evaporation, the target is cooled and an optimum range of ion energies is selected. Since it is rather difficult to achieve a sufficiently intense flux of low-energy ions, most experiments were performed using glow discharge ions. Akishin et al.[45] examined PTFE and PMMA sputtering in 5- and 50-MHz discharges in oxygen and nitrogen. An anomalous PTFE sputtering was observed by using 5−40-eV ions. Interestingly, there is a narrow range of ion energies where the sputtering coefficient drops as ion energy increases. The authors attribute this to a focusing of the energy transfer to the polymer lattice. It was shown that, with 6-eV oxygen ions, the yield of sputtered products was 200 amu per ion. Considering that cleaving the macromolecular backbone in two places requires 7.5 eV, it can be assumed that this is not a one-stage process. More likely, it would seem that the molecular chain is first ruptured by an initial impacting ion, and then a second impacting ion knocks the fragment from the target. Filatov et al.[46] found that the sputtering coefficient decreases with longer exposure time and higher ion flux intensity, and increases with the mass of the incident ions.

Polymer sputtering experiments with plasma ions require a gas in which it is possible to initiate an electric discharge. However, gaseous products are evolved from the polymer during its sputtering, in kind and quantities that are themselves sufficient to support a plasma. Such a self-supporting process, in which gas is supplied only when the discharge is started, can be achieved only at distinct combinations of discharge power and chamber evacuation rate. Discharge ignition can also be achieved by short-term evaporation of the target caused by a laser pulse, after which the discharge is sustained in the gaseous medium thus formed.[47] In this case, target decomposition is accompanied by secondary plasma decomposition of the gaseous fragments. There are many articles in English on polymer sputtering; therefore, we do not consider the subject in detail here.

Ion beam sputtering of PTFE was investigated by Weissmantel,[48] and later by Rost and Reisse.[49] The yield of gaseous fragments (CF_2) during sputtering was found to be 2−3 orders of magnitude greater than that for inorganic targets. For 3−10-keV Ar and Ne ions, the constant power density yield of sputtered fragments is proportional to ion mass and energy. Perhaps general interest in polymer film deposition by ion sputtering has been slow to develop due to the intricate nature of the process and the lack of advantages it offers compared with other methods of polymer film deposition.

2.3. Laser-Induced Destruction of Polymers

An advantage of laser treatment is the ability to vary the power impinging upon the polymer over a wide range. Most experiments have been performed using ruby, yttrium−aluminum garnet (YAG), neodymium glass, and carbon dioxide (CO_2) lasers. More recently, reports have appeared on the use of UV lasers.[50−56] The photophysical and photochemical processes induced in polymers by such irradiation are interesting from both scientific and practical viewpoints. The selective activation of certain chemical bonds might provide a basis for targeted chemical transformations. Such processes have been discussed in summary reviews by Talrose and Barashev[57] and by Bunkin et al.[58] Ilyasov and co-workers[59] came to the conclusion that IR laser irradiation of certain polymers can provoke chemical reactions which lead to the formation of polymers with improved mechanical properties. Parkhomenko et al.[60] and Nesterikhin et al.[61] carried out the selective excitation of complex biological molecules in the condensed state. Krasovsky et al.[62] suggested the existence of nonthermal processes in PTFE under CO_2 laser irradiation.

Mirkin and co-workers[63,64] encountered crack generation in PMMA, PS, and PC under pulsed laser irradiation. Ashkinazi et al.[65] and Sultanov[66] suggested that these cracks were the result of hypersonic waves generated by the laser pulse in the polymer. Novikov[67] postulated that one of the reasons for these cracks could be radiation-induced gas liberation. The mechanism of laser radiation absorption remains obscure, in particular when no known absorption bands coincide with the radiation wavelength. Mirkin et al.[63,64] suggested that certain defects in the polymer structure act as absorption centers:

(i) structural micro-heterogeneities smaller than a micrometer caused by local stress fields;
(ii) scattering centers of the same size; and
(iii) nontransparent inclusions larger than a micrometer.

Novikov[67] suggests that release energy centers in pure polymer, free from foreign inclusions, are microstructure defects associated with local stressed microdomains.

Examination of the bright glow preceding polymer failure shows that the temperature of the emitter is over 7000 K. Polymer gassification at sites close to the laser-heated spot proceeds extremely quickly, giving a pressure jump of the order of 200 MPa. Under these conditions, the plasma gas is the laser radiation absorber. Energy liberation is localized closer and closer to the absorption center, leading to an avalanche process.

Mikhailova et al.[68] showed that the composition of gas which occupies these cracks is similar to that resulting from polymer photolysis proceeding via side-branch scission. Rather than by thermal action, the avalanche degradation process is initiated by photodegradation of stressed PMMA molecules at microdefect boundaries. The scission of these stressed molecules leads to breakdown in the electric field formed by oriented dipoles of the macromolecular side chains. Plasma generated at this point initiates the avalanche process. Babajan et al.[69] suggest that absorption could occur in the crack-rich surface layers of transparent dielectrics.

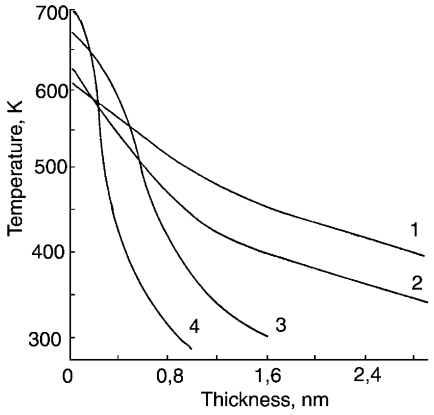

Figure 6. Temperature profile across PMMA thickness in the spot center during CO_2 laser irradiation at the following intensities: (1) 214, (2) 247, (3) 314, and (4) 419 kW/m^2.

All work mentioned so far has utilzed pulsed lasers of low average power. Less attention has been given to interactions of polymers with higher power laser radiation. Novikov and Kholodilov[70] examined PMMA, PS, and PC behavior under CO_2 laser irradiation with an average intensity of 250, 420, and 500 kW/m^2. When these polymers are exposed in air, they degrade and evaporate, giving a condensate-droplet zone on the front surface of the sample. The relative amounts of solid, liquid, and gas phases in this zone depend on input power. Only vapor and a limited amount of fibrils were ejected during PC exposure. The depth to which the polymer was heated decreased with the radiation power intensity. This is due to the intense evaporation activity as well as to the fast movement of the polymer−vapor boundary. The surface temperature was 710 K for PMMA, 560 K for PSF, and 1000 K for PC, and the time needed for a steady-state temperature distribution was between 0.3 and 4 s. It was concluded that depolymerization occurs by a radical mechanism. Figure 6 summarizes the dependence of the temperature profile across a PMMA specimen on the power density of the incident laser radiation. The authors proposed a mathematical description of the steady-state decomposition of polymer by laser radiation. This theoretical relation is applicable only to the moderate laser intensity case, where the activation energy for degradation does not depend on the rate of energy supply.

Tolstopyatov[71] studied the kinetic characteristics of PTFE, P(TFE-E), PC, PVDF, and PPX decomposition produced by 35-W laser radiation and 0.5 MW/m^2 intensity at wavelengths of 10.6 (CO_2) and 1.06 μm (YAG). CO_2 laser irradiation produced a constant degradation rate for all polymers after a 2−3-s induction period. PVDF produced the minimum decomposition rate, while the maximum rate, for PTFE, was 5 times higher. The decomposition rate under YAG laser irradiation was steady for PC and PTFE, but grew with time for PVDF and P(TFE-E). Decomposition rates were several times lower for YAG laser action than for CO_2. The authors explain these peculiarities by a higher reflection coefficient

and transparency of polymers for radiation of 1.06-μm wavelength.

Grakovich et al.[72] studied PPX decomposition by CO_2 laser at intensities of 0.1−3 MW/m^2. At the higher irradiation intensities, a fine powder is recovered along with the evolved gases. Both the powder and a condensate were lettuce-yellow, which is suggestive of the presence of *trans*-stillbene structures in these degradation products.

Bykovsky et al.[73] examined the effect of nanosecond pulse radiation of a powerful light with a wavelength in the 2.4−4.2-μm range. The pulse energy exceeded 30 mJ. UV lasers with 266- and 354-nm wavelength were also used. Cellulose, PSF, and epoxy polymer were exposed in this way. The authors investigated these photophysical and photochemical processes by dynamic time-of-flight mass spectrometry in the collision-free regime. Comparing the results of IR and UV irradiation, the authors concluded that both types of laser treatment with a 10^{10}−10^{18} W/m^2 pulse intensity lead to the thermal dissociation of macromolecules on the target surface, but not in the gaseous phase.

Said-Galiev et al.[74] studied the effect of CO_2 laser radiation on aromatic heterochain polymers in air. This laser treatment cross-linked the surface layer, which sometimes improved mechanical characteristics. Cross-linking under irradiation is characteristic for aromatic polymers. Further exposure of cross-linked PC and PhN leads to degradation, charring, and formation of a porous carbonized residue.[43] Cross-linked PE degrades under the action of a CO_2 laser, with the formation of paraffin-like products.[44]

Tolstopyatov et al.[18] concluded that degradation, evaporation, and cross-linking proceed simultaneously upon laser irradiation of aromatic polymers. Among the evaporated products of decomposition, only those with intact side groups (i.e., having the structure of the original polymer) were observed. Apparently, polymer fragments sustaining damage in the side chain quickly cross-link and are therefore not able to evaporate. Tolstopyatov[44] confirmed the inverse dependence of the thickness of the polymer layer heated upon irradiation intensity. Thus, the thickness of the melted layer of compressed PCTFE powder is about 0.1 mm under CO_2 laser irradiation at an intensity of 1−2 MW/m^2, and as much as 5 mm under an intensity of 50 kW/m^2.

Interesting results were obtained when PTFE was irradiated by a CO_2 laser in a vacuum.[62] No temperature variation was induced in the zone of exposure as a result of increasing the irradiation intensity from 0.2 to 1.5 MW/m^2. It was steady at 805 ±15 K.[75] The only variability observed was in the rate of liberation of gaseous products. The mass spectrum of the gaseous products emitted during PTFE laser beam evaporation is similar to that resulting from the products of low-temperature pyrolysis.[31,43] The average molecular weight of the liberated gas determined by gas density measurements was found to be 108−112 Da. Fragments with higher molecular weight were absent. Along with the gaseous fraction, wool and fibers were also ejected from the exposed zone (Figure 7). Figures 8 and 9 show XRD and DSC

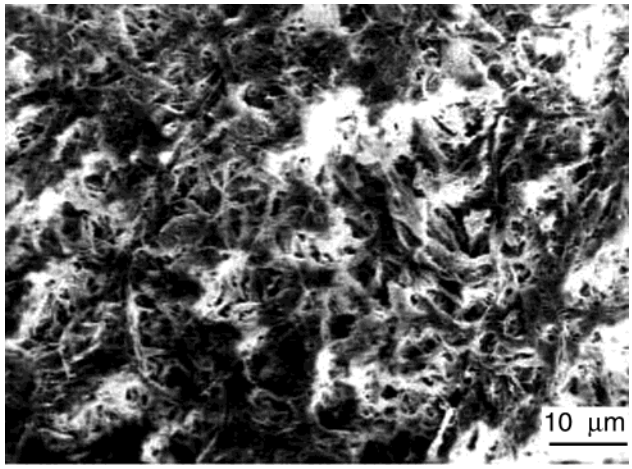

Figure 7. SEM image of PTFE wool.

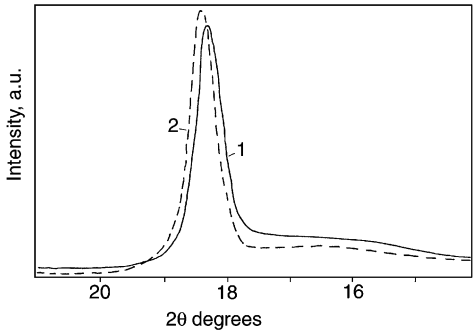

Figure 8. X-ray diffraction of (1) PTFE fibers and (2) bulk PTFE.

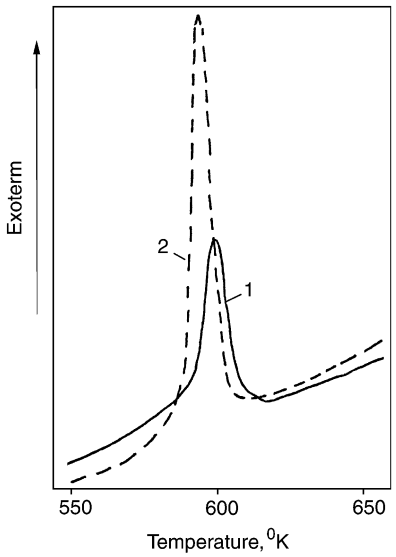

Figure 9. Differential scanning calorimetry of (1) PTFE fibers and (2) bulk PTFE.

comparisons between PTFE fibers and commercial bulk PTFE. Some differences (including a slight increase of the identity period) are evident, although the source of these differences remains unclear. Such small differences between the original polymer and the fibers seem to correlate with the qualitative difference between the behaviors of these materials under CO_2 laser irradiation. When these gathered fibers were later exposed to laser irradiation in a vacuum, products capable of condensing at room temperature were formed.

Krasovsky et al.[62] proposed a model for the decomposition of PTFE under CO_2 laser irradiation. The model assumes that the PTFE bulk consists of two modifications having differing responses to laser exposure. One component unzips easily to monomer under irradiation at a low temperature (805 K), while the second slowly degrades to form a wide range of products, including the heavies, being "cooled" by the monomer generated by the first component. The second component forms a viscous molten film on the surface which is ripped through by the efflux of monomer and drawn out into fibers. But at chamber pressure over 1000 Pa, fiber formation is no longer significant. The irradiation of PTFE at other wavelengths (1.06, 0.157, and 0.248 μm) produced no fibers, but did give condensable gaseous products. Perhaps such a behavior is due to the unique combination of the unusually good high-temperature dimensional stability and the near coincidence of the CO_2 laser radiation wavelength to a C_2F_4 absorption band. The more C_2F_4 released during irradiation, the more absorption, resulting in a process with positive feedback.

Tovstonog[76] irradiated (32.5 MW/m^2) PTFE in a closed vessel at atmospheric pressure. This author observed two different phenomena:

(i) Monomer is formed by irradiation. It partially escapes owing to imperfect seal of the vessel, and partially polymerizes on the vessel walls, producing a white powder of secondary PTFE.
(ii) A bright flash occurs during irradiation after an induction period.

The glow zone temperature was estimated to be 2500−2800 K. Carbonized products were also formed. The author suggests this to be the result of a secondary reaction, such as

$$2C_2F_2 = 3C + CF_4$$

proceeding through multiple intermediate stages. It should be noted that the final gas pressure in the vessel was 0.35−0.5 MPa, which is higher than that at the start (1 atm = 0.1013 MPa).

Garrison and Srinivasan[77] developed microscopic photochemical and photothermal models for laser ablation of PMMA. They showed that their photochemical model describes the processes in PMMA under UV laser irradiation (193 nm), while their photothermal model better describes the processes under visible laser irradiation (532 nm). Hill and Soong[78] developed a model for laser marking of thin polymeric films. The ablation threshold is caused by the internal energy of the depolymerization process. The temperature of the film surface is determined by the balance between the absorbed laser energy and the energy needed for depolymerization and evaporation of the monomer. These processes also are responsible for the observation that only a very thin surface layer is heated to high temperature.

New experimental techniques have increased research activity in the laser treatment of polymers. D. D. Dlott et al.[79−82] irradiated PMMA film using a 1.06-μm laser. The processes occurring were determined using a "molecular thermometer" as well as picosecond time-resolved coherent Raman spectroscopy (CARS). In situ methyl methacrylate formation was verified to occur directly under laser radiation and not through secondary reactions.[81] The CARS spectra of PMMA films under laser action are shown in Figure 10. The bathochromic shift of the PMMA peak is attributable to MMA generation by thermal decomposition. The ablation threshold temperature was 600 °C, while the maximum temperature reached was 715 °C,[79] as presented in Figure 11. At the ablation threshold, the depolymerization is slow and most bond cleavage occurs by pyrolysis. Above the threshold, the depolymerization by thermally activated unzipping becomes comparable to pyrolysis. The scheme of the processes is presented in Figure 12. It was also demonstrated that ultrafast thermal heating involves two stages, interchain and intrachain excitation. Phonon excitation occurs 2 orders

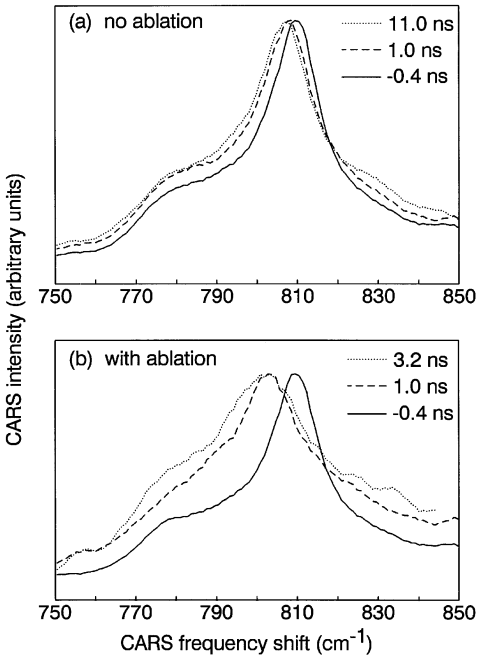

Figure 10. CARS spectra of PMMA films under laser irradiation. Reprinted with permission from ref 81. Copyright 1994 American Institute of Physics.

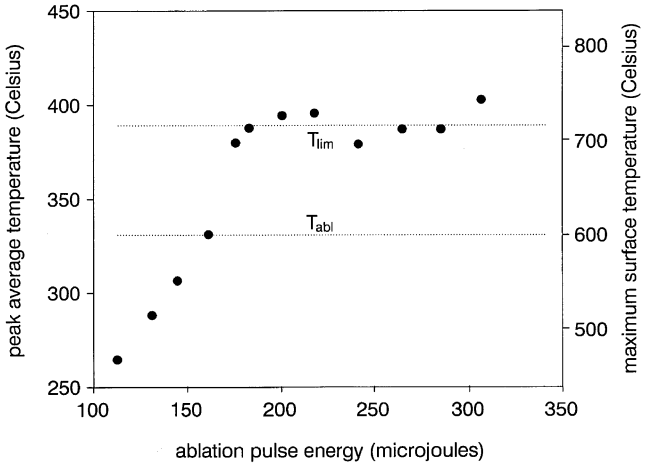

Figure 11. Peak temperature vs ablation pulse energy. Reprinted with permission from ref 79. Copyright 1992 American Institute of Physics.

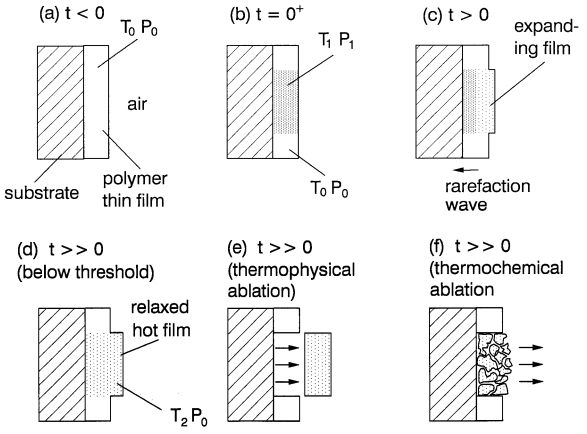

Figure 12. Scheme of the ablation processes. Reprinted with permission from ref 82. Copyright 1995 American Institute of Physics.

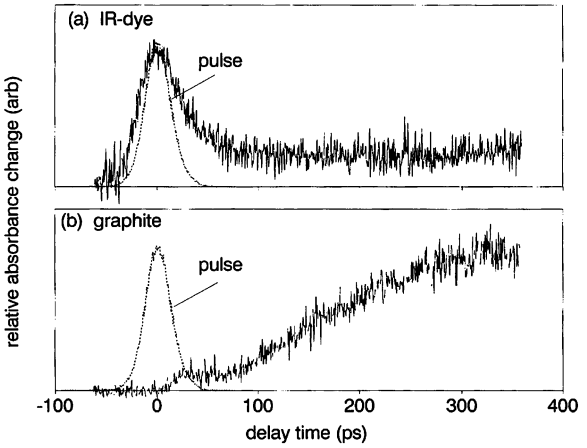

Figure 13. Kinetics of dye- and graphite-filled polymer film cooling. Reprinted with permission from ref 80. Copyright 1994 American Institute of Physics.

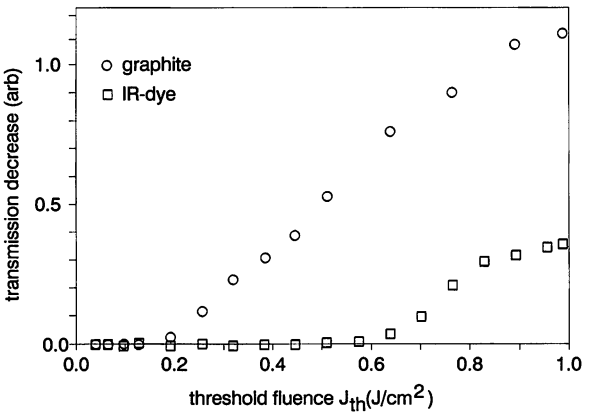

Figure 14. Threshold fluence for dye- and graphite-filled polymer film. Reprinted with permission from ref 80. Copyright 1994 American Institute of Physics.

of magnitude faster than vibrational excitation. The thermal equilibration time was estimated to be 50 ps in a dye-filled PMMA film. Small absorptive particles lower the ablation threshold, as shown in Figures 13 and 14. This is due to the fact that thermal decomposition begins on the particle surface, but need not heat up the entire volume (particle temperature equilibrates with the bulk polymer in 300 ps).

Tsunekawa, Nishio, and Sato[54,83,84] studied PMMA and PS ablation by a 308-nm laser using multiphoton ionization mass spectrometry (at 248 nm). All peaks were understood as having been derived from MMA monomer or dimer splitting under the 248-nm laser ionization action. The peaks from PS were assigned to a styrene monomer. The authors suggest that these results confirm unzipping reactions in PMMA and PS under laser irradiation. They measured the velocity distributions of neutral fragments emitted from the polymer surface. Using Maxwell−Boltzmann distributions, the temperature for MMA was estimated to be 600 K, and for styrene, 1100 K. Since PMMA has a negligible absorption at 308 nm, the ablation must be due to either thermal or multiphoton events. PS absorbs strongly at 308 nm, and the ablated products' character indicates the photothermal nature of the process.

Nishio et al.[55] discovered a remarkable effect of UV laser wavelength in PAN ablation. For the 308-nm laser, the chemical structure of the deposited film is the same as the original polymer. This suggests a purely thermal process which involves the ablation of microclusters. On ablation with 248-nm irradiation, cyclization of nitrile groups occurs. With 193-nm irradiation, the nitrile groups are eliminated almost completely, and the resulting film is a polyacetylene-like polymer. The latter two cases indicate the extent to which photochemical reactions occur.

Kannari et al.[50,51] obtained films using a 157-nm laser for PTFE irradiation. Norton and his coauthors[52,53] used a nanosecond-pulsed 248-nm laser. They arrived at an interesting result: the activation energy for the formation of TFE from PTFE is 0.9 eV at a radiation intensity about 10 kJ/m^2, and about 0.2 eV at 30−35 kJ/m^2, both of which are markedly less than the activation energy for thermal degradation (about 3.5 eV). Tolstopyatov[44] obtained a similar result when irradiating PTFE with a CO_2 laser of lower intensity (1 MW/m^2).

Inayoshi et al.[85] used XeCl and CO_2 lasers for PTFE decomposition. The CO_2 laser power was varied from 5 to 15 W. Deposition rates as high as 1 μm/min were obtained at 7 W for the CO_2 laser, while for the XeCl laser the deposition rate was only 8 nm/min. It seems that the XeCl laser irradiation leads truly to chemical decomposition and secondary polymerization of small fragments, while the CO_2 laser gives emitting clusters of the original polymer along with small fragments. The same team,[86] as well as Zhang and Katoh,[87,88] studied PTFE and PFEP decomposition by synchrotron radiation (SR). The ablation rate for PTFE was as high as several micrometers per minute. The PFEP ablation rate was even higher. Strong ion signals were observed for C, F, CF, CF_2, and CF_3 fragments. Moreover, more ion signals of fragments with masses over 300 amu were recorded.[86] Similar results were obtained by Zhang with other coauthors.[87,88] They compared the composition of gaseous products of PTFE decomposition by various methods. Mass spectra for PTFE degradation products obtained by synchrotron radiation evaporation, laser beam, and thermal evaporation are summarized in Figure 15. One concludes that the mech-

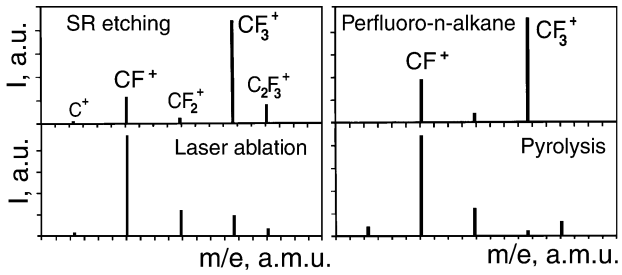

Figure 15. Mass spectra of PTFE degradation products: synchrotron radiation evaporation, laser beam evaporation, thermal evaporation, and perfluoro-*n*-alkane gas. Reprinted with permission from ref 88. Copyright 1999 Elsevier Science.

anism of PTFE decomposition by synchrotron radiation is photochemical, while that by UV laser beam is a thermal unzipping, yielding almost pure monomer. PVDF and P(TFE-E) films also were successfully deposited by synchrotron radiation.

The latest development is deposition of a poly(ethylene glycol) (PEG) polymer film by resonant laser beam evaporation, using an IR free electron pulsed laser that allows one to tune the incident radiation anywhere in the 2−10-μm range.[89] When the irradiation wavelength (i.e., frequency) coincided with the CH_2 group's vibration frequency, complete macromolecules were transmitted from the target to the substrate. This conclusion is supported by IR spectroscopy, electrospray ionization mass spectrometry, and matrix-assisted laser desorption/ionization spectroscopy data, which together indicated an average molecular weight for the film of 1518 (2.9-μm irradiation) or 1528 amu (3.4-μm irradiation). The average molecular weight of the target polymer was 1538 amu. That result is in agreement with the theoretical determination of the maximum size of a molecule that can be evaporated without destruction.

Given the research trends in the this field, interest in electron beam, laser beam, and synchrotron radiation evaporation of PTFE will surely continue. This polymer possesses uncommon properties under irradiation which we need to learn more about.

These experimental results on in vacuo polymer destruction with various energy sources lead us to conclude that destruction processes are determined by the chemical nature of a polymer as well as by the energy input rate from the pre-degradation to the evaporation of the destruction products.

Theoretical modeling for describing various aspects of laser-induced degradation and ablation of polymers continues, in particular in the Garrison[90,91] and Arnold[92−94] groups.

2.4. Classification of the Energy Actions on Polymers

The following energy action classification scheme should be useful in accurately describing important aspects of polymer thin-film technology:

(i) *Contact heating* is characterized by a slow transition from the pre-degraded state into decomposition, due to the inherently low thermal conductivity of polymers. Degradation itself is close to an equilibrium process, in which the weakest links are first to rupture. The comparatively slow rate of energy input enlarges the size of the destruction volume, and secondary reactions in the bulk polymer contribute considerably to the product mix.

(ii) *Laser irradiation*. Here, the depth of the destruction zone is determined by the polymer's optical absorption at the laser radiation wavelength, which ranges from 1 to 90 μm. The rate of energy input into the polymer can be rather high. This leads to nonequilibrium degradation and expands the range types of cleaved chemical bonds. Account should be taken of the possible surface carbonization of some polymers, which reduces their transparency and enhances subsequent polymer degradation as a result of the greater energy capture by the carbonized layer, in a mode similar to high-temperature contact heating. Secondary processes in the gaseous phase are comparatively small.

(iii) *Synchrotron irradiation*. The radiation wavelength ranges from 1.4 to 10 nm. The absorption and energy supply mechanisms are like those of laser irradiation, but the photon energies are much higher, which gives the possibility of both rupturing more chemical link types and introducing a much higher energy density. Synchrotron radiation evaporation involves mostly photochemical mechanisms of polymer decomposition.

(iv) *Irradiation by accelerated electrons*. Penetration depths for 1−7-keV energy electrons are up to 1 μm. A high rate of energy input is possible. One must take into account local nonuniform distribution of excitation along the molecular chain, which widens the range of degradation pathways, as well as the composition of the evaporated fragments. Secondary processes in the polymer are minimal. However, secondary processes are possible in the gaseous phase, activated by electron collisions.

(v) *Ion irradiation*. The main distinction from previous methods is that the mechanism of fragment formation is physical sputtering, not thermal destruction. Treated polymer depth is minimal. Industrial uses include mainly ion-plasma treatment, which permits additional dissociation in the gaseous phase.

2.5. Gas-Phase Geometrical Distribution of Destruction Products and Their Activation

The total chamber pressure depends on the competition between gas liberation from the heated polymer, active fragment condensation, and evacuation of the more volatile fragments from the chamber. Polymer decomposition products may comprise both neutral and charged fragments, as well as free mono- and diradicals. The sticking probability of the fragments depends on both the thermodynamic and the kinetic characteristics of the entire system. Depending on the fragments' chemical activity, their velocity, their flux density, and the nature and temperature of the substrate, the sticking probability can varied over a wide range. Increases in chemical activity, molecular weight, and flux density, and decreases in substrate temperature, increase the sticking probability.

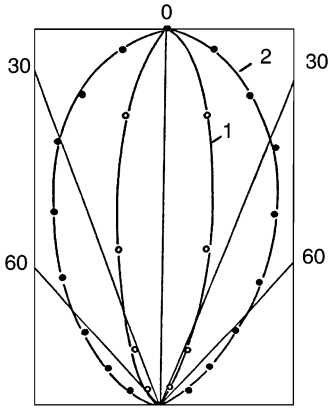

Figure 16. Polarogram of molecular flow of PCTFE evaporation products, produced by laser beam evaporation of (1) 40 and (2) 4 W.

Molten polymer droplet ejection is a problem to be avoided in thin-film technology. Droplet formation depends on the type and parameters of energy input, as well as on the polymer's structure. The decisive factor here is a combination of the depth of energy penetration, the rate of formation of gaseous products, and the polymer melt viscosity. The only thermoplastic polymer producing no drops is PTFE, which has an extraordinarily high melt viscosity. Cross-linked polymers produce a pure fragment flow, and only at energy intensities higher than 0.3−1 MW/m^2 do they start producing a few fibrils or powder particles. Melt splashing can be mitigated by the following methods: the use of heated screens[95] or filters,[96−98] the proper choice of evaporation regimes with small deposition rate,[98,99] feeding the polymer to the heated surface in small portions,[95] and pressing the powered polymer into a matrix of metal powder.[96] Gritsenko and co-workers[96,97] observed no reduction of condensed-phase yield while using a metal filter in the evaporation of PE, PP, PCA, or PVDF. In contrast, Luff and White[98] found a 5-fold reduction in condensed phase yield using a quartz wool filter.

The angular distribution of fragment flow emitted from a point on a planar surface obeys a cosine law, much as in the case of thermal evaporation. However, the distribution is distorted because the crater bottom is nonplanar. According to Tolstopyatov,[44] a distinct contribution to distortion of the initial angular distribution of vapor emission intensity is introduced by collisions of the emitted molecules with each other. Gritsenko determined that during PTFE evaporation from a crucible, this indicator of the fragment flow was close to being cosine in shape. Krasovsky and Tolstopyatov[12] showed that the fragment flow produced by a 40-W CO_2 laser with a beam cross-section of 5×10^{-5} m^2 is shaped approximately as a $\cos^n \theta$ function, where $n = 6-30$ (Figure 16). For similar conditions, Stephens et al.[100] found $n = 6$. These variances can be explained by differences in the radial distribution of irradiation density for different individual lasers as well as by any procedures taken to avoid crater formation. Fragment flow development is affected by fragment self-interaction. The contribution of such interactions increases with irradiation intensity. Estimates from two independent

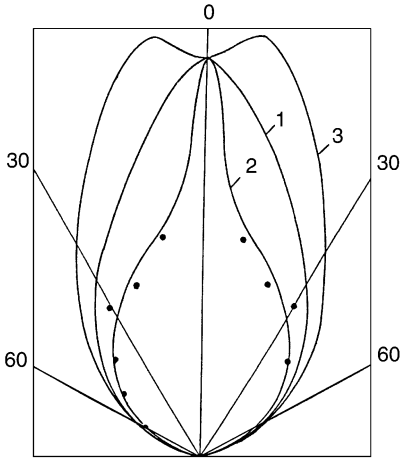

Figure 17. Polarogram of molecular flow emitted by electron beam evaporation of PTFE: (1) accelerating voltage, 2.0 kV; (2) accelerating voltage, 3.6 kV; (3) glow discharge gun.

methods agree with this proposal.[44] But Garrison and Srinivasan[77] calculate that in the case of photochemical processes the distribution angle is narrow (30° of surface normal), and in the case of photothermal processes it is wide (60−70°). It might be suggested that in the case of PTFE destruction by a CO_2 laser, the photochemical mechanism is taking place simultaneously with the photothermal mechanism. The former can contribute to the fragment flow shape significantly.

Electron beam evaporation is characterized by a wider variety of fragment flow features. Apart from the expanded range of polymer decomposition products rich in heavier fragments, some products may also be electrically charged. Zadorozhny[33] showed that the plume of fragments emitted during PTFE and PCTFE electron beam evaporation had a nearly cosine shape (within 10%). Silantiev[42] encountered crater formation; hence, his experimental dependence was approximately $\cos^3 \theta$. Tolstopyatov and Krasovsky[12,43] obtained a more complex spatial distribution of fragments during electron beam evaporation of PTFE (Figure 17). This flow shape looked like a superposition of two components: a narrow central beam and wider beam approximating cosine shape. Further experiments[44] demonstrated that the narrower component consisted of molecular fragments carrying negative charge. Since a positively charged electrode, coaxial to the flow, is situated near the condensation surface, ion fragments are expelled from the flow, concentrated, and focused into a narrow beam. Varying electrode potential and position with respect to the flow axis changes the flow configuration. The cause of Zadorozhny's[33] double-hump-shaped fragment flow from a planar surface during electron beam evaporation remains obscure. In addition to its cosine shape, the flow is similar to that achieved by suppressing the nearly axial central flow (the opposite of the expulsion seen in ref 47). Gritsenko obtained both of the above-mentioned distribution types for PTFE, using the same crucible[28] but modifying the activator geometry. This suggests that the effects are caused by charged particles, but whether this is due to the influence of different

spatial distribution of activating electrons or activated charged fragments has not yet been decided.

The question of the state of charge possessed by particles emitted from the polymer surface has been around from the beginning of experimental work. Belyi at al.[30] showed that ions are absent in the thermal degradation of PCA. Tolstopyatov[47] could not find ions (less than 1 in 10^9) among the products generated by a CO_2 laser operating at power densities up to 10 MW/m^2. Ionization during evaporation does, however, arise at higher laser intensities. Norton et al.[52,53] recorded both positive and negative ions among the PTFE degradation products at 248-nm laser wavelength, 20-ns pulse duration, and 12−15 kJ/m^2 intensity (0.6−0.75 TW/m^2). The positive ions included species up to C_4F_7 in size, while negative species were limited to smaller fragments (F, C_3, CF_3).

Fragment flow can be activated by either accelerated electrons, glow discharge, or UV light. Excitation and ionization of the fragments as well as modification of fragment composition are all possibilities. The physicochemical processes occurring upon activation are similar to those occurring in film deposition starting with low-molecular-weight compounds, as in the case of plasma polymerization. Yet films obtained from the subject technologies are quantitatively different. Since the fragments have higher molecular weight, changes in repeat unit structure are considerably smaller. The chemical reactivity of the evaporated fragments also shrinks the comparative effect of the activation. A plasma struck in a supporting gas atmosphere activates each monomer molecule, and the probability of secondary reactivation and splitting of the already initially activated molecule is high. As a result, the film produced is highly crosslinked and has a deficiency of H and F. In the case of activation during evaporation in a comparatively high vacuum, the plasma action is significantly smaller — only one hit may be possible. Furthermore, we tend to have multiple-repeat-unit evaporated particles — so being hit by an electron results in less damage than if a monomer-sized unit were hit. So, the influence on both deposition rate and film structure is less.

It was discovered during mass spectroscopic studies of PE, PP, PVDF, and PCA pyrolysis products that accelerated electrons led not only to excitation and ionization of fragments, but also to their dissociation. As a result, an additional several percent hydrogen is freed up, and the unsaturated fragment content increases.[28] Similar treatment of PTFE evaporation products led to an even more significant modification of the gas-phase composition (Figure 18): the relative intensity of CF_3 and C_3F_5 fragments was increased, and also fragments with high content of carbon appeared. The concentration of CF and C_2F_4 fragments decreased. It should be mentioned that products of PTFE pyrolysis in a quasi-closed volume differed in composition (section 2.1) and could not be activated by electron impact.

During gas-phase activation, it is possible simultaneously to activate the film surface with a directed electron beam, by charged particles of a plasma, or by light. Such irradiation of the growing film considerably influences its properties.

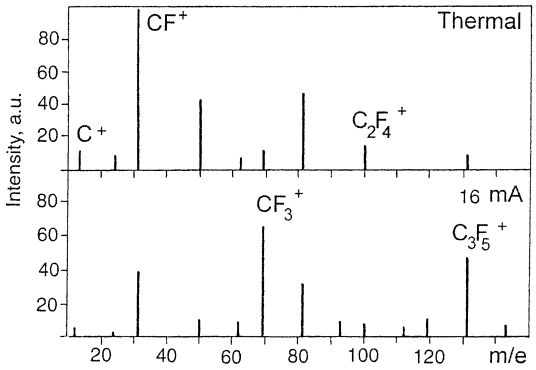

Figure 18. Mass spectra of PTFE evaporation products under the following conditions: (1) thermal evaporation from a crucible; (2) thermal evaporation from a crucible with activation by accelerated electrons at 3 kV and 16 mA.

2.6. Conclusions

In summary, we find that the status of studies of thermally induced degradation is mature. Work continues on newly synthesized polymers and on all polymers under severe degradation regimes (high-power pulse, hostile environments, etc.). One particular area of interest remaining is degradation induced by the action of high-energy electrons or plasma. Work on laser-produced effects in polymers, including degradation and other photostimulated processes, is growing fast.

3. Polymer Film Growth and Structure

3.1. Polymer Film Formation on Solid Surfaces in a Vacuum

The chemical and physical processes occurring on the substrate surface depend on the chemical activity of the vapor as well as on certain kinetic and thermodynamic factors, such as the fragment flux intensity as well as the nature and the temperature of the substrate. Inactive molecules of low molecular weight form a dynamic equilibrium layer on the surface, the parameters of which depend on the chamber pressure and temperature. Winters[101] estimated the sticking probability on a silicone substrate for a number of small fluorine-containing stable gas molecules to be less than 10^{-7} at 293 K and a pressure of 10^{-1}−10^{-2} Pa. But the sticking probability for the reactive CF_3 radical is in the 0.08−0.7 range. The sticking probabilities on chemically active surfaces, e.g., growing film, should be higher for both active and inactive fragments. The ability of smaller fragments to migrate is greater; hence, migration ability makes a considerable contribution to the polymer film growth processes. The largest fragments will have sticking probabilities approaching unity, and will be nearly unable to migrate any appreciable distance laterally over the surface at 293 K. Their participation in chemical processes is governed rather by the mobility of their reactive end segments.

Apparently, the processes on the substrate will respond to the concentration of each type of fragment.

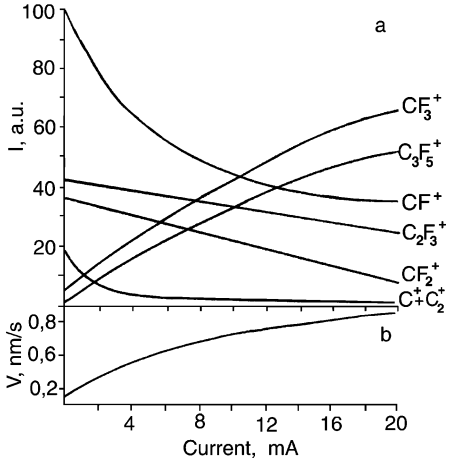

Figure 19. Concentration of some PTFE degradation products (a) and deposition rate of the film (b) vs activation current ($V = 3$ kV). Distance from evaporator to quartz microbalance was 300 mm.

Krasovsky and Yurkevich[102] studied the influence of the pressure of the gaseous medium, the distance between evaporator and substrate, and the PCA evaporation rate on film growth kinetics. Increasing pressure and decreasing distance gave an increasing in the growth rate. But the interpretation of the results of this experiment might be improved if one takes into account that the chamber pressure is not a basic independent parameter. Indeed, it depends on polymer evaporation flux, the chamber evacuation rate, and the injection into the chamber of any additional gas. By varying pressure through different means, we can achieve different results. In essence, the authors[102] measured film growth rate vs evaporation flux intensity, which is indeed an independent parameter, although the pressure of gaseous products is proportional to it. These results are unique to the particular apparatus used, and can be used qualitatively to characterize the regularity of the process. Similar results were obtained by Gritsenko et al. during PE, PP, PCA, PVDF, and PCTFE thermal evaporation. It was found in general that the ability of the polymer vapors to grow films was limited at certain pressures in the chamber, despite further increases in evaporation intensity (see Figure 1). Gritsenko and co-workers studied the kinetics of PTFE film growth as well as the gaseous phase composition upon the electron activation of PTFE degradation products.[103] The film growth rate rose under electron activation in a manner which correlates with the quantity of CF_3 and C_3F_5 fragments, as presented in Figure 19. The growth of the polymer chain was supposed to have resulted from the electrically neutral C_3F_5 fragments, but CF_3 fragments also can be found in the growth process. The author suggested that these results might be explainable in terms of the activation−chemisorption model developed by Vinogradov[104] for the processes of film formation during plasma polymerization, although a step-by-step diradical attachment mechanism like that for PPX growth might also be considered. To clarify the growth mechanism, a complex investigation involving mass spectrometry of both positive and negative ions was required. Recently, Wijesundara et al.[105] studied PS surface modification by CF_3 and C_3F_5 positive ions in the 25−100-eV energy range with an accuracy of l eV. A special ion source was used. XPS revealed that the chemical structures of the deposits were consistent with a plasma-polymerized fluoropolymer. Increasing ion energy gave films containing more CF_n groups other than CF_3. But the maximum concentration of $-CF_2-$ groups was achieved when using 50-eV ions. The authors[105] considered their results as indicative that a fluoropolymer film is grown more effectively from C_3F_5 ions than from CF_3 ions. These results confirmed the mechanism of PTFE film growth proposed by Gritsenko: both C_3F_5 and CF_3 fragments play a role in film growth, but to differing extents.

Luff and White[98] exposed growing PE film to UV radiation. The rate of film growth did not change, but the material hardness and brittleness rose and the film became insoluble. Polishchuk[106] used accelerated electrons to irradiate the condensation surface during PTFE electron beam evaporation. Obviously, interactions between electrons and molecular fragments in the gaseous phase were unavoidable. Irradiation under all conditions reduced the film growth rate, indicating that a degradation process accompanies polymerization. The formation of a cross-linked structure provided further evidence that degradation is a significant factor in film growth under irradiation.

Gritsenko,[107,108] Silantiev,[42] and Tolstopyatov[44] all used the RF discharge for activating decomposition products. In the first work, film growth kinetics were found to be independent of plasma treatment. It should be noted, however, that this result was observed only for comparatively small RF power levels. During electron beam evaporation of PCTFE, a proportionate reduction in growth rate was detected upon increasing discharge power, while for PTFE decomposition a slight increase was observed at the lower powers and then a decline in growth rate at the higher power range. A similar dependence was found upon the plasma activation of laser beam evaporation products of PC, PSF, and PhN. For PCTFE, P(TFE-E), and P(CTFE-E), a reduction in the deposition rate with increasing power was observed. In the case of the chlorinated polymers, the rate decrease was due to the fact that chlorine atoms have the weakest binding energy, and thus were cleaved off more easily, not to take part in the film growth. The increase in the growth rate at low powers for other polymers could be explained by the production of a greater amount of smaller fragments during decomposition, which could not be polymerized at the extent of activation employed.

Mass-spectral analysis of the noncondensing fraction and IR spectroscopy of the films lead us to conclude that the main contribution to film formation is from chain fragments with largely unmodified chemical structure. Some of the condensed fragments possess defects in chemical structure, such as in particular the lack of side groups or atoms. Evidence for this conclusion includes the presence of components in the gaseous phase originating from side groups, as well as EPR data, and measurements of dielectric characteristics (tg δ) with alternating cur-

Table 5. PCTFE Film Molecular Weight vs Substrate Conditions

substrate temperature and irradiation			molecular weight, in solutions	
temp, K	electron energy, eV	current density, A/m^2	mean viscous, 2,5-DCTFB[a]	mean digital, Camfora
78	−		5 000	1 500
217	−		10 000	2 900
323	−		40 000	5 600
373	−		90 000	20 900
423	−		120 000	36 400
473	−		140 000	50 600
323	500−100	1	55 000	6 200
323	100−150	2	145 000	55 600
323	200−500	3−5	80 000	2 270
bulk polymer	−		20 0 000	−

[a] 2,5-DCTFB, 2,5-dichlorotrifluorobenzene.

rent which are strongly affected by molecular symmetry and polarity. That the content of the defective fragments is not high is supported by the identity of the films with the initial polymers by IR spectroscopy.

The potential chemical activity of evaporation products, suggesting the presence of diradical fragments therein, could be recognized by their interaction with each other or with unsaturated compounds on the condensation surface. A macromolecule similar to the initial one should be regenerated. The prerequisites for favorable film growth here are (i) the absence of foreign impurities in the gaseous medium, and especially of atoms and monoradicals capable of arresting the chain growth; and (ii) a sufficiently high mobility of the fragment as a whole, or of fragment segments containing free radicals.

Most researchers feel that the macromolecule reconstruction takes place in the growing film. But the final molecular weight in the film is smaller than that in the starting polymer. The mobility of the diradicals diminishes with increasing molecular weight, and as a result there arises a likelihood that, at a certain stage of the process, the end segment would be blocked by the surrounding inactive molecules. That is important, whether the end segment be located in the film bulk or on its surface. In the latter case, there is a further possibility that macrochain increments as a result of active fragments arriving from the gaseous medium. Such a mechanism is thought to take place during PPX synthesis from the gaseous phase.[109] The probability of interaction between macroradical and diradical is proportional to the mobility of the latter and to its lifetime on the surface before it desorbs. Note that both factors are temperature dependent. The factor which limits PPX synthesis from *p*-xylylene is the lifetime of the diradicals on the surface, which become so small at substrate temperatures above 300 K that film growth ceases. A similar situation arises in the condensation of other decomposition products, but at a higher temperature. Therefore, moderate heating reduces the film growth rate, but intensifies polymerization processes and increases the polymer molecular weight. Table 5 gives PCTFE and PTFE average molecular weights at various condensation temperatures.[33] The film molecular weight approaches that of the starting polymer, which is amazing in view of the great number of monoradicals capable of interrupting chain growth.

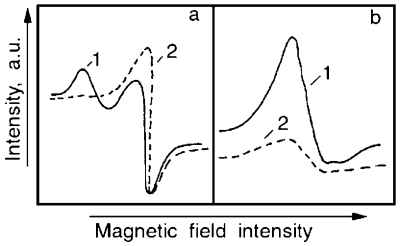

Figure 20. Electron paramagnetic resonance spectra of films deposited by laser beam evaporation of PC (a) and PCTFE (b): (1) as-deposited and (2) after 800 ks of storage.

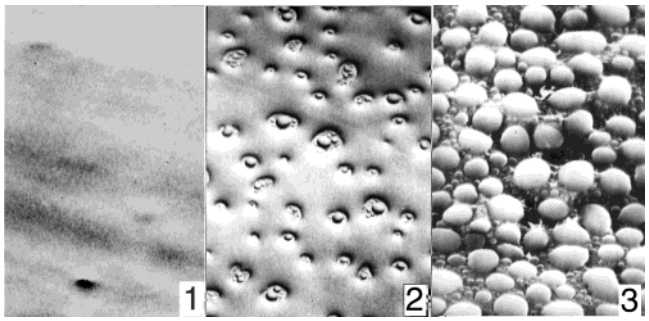

Figure 21. SEM images of PC film surface, deposited by laser beam evaporation, vs substrate temperature: (1) 293, (2) 360, and (3) 430 K.

The study[110] gives indirect data about the predominantly surface character of fragment interactions on condensation. While the condensation rate increases from 5 to 230 nm/s, the concentration of free radicals in the film grows 400-fold. Since the deposition rate was controlled by changing the target−substrate distance only, the concentration of free radicals can vary only due to their interaction on the surface. The data indicate that the interaction time of free radicals on the surface is roughly the same as their lifetime on the surface; i.e., the time interval terminated with the condensing of the subsequent layer.

Evidence of insufficient mobility of free radicals or molecular chain segments in the film bulk at room temperature is given in ref 44. A considerable variety of free radicals (Figure 20) were detected using EPR in films produced by laser beam evaporation of PCF, PCTFE, and PC at 50 nm/s. Storage of the PCTFE film for 600 ks under conventional conditions leads to a double decrease in free radical concentration. Storage of PC and PSF films for 30 Ms did not considerably change the intensity and pattern of EPR spectra. Decay of free radicals in film is assumed to result from their interaction, as well as reactions with oxygen and with hydroxyl diffusing into the film from the atmosphere. The following data confirm the insufficient mobility of molecular fragments on a surface at room temperature. When the products of PC laser beam evaporation condense on a lyophobic (PTFE) surface at room temperature, a homogeneous film is formed[44] (Figure 21, panel 1). At elevated temperatures, the defective film or islet condensate is formed (Figure 21, panels 2 and 3). A similar picture is observed upon the condensation of evaporation products of other polymers. These observations

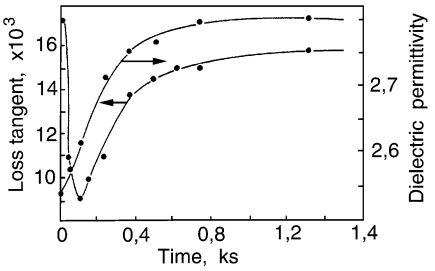

Figure 22. Dielectric permittivity (ϵ) and loss tangent (tg δ) of as-deposited PCTFE films vs endurance time.

prove that a continuous film is formed on a lyophobic surface at low temperature only because of the instantaneous energy loss of molecular fragments on collision with the surface and the resulting reduction of their mobility. Of interest is the evolution of a film with free radicals "frozen" during aging. Films prepared by plasma-induced polymerization from monomer contain free radicals and are inclined to change on aging, resulting in changes in their properties, which become, as a rule, impaired. To stabilize the material, the film is saturated by thermal treatment in a hydrogen atmosphere. As a result, the material loses its chemical activity. The aging phenomenon in such an extreme form was not observed in films formed by polymer evaporation. This is explained by a smaller content of chemical defects. Cracking was not observed during aging of these films. Thermal treatment in a vacuum of the films, prepared by laser beam evaporation of PCTFE,[44] reduces the free radicals' concentration. Such processes may be assisted by alternating electric fields applied to the film. Krasovsky et al.[111] observed more than a factor of 2 change of the loss tangent (tg δ) and 10% change in dielectric permittivity (ϵ) of the films formed by PCTFE during storage under the measuring voltage stress (Figure 22). Irreversible growth of ϵ proves that the material polarity has increased. This correlates with the proposed mechanism of oxygen and hydroxyl attachment to free radicals. It should be noted that, without constant voltage stress during aging, i.e., when voltage is applied only at the moment of measurement, the growth of ϵ and tg δ proceeds much more slowly. The same authors observed an irreversible increment of ϵ and tg δ at cyclic heating−cooling in the 290−393 K range of as-deposited films (Figure 23). It appears that a 25% increase of ϵ during the first step of heating is caused by the compacting of initially microporous material. Dielectric loss tangent varied in a complex way: at temperatures above 410 K, it abruptly and irreversibly increased. This phenomenon was caused by the cracking of the thin upper layer film of metal bonded to polymer. This is the result of a mismatch in coefficients of thermal expansion (metal vs polymer) and the growth of supermolecular structure in the polymer.

Thus, the polymer-evaporated film material is affected by aging. The process of material stabilization under ambient conditions can take a long time. Reducing the deposition rate gave a more stable film. Tolstopyatov[44] observed considerable changes in film properties after a 10-year aging under ambient conditions. PC film, deposited by laser beam evaporation

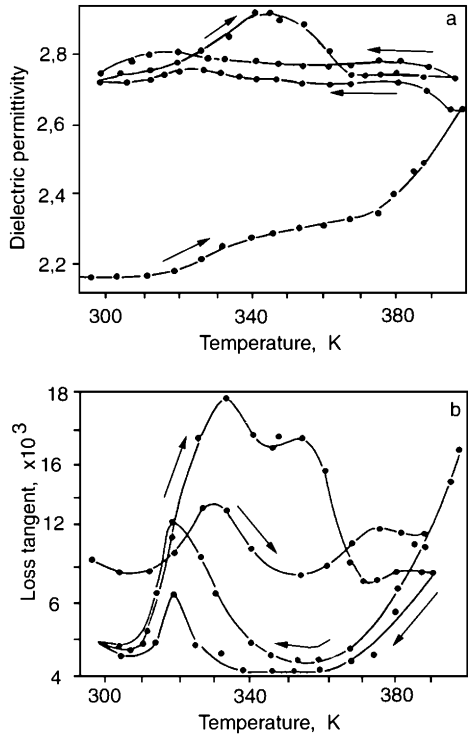

Figure 23. Thermal cycling influence on ϵ (a) and tg δ (b) of PCTFE films.

with RF discharge, exhibited superior solvent resistance. The 5−8-μm-thick film of PTFE on titanium possessed satisfactory cohesion and adhesion as deposited by electron beam evaporation. After 10 years, the film had differentiated into two layers: (i) the upper layer, 60−70% of the film thickness, had properties similar to the as-deposited film; and (ii) the remainder, next to the substrate, had higher strength and adhesion, similar to the original polymer. Structural rearrangements catalyzed by the Ti were presumed to have taken place in the film.

As is known, the lower the mass (size) of particles from which an organic film is formed, the higher the material's inclination toward crystallization. The three-dimensional shape of the molecule and intermolecular forces also play important roles in the crystallization process. Films polymerized from TFE[111] as well as from *p*-xylylene are highly crystalline. Larger fragments decrease crystallization, a matter related to reduced fragment mobility. Asymmetry in the fragment structure additionally reduces crystallinity. For example, a PTFE film formed from the products of electron beam evaporation has a lower degree of crystallinity, which can vary in response to the deposition rate (Figure 24).[44] The crystallization of a material is favored when molecular chains have a highly regular structure. Structural defects reduce their ability to crystallize. Crystallization is suppressed as a second component is introduced. Krasovsky and Belyi[112] proved this by the co-evaporation of polymers and metals. Tolstopyatov[44] prepared amorphous films by simultaneous laser beam evaporation of PSF and PCTFE.

Film composition is also dependent on the characteristics of the condensation surface. Rogachev and Kazachenko[113−115] conducted an investigation of films

Table 6. Refractive Indices of PTFE Films

electron current, mA	thickness, nm	refractive index		structure	
		before annealing	after annealing	before annealing	after annealing
0	31.9	1.36	1.42	crystal	crystal
10	26.4	1.33	1.39	amorphous	crystal
20	26.7	1.32	1.37	amorphous	crystal
20 + 30 W RF	28.3	1.38	1.38	amorphous	amorphous
20 + 30 W RF	600.0	1.42	1.42	amorphous	amorphous

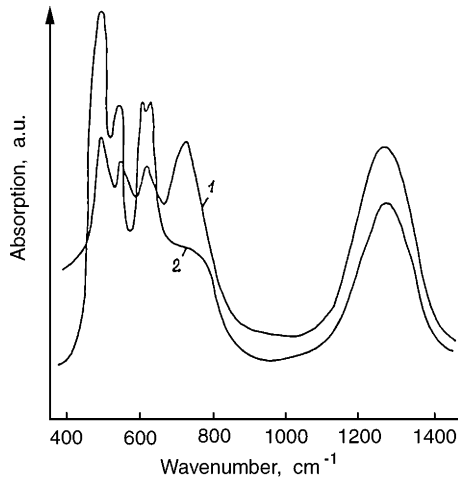

Figure 24. IR spectra of PTFE films deposited by electron beam evaporation at the following rates: (1) 9 and (2) 50 nm/s.

deposited by discharge-activated electron beam evaporation of PTFE. Electron spectroscopy for chemical analysis (ESCA), IR spectroscopy, and secondary ion mass spectroscopy showed that the polymer layer adjoining the substrate had a composition different from that of the rest of the film. Its molecular chains contain hydrogen in their side groups. The macromolecular chains of this layer (0.5 μm thick) tend to be oriented normal to the condensation surface. The refractive index of these films is quite low. The authors also noted that the material, as deposited, is surprisingly deliquescent.

Gritsenko[107,108] investigated films deposited from the products of PTFE thermal evaporation, activated by accelerated electrons and RF discharge, and observed that the refractive index increases with thickness up to 0.5 μm, at which thickness it approaches that of the bulk material (Table 6). The refractive index of films produced with RF discharge activation remains unchanged after annealing, while without such activation it increases somewhat. A variation of refractive index throughout its thickness was observed in a film formed by laser beam evaporation of PSF,[44] with a maximum value next to the substrate. Usui and coauthors have been carrying out "ionization-assisted" deposition of various polymers and dyes since the mid-1980s.[8,116−118] Their PE films have molecular weights of about 1000 Da with a narrow distribution. Their PTFE films have a molecular weight in the range of several thousands of daltons. The PE film crystallinity was greater by that method. This effect could be explained as resulting from an extra decomposition of the evaporated PE fragments by the accelerated electrons, producing a film with lower molecular mass. The PTFE film had a uniaxial crystal orientation, with its molecular chains lying in the plane of the surface. Usui's PTFE film properties agree well with those reported by Gritsenko, obtained employing the same method. But the effect of the "ionization" method on the treatment of PTFE destruction products is more complex, as discussed by Gritsenko.[29,103]

3.2. Morphology and Structure of Polymer Films

Krasovsky[112,119] used TEM to study film formation resulting from the thermal evaporation of PTFE, PE, PCA, and PA. PTFE formed highly crystalline three-dimensional aggregates up to 1 μm in size. A highly crystalline film with a globular−fibrillar structure was formed from PE vapors. The film growth was noted to proceed with a "propagation" of the original structures of dendritic type which overlie one another. Depending on evaporation and condensation conditions, heterochain polymers (PCA, PA) could have different types of aggregation. Suzuki and his coauthors[120] deposited films by the thermal evaporation of poly(acrylonitrile). Film which was deposited from untreated PAN powder was made up of blocks up to 30 μm in size, while film which was deposited using powder previously annealed in air at 200 °C exhibited a smoothness even at the submicrometer level. The IR spectrum of the film agreed well with that of the source powder. It also indicated the high concentration of −C=N− and −C=C− conjugated bonds expected after high-temperature annealing. The PAN films were annealed in a nitrogen atmosphere to convert them into the semiconductive state. Shrinet et al.[121] deposited a thin Mylar (PET) film by thermal evaporation. The IR spectrum of the film agreed well with that of the original PET.

Kabayev et al.[122,123] investigated films produced by the thermal evaporation of PE and PET using TEM and IR spectroscopy. The PE film displayed both crystallinity and vinyl end-group content higher than those for bulk PE. The PET film was amorphous and had high concentrations of COOH and $COOCHCH_2$ moieties. The groups were homogeneously distributed throughout the film. Gritsenko[28] observed cracking and peeling-off after several weeks of storage of the PET film at ambient conditions.

Komakine et al.[124] deposited films of poly(1,4-phenylene) by thermal evaporation. They found that evaporation of PPP produced highly crystalline films. Miyashita and Kaneko[125] pointed out that the crystallinity of deposited PPP films is much greater than that of the original powder. SEM and AFM studies showed that the PPP film consists of crystalline particles about 100 nm in size as well as amorphous domains (Figure 25). Calculations from IR spectroscopy data on the PPP film gave an average chain

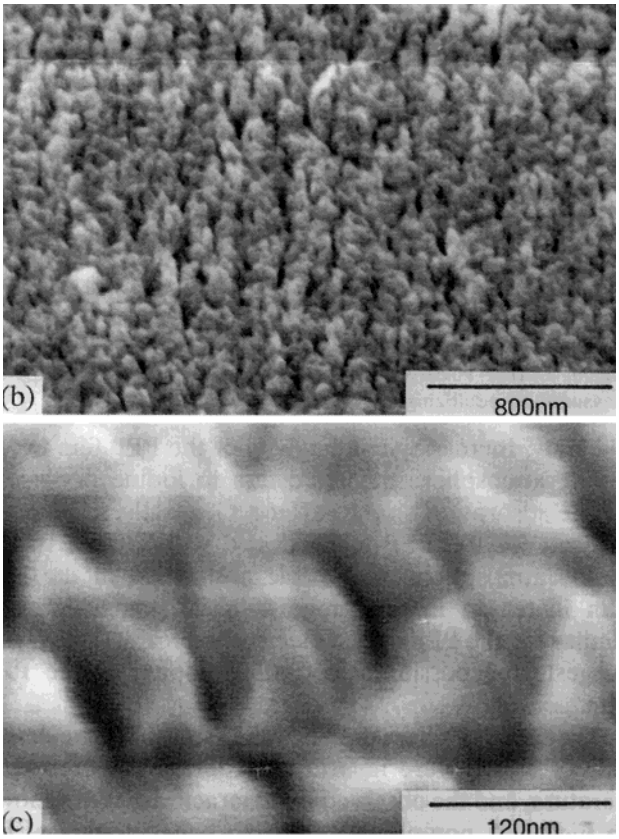

Figure 25. SEM micrographs of 50-nm-thick PPP film.

length of about 9.3 monomer units, which is almost half of that of the initial PPP molecules in the powder.

De Wilde[126] studied the structure of PTFE films deposited by electron beam evaporation using IR spectroscopy. The IR spectra of the deposited film had the same shape as the IR spectra of original PTFE, but the macromolecular chain was shorter and more branched. The film was amorphous. Its glass transition temperature (t_g) was found from measurements of the dielectric properties to be near 51 °C, confirming that the molecules were smaller and more branched. The effects of condensation conditions and thickness on the morphology of films produced by PE, PP, PCA, PTFE, and PCTFE thermal evaporation were studied by Gritsenko and his coauthors.[127,128] The morphology of these films is presented in Figure 26. Deposited at a substrate temperature of 293 K and rates above 0.5 nm/s, PE and PP films became continuous at a thickness of 10 nm. No structure was observed at 120000× magnification up to 100 nm of film thickness. Deposition rates below 0.3 nm/s did not support continuous film formation. Hogarth and Iqbal[129] previously observed similar results at low PP film growth rates. At high growth rates, surface folds appeared in PE and PP films at 100 nm thickness. PCA film continuity was possible at 40 nm thickness, but it had structural formations up to 150 nm in size. The PVDF film became continuous at 40 nm and the PCTFE film at 10 nm thickness, their morphology smooth up to several μm in thickness.[127,128] PTFE film deposited with electron activation of evaporation products was continuous at thickness of greater than 10 nm. The rate of PTFE film growth and RF

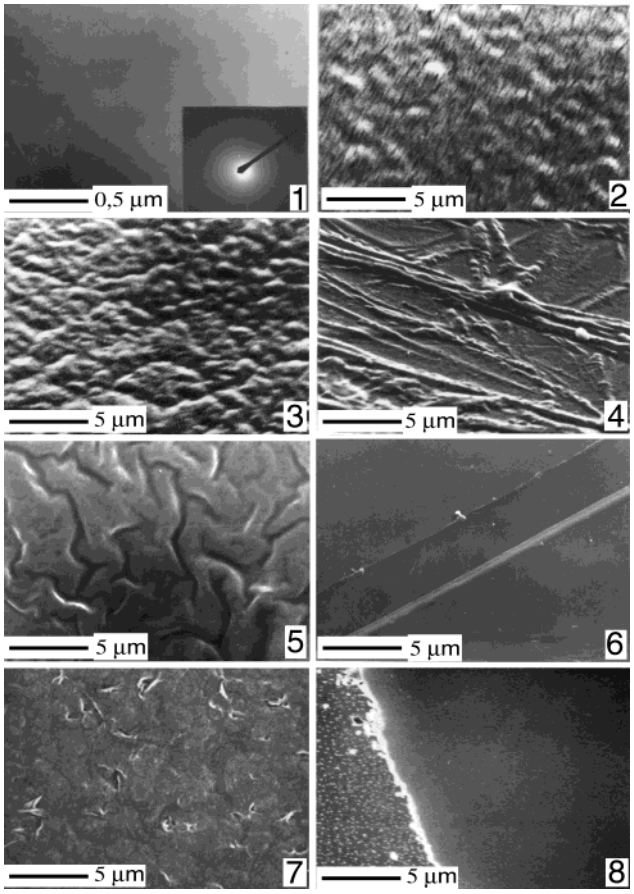

Figure 26. Electron microscopy images of polymer films. TEM: (1) PE, 50 nm thick. SEM: (2) PE, 100 nm; (3) PP, 250 nm, growth rate 1.5 nm/s; (4) PP, 250 nm, growth rate 0.1 nm/s; (5) PCA, 250 nm, growth rate 1.5 nm/s; (6) PTFE, 500 nm, growth rate 1 nm/s; (7) PTFE, 500 nm, deposited at substrate temperature 200 °C; (8) PTFE, 200 nm, polymerized by plasma (50 Hz).

activation did not seem to affect its morphology. The film was made up of 5−8 nm -thick microfibrilles whose long axes tended to lie in the surface plane. When these films are deposited at elevated temperature, the surface folds enlargement was dependent on material thermal stability. Enlargement beginning was registered for PE, PP at 340 K, for PVDF and PCTFE at 350 K, for PTFE at 500 K.

The morphology of films produced by laser beam evaporation depended on the nature of the material as well as the condensation conditions.[12,44] While PC films were smooth, PTFE and PC had a relief of about 1 μm. The homogeneity of PSF films improved when the films were deposited on a warmer substrate or after annealing, but these films had high internal stress. The IR spectra of PC and PSF films deposited by laser beam evaporation agreed well with those of the original polymers (Figures 27 and 28), in contrast to the observation with films deposited by thermal evaporation.

Inayoshi and co-workers[85,86] studied the morphology of the PTFE films produced by CO_2 laser beam evaporation. The film relief is shown in Figure 29. The film deposited at 20 °C seems to be composed of lumps of up to micrometer size, while that deposited at 100 °C is comparatively smooth. The surface of a film deposited by a XeCl laser was smooth even at

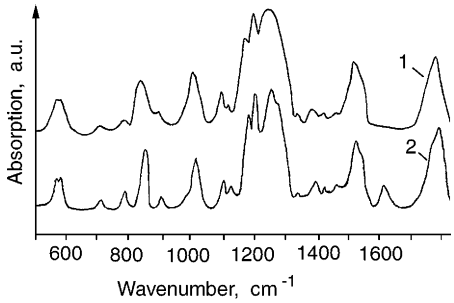

Figure 27. IR spectra of original PC and film, deposited by laser beam evaporation.

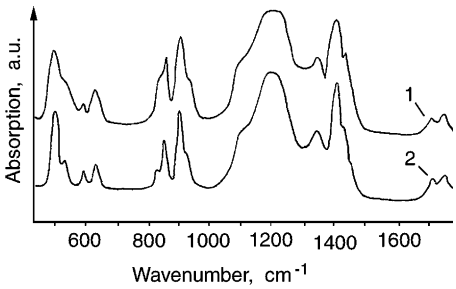

Figure 28. IR spectra of original PSF and film, deposited by laser beam evaporation.

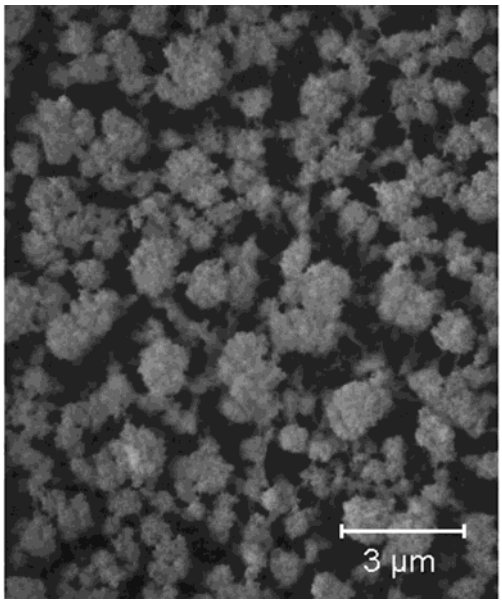

Figure 29. Surface relief of PTFE film deposited by CO_2 laser beam. Reprinted with permission from ref 85. Copyright 1996 American Vacuum Society.

20 °C. These results suggest that polymer evaporation by a CO_2 laser is associated with a release of large clusters which are not completely decomposed. The same team studied the influence of substrate temperature on the structure of films grown by the synchrotron radiation evaporation of PTFE and PFEP (Figures 30 and 31). Films deposited at 20 °C seem to be made up of poles. This may be due to the high flux of the active CFx species. The growth of many macromolecular chains occurs simultaneously, but that is possible in only one direction—perpendicular to the substrate surface. In this case, the kinetics of solid growth is more influential than the thermodynamics. Higher temperature gives smoother morphology. This fact suggests that the

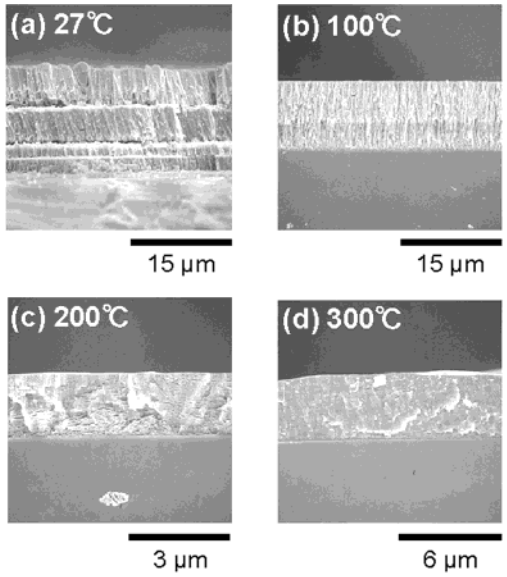

Figure 30. Substrate temperature influence on the structure of the PTFE films grown by synchrotron radiation evaporation. Reprinted with permission from ref 86. Copyright 1999 American Vacuum Society.

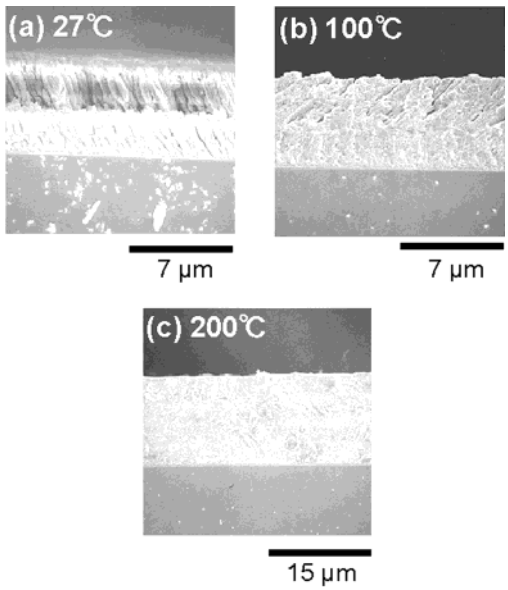

Figure 31. Substrate temperature influence on the structure of the PFEP films grown by synchrotron radiation evaporation. Reprinted with permission from ref 86. Copyright 1999 American Vacuum Society.

film material has a higher degree of polymerization. Zhang et al.[87,88] obtained similar results. Figure 32 compares the morphologies of PTFE films deposited by thermal, laser beam, and synchrotron radiation evaporation. The film deposited by synchrotron radiation evaporation had the smoothest morphology. ESCA data, presented in Figure 33, show more CF_3 groups in the film. Warmer substrate during film growth gave a reduction in CF_3 groups, which is additional proof of a higher degree of polymerization. The axes of the PTFE polymer chains are highly ordered and perpendicular to surface plane. The authors estimated the PTFE film molecular weight to be between 1500 and 8500 Da. The morphology of fluoropolymer films produced by electron beam evaporation was studied by Zadorozhny.[33] Under optimal

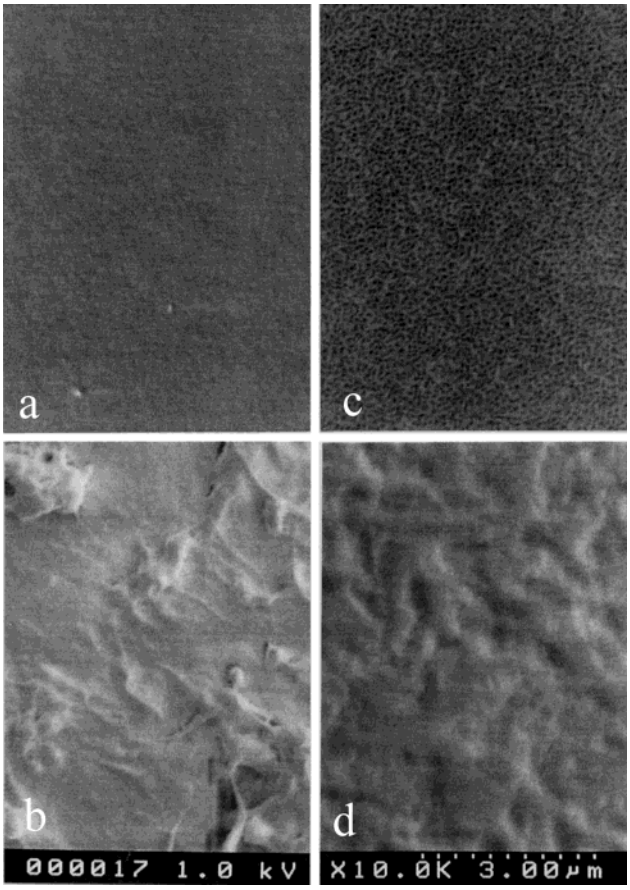

Figure 32. Surface relief of the PTFE films deposited by (a) synchrotron radiation, substrate temperature 20 °C; (b) laser beam evaporation, substrate temperature 20 °C; (c) thermal evaporation, substrate temperature 20 °C; and (d) thermal evaporation, substrate temperature 200 °C. Reprinted with permission from ref 88. Copyright 2001 Elsevier Science.

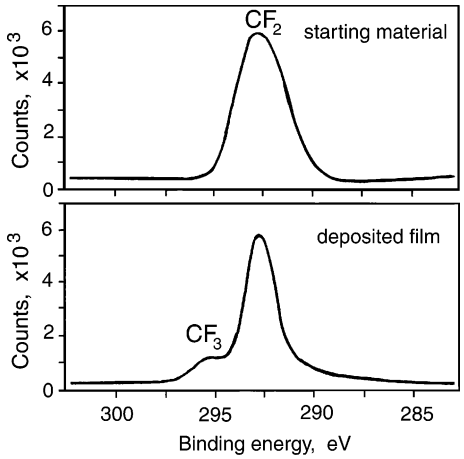

Figure 33. ESCA of PTFE film grown by synchrotron radiation evaporation. Reprinted with permission from ref 87. Copyright 1999 Elsevier Science.

conditions of decomposition, and at a substrate temperature above 450 K, the films formed from PTFE and PCTFE have typical striated and fibrillar structures. He also studied the effect of electron beam irradiation during growth on the refractive indices of the films.

It is clear from the data in Table 7 that, for films of all materials, maximum refractive index results

Table 7. Effect on Refractive Index of Irradiating Growing Film by 2 keV Electrons

	refractive index at current density, A/m^2		
polymer	1	2.5	5
PTFE	1.41	1.406	1.39
PE	1.57	1.57	1.54
P(VDF−FEP)[a]	1.44	1.42	1.40
ML-20	1.57	1.55	1.51

[a] P(VDF−FEP), vinylidene fluoride and hexafluoropropylene copolymer.

with minimal exposure to accelerated electrons. These data are evidence that electron irradiation gives a lower density film.

Polishchuk[106] investigated the structure of films deposited by electron beam evaporation of PTFE, including irradiation of the growing film with an electron beam. He established a correlation between substrate temperature and film structure. A fibrillar structure is formed at 500 K, which becomes spherulitic after annealing in a vacuum at 600 K. Exposure of the growing film to an electron beam (up to 1.5 A/m^2 in current density) induces the formation of a globular structure with spherulitic inclusions. The author presumes this to result from the low molecular weight of such films and, consequently, the high mobility of the molecular chains. At 2.5−3.5 A/m^2, a fibrillar−stack structure is formed. Annealing for 7 ks at 600 K in a vacuum reduces the crystallinity of the film. At higher current densities, crystallinity grows and molecular weight decreases. These data disagree with the results of other researchers, who observed increased cross-linking under similar conditions.

Silantiev[42] investigated the morphology of films obtained by a gas discharge electron beam gun. For condensations under 293 K, PTFE films have heterogeneities about 1−5 μm in size and appeared to be made up of lumps. PCTFE films deposited at substrate temperatures up to 350 K displayed no such structural formations and were amorphous. Films deposited at 430 K showed striations and stack structures. At condensation temperatures above 430 K, upon substrate exposure to a 3-W RF discharge, a densely packed stack structure was formed. Increasing the discharge power to 10 W expanded the stack size. Further increasing the discharge power resulted in a brittle film. It should be noted that PTFE films produced by different methods at a comparatively high pressure and 293 K are lumpy. It is possible that an initial aggregation of active particles into clusters proceeds in the gaseous phase. Kruglyak et al.[130] found that, in the case of electron beam evaporation of PE, the degree of film crystallinity declined with a decreasing rate deposition and an increasing condensation temperature. Electron beam irradiation of the films during their growth led to cross-linking.

The IR spectra of 10-μm-thick films produced by thermal evaporation were studied by Gritsenko and coauthors.[103,107,131] The IR spectra of PP and PVDF films are presented in Figures 34 and 35. The IR spectra of PE, PP, PVDF, and PCTFE films agreed well with those of the starting polymers. The degree

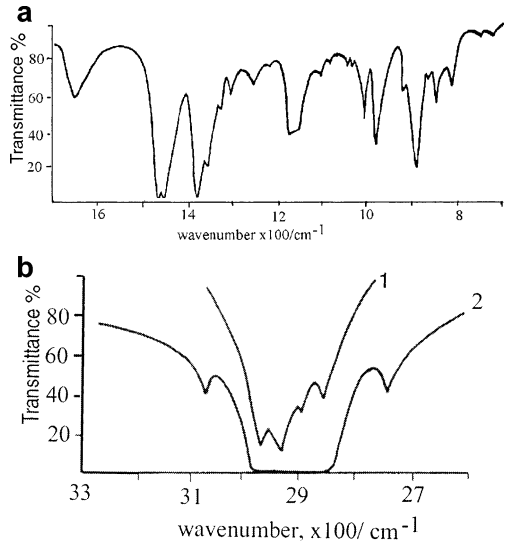

Figure 34. (a) IR spectrum of 10-μm-thick PP film, deposited by thermal evaporation. (b) IR spectrum of the same PP film in the 2700−3300 cm^{-1} region: (1) 1 μm thickness and (2) 10 μm thickness.

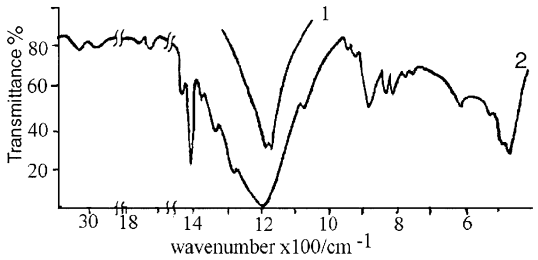

Figure 35. IR spectra of PVDF films deposited by thermal evaporation: (1) 1 μm thickness and (2) 10 μm thickness.

of PE film crystallinity was estimated at 45%. An increase in the double bond content, as well as vinyl, vinylene, and vinylidene groups, was disclosed. This suggests a great number of side chains. A similar conclusion was made for PP, PVDF, and PCTFE. The amount of isotactic PP was estimated to be 20% for films obtained by using a porous filter and 40% for those obtained by evaporating pressed powder. The degree of crystallinity in PVDF films was about 30%.

Considering that TEM examinations of all these films (that had 50-nm thickness!) showed amorphous structure (while IR spectra showed not a small amount of crystal phase), it is suggested that material is ordered and crystallized with film thickness growth due to supermolecular structure formation, as is clearly seen in SEM.

Hogarth and Iqbal[129] studied the thickness dependence of PP film structure using TEM. The line width of the diffraction patterns narrows as film thickness increases from 15 to 160 nm, both before and after annealing. Annealing gives further line width narrowing. This effect was stronger for thicker films. For a thicker film, crystallinity was greater. These results can be explained by a nonequilibrium state of thin-film material caused by the surface energy of the substrate. But a dimensional restriction for crystal growth in the perpendicular direction must be considered.

As Fritz[132] observed for layers of comparatively low-molecular-weight dyes, their structure begins to develop under a strong influence of the substrate, and as a rule, it is different there (near the substrate interface) from the bulk. The film structure tends to transform into the bulk structure at thicknesses which depend on the substrate and compound used. It can be anywhere from several monolayers up to about 100 nm.

Nagayama et al.[133] studied the orientation of low-molecular-weight PTFE films and perfluorotetracosane (PFT) by near-edge X-ray photoelectron spectroscopy (XPS) absorption. They found that PFT molecules grew in a highly oriented manner perpendicular to the substrate and were not changed in their orientation by rubbing with a cloth. PTFE molecules, on the other hand, grew parallel to the substrate and were easily oriented with their chains along the rubbing direction. The difference may result from the fact that comparatively long PTFE chains cannot be altered to their original structure after rubbing, due to the difficulties of moving larger molecules over a longer distance. The comparatively smaller chains of PFT are more easily relaxed. The stronger anchoring of chain ends to the substrate in the PFT film also must be taken into account.

A comparison of IR spectra of PCA films produced by evaporation from a boat and from a porous metal filter was reported by Khimchenko et al.[27] The IR spectrum of the film deposited from a boat showed a superposition of PCA α- and β-phase spectra. IR spectrum of the film produced using the porous filter is different. The intensity of −NH− and amide groups is considerably lower. Ether and hydroperoxide bonds appear, as well as a number of cross-links. This is explained in the latter case (porous metal filter) by the complete decomposition of PCA and film formation exclusively from the resulting molecular flow, while in the former case (boat) microdrops also play a role in film formation. The cross-links' appearance can be attributed to the participation of fragments smaller than a repeat unit in the film formation. This work shows that, during thermal evaporation of heterochain polymers, side reactions can take place which result in a significant modification to the chemical structure of the film. From the increased intensity of 735 and 703 cm^{-1} absorption bands, Silantiev[42] concluded that RF activation of the molecular flow increased crystallinity of PTFE films. But according to Painter et al.,[135] these bands should be attributed rather to the amorphous phase. We are inclined to another view: RF activation produces cross-links in the film material, preventing crystallization and thus leading to an amorphous film structure.

The IR spectra of films deposited from PTFE decomposition products under activation by both an electron impact and RF discharge are depicted in Figure 36. The main bands are attributed to bulk PTFE 15_7 spiral conformation. Bands at 780 and 630 cm^{-1} were supposed to correspond to conformation 10_3 of PTFE spiral.[134] The existence of such conformation was predicted.[135] IR spectra, density measurements, and diffraction patterns showed that the structure of the thermally deposited film is highly crystalline. An increase in electron activation current

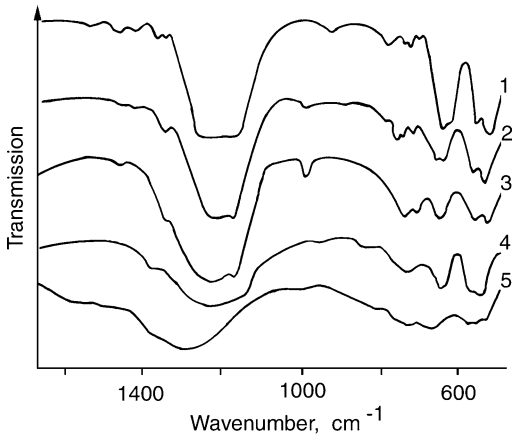

Figure 36. IR spectra of 10-μm-thick PTFE films, deposited under the following conditions: (1) thermal evaporation, (2) with activation current 10 mA, (3) with activation current 20 mA, (4) with activation current 20 mA and additional 40.68-MHz 30-W discharge, (5) with activation current 20 mA and 40.68-MHz 70-W discharge. Acceleration voltage, 3 kV.

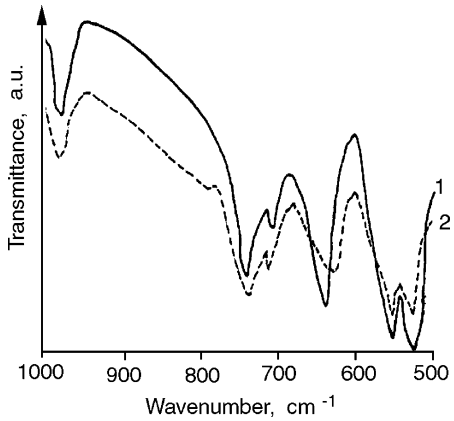

Figure 37. IR spectra of PTFE film, recorded at (1) room temperature and (2) elevated (200 °C) temperature.

makes the films amorphous and increases the content of double bonds and side branches. The mass spectrum of the degradation products of deposited PTFE film showed an increased quantity of the CF_3 and C_3F_5 fragments. This is the confirmation that the macromolecules in the film are shorter and more branched than the original ones. Figure 37 presents IR spectra of a PTFE film recorded at 200 °C. They coincide well with a reference spectrum.[135] After annealing of the amorphous films in a vacuum at 500 K for 36 ks, the IR spectrum becomes identical to that of the crystalline film. The cross-link content was estimated to be low and the macromolecular structure to be mainly linear. More extensive modification of the film structure was produced by the simultaneous action of electron impact and a 40.68-MHz discharge. A 30-W discharge leads to a widening of IR spectra bands, although in general they correlate with the bands of the bulk PTFE IR spectra. Noticeable cross-links were formed, but with preserved linear structure of macromolecules. Increasing the power to 70 W leads to a highly cross-linked, branched structure with a high double bond content. The IR spectra of films deposited with RF activation do not change upon annealing, except for a slight

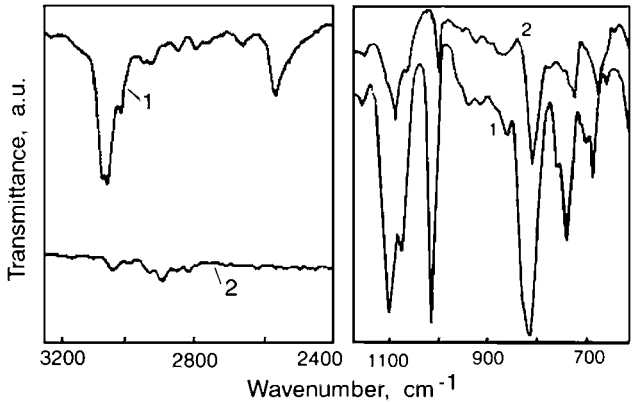

Figure 38. IR spectra of PPS films, deposited by (a) (1) thermal evaporation or laser beam evaporation and (2) thermal evaporation using Cu powder evaporator; (b) (1) thermal evaporation from a boat and (2) laser beam evaporation.

reduction of the bandwidth.[108,131] This supports the contention that films obtained without discharge are negligibly cross-linked and those with discharge activation are highly cross-linked.

Zadorozhny[136] reported the thermal and electron beam evaporation of poly(vinylcarbazole) (PVK) and poly(epoxyvinylcarbazole) (PEVK). He produced smooth films, but no other characteristics were given. Gritsenko[28] discovered that replicate cycles of CO_2 laser beam evaporation from the same PEVK target led to changes in the deposited film. At first, an almost noncondensing fraction was emitted, followed by more and more condensable molecular flow formation upon repeated laser action on the same target. The resulting film could not be considered as classic PEVK. Touihri and his coauthors[137] reported success with PVK thermal evaporation. They reported that polymer chains are significantly shorter than in the original polymer. PPS films were deposited using UV and visible laser irradiation.[138,139] These films contained many macrodrops up to 10 μm in size. Elevating the substrate temperature during deposition reduced the size of the macrodrops but increased their quantity. XRD showed that film deposited at room temperature was amorphous, while at 125 °C it was crystalline. The ESCA indicated that the film contained some side products of decomposition. Gritsenko et al.[140] evaporated PPS samples with varying thermal pretreatment by thermal and CO_2 laser beam evaporation and with additional RF activation. It was found that laser beam evaporation with RF activation of previously annealed PPS led to the formation of the best-quality film. The IR spectrum of this film is almost identical to that of the original PPS, although minor differences are present (Figure 38a,b). Films evaporated using a composite Cu powder evaporator did not contain benzene rings (Figure 38a), like that of PC. The film deposited by laser beam evaporation was clear and transparent, although AFM showed that the film contained nanosized pores. From these data, it could be concluded that PPS nanoclusters with the original chemical structure were emitted from the target, along with low-molecular-weight products of decomposition, and the film grew mainly from these clusters. The RF

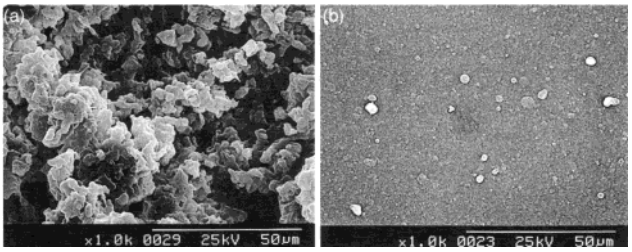

Figure 39. Surface relief of PAN film deposited by laser beam evaporation at the following wavelengths: (a) 308 and (b) 248 nm. Reprinted with permission from ref 55. Copyright 1996 Elsevier Science.

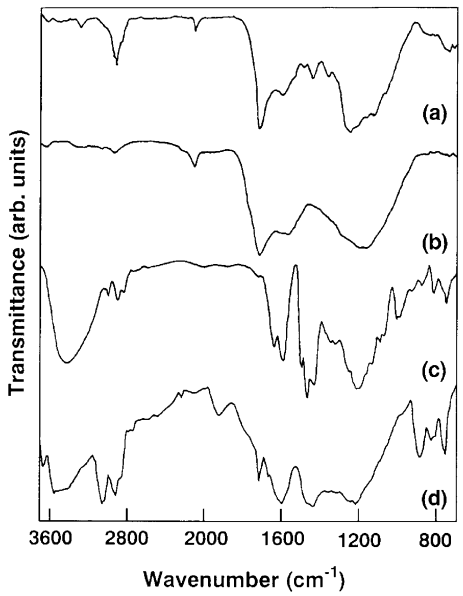

Figure 40. IR spectra of PAS: (a) film from phenol−formaldehyde resin; (b) film from pyrolytic PAS; (c) phenol−formaldehyde resin; and (d) pyrolytic PAS targets. Reprinted with permission from ref 141. Copyright 1996 Elsevier Science.

discharge activated their surface and promoted chemical links between clusters, forming the most stable films.

Das and co-workers[139] studied the influence of proton implantation into deposited PPS films. The polymer was strongly resistant to 100 keV protons up to a total dose of 10^{15} ions/cm^2. The carbon concentration was increased by 17-fold, while the sulfur concentration was significantly decreased. Nishio et al.[141−143] reported semiconductive thin-film deposition by UV pulsed laser beam evaporation of PAN and polyacenic (PAS) materials. The surface relief of the PAN films is shown in Figure 39. The films deposited using a 308-nm laser beam seem to be composed of large clusters, while those deposited using a 248-nm laser beam are comparatively smooth, although some grains up to several micrometers are still present. Their IR spectra indicate the greatest proximity in the film deposited by the 308-nm laser beam, then that deposited at 248 nm with low fluence, and that deposited at 193 nm is the most unsuitable (Figure 40). XPS data showed that all films have different compositions, but the films deposited using 248 nm at high fluence and using 193-nm irradiation both showed a lack of nitrogen. Figure 41 presents the film chemical structure variations vs laser wavelength. The deposition of PAS polymer film using a 308-nm laser beam resulted in a film that seems to be composed of microdrops up to 0.5 μm in size (Figure 42).

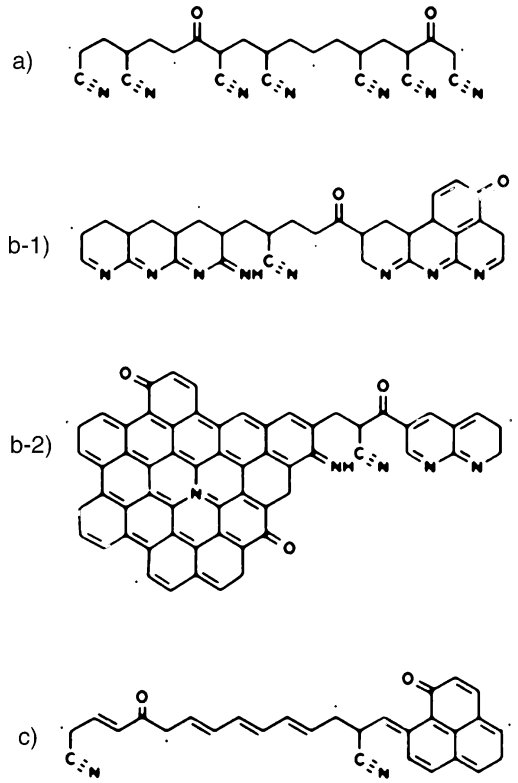

Figure 41. Chemical structure of films prepared by PAN laser beam evaporation vs laser wavelength and fluence: (a) at 308 nm with low fluence; (b) (1) at 248 nm with low fluence, and (2) at 248 nm with high fluence; (c) at 193 nm. Reprinted with permission from ref 142. Copyright 1996 American Institute of Physics.

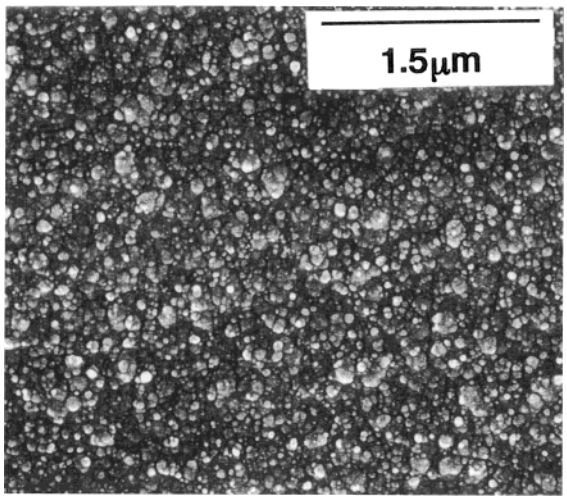

Figure 42. Surface relief of PAS film deposited by laser beam evaporation of phenol−formaldehyde resin. Reprinted with permission from ref 141. Copyright 1996 Elsevier Science.

Agabekov and co-workers[38,39] studied the structure and properties of deposited 0.1−1-μm-thick films of PCHD and cross-linked PCHD (CPCHD). As deposited, the film structure is amorphous. The mass spectra of the destruction products of the deposited film featured more intensive peaks over 200 amu

Table 8. Properties of Films Deposited at a CO_2 Laser Beam Power of 10 W

radical assistance	substrate temp, °C	deposition rate, nm/min	film properties
no	30	1570	cauliflower-like, soft
no	100	–	granular
O_2 microwave plasma	30	–	fibrillar
O_2 microwave plasma	100	23	flat, transparent, hard
H_2O microwave plasma	30	–	
H_2O microwave plasma	100	14	flat, transparent, hard

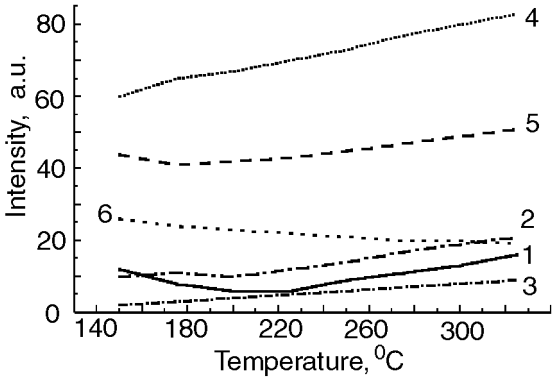

Figure 43. Concentration of degradation products of deposited CPCHD film vs temperature: (1) 18, (2) 20, (3) 44, (4) 81, (5) 105, and (6) 166 amu.

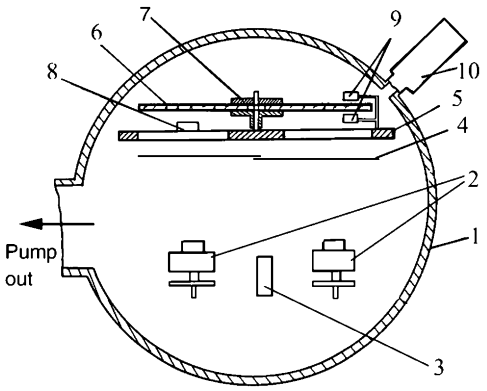

Figure 44. Cross section of chamber for thermal and combined film deposition with electron activation: (1) wall, (2) electron beam evaporators, (3) crucible heated by electric current, (4) shutter, (5) shield with windows, (6) substrate, (7) gear for substrate rotating, (8) quartz crystal (thickness), (9) transmittance and reflectance in situ, (10) mass spectrometer.

compared with the mass spectra of the original polymers (Figure 43). The authors suggest that the film was formed mainly from oligomeric decomposition products. The final film structure differs somewhat from that of the original polymer. It was found that some bands of its IR and NMR spectra can be attributed to the formation of benzene rings, moreover, conjugated up to three rings. The spin concentration in CPHD film was 10^{19}, while in the original powder it was 5×10^{17} spins/gramm. These films are soluble in organic solvents, unlike the original polymers. After exposure to UV radiation in the air, the films became insoluble, and their oxygen content increased. The authors think that the film is cross-linked under UV irradiation through photo-oxidation.

Lee and his coauthors[144] studied the deposition of very thin films of the conductive polymer PANI, prepared by the thermal evaporation of emeraldine. They conclude from high-resolution electron energy loss spectroscopy that the initial layer is made up of relatively short PANI oligomers. As film thickness builds, these oligomers react with one another to form longer polymer chains. The chemical nature of the substrate had an influence on the final degree of PANI film oxidation. Li et al.[145] deposited PANI film using a specially designed crucible. The morphology of this PANI film consisted of grains up to several micrometers in size. Gritsenko[28] deposited PANI film by laser beam evaporation. This film was a leucoemeraldine base, and also may consist of some reduced oligomers.

Fujii et al.[146] deposited polysiloxane films using CO_2 laser beam evaporation of a polysiloxane target, assisted by a remote radical source. A 2.45-GHz discharge in O_2 or H_2O supplied the radicals. At 5-W irradiation, a smooth film was deposited, while at 10 W a clustered "film" was grown at a substrate temperature of 30 °C. Raising the temperature to 100 °C gave a smooth film at 10 W. The variations of film structure vs deposition conditions are shown in Table 8.

Nakao et al. deposited poly(diacetylene) (PDA) films by the thermal evaporation of PDA with $(CH_2)_4$-$OCONHCH_2CH_3$ side groups.[147] The PDA film was grown on a PET sublayer that was previously rubbed with a cloth. The film was unidirectionally oriented with the PET sublayer.

3.3. Composite Film Deposition and Characteristics

Since the equipment and operating regimes for polymer evaporation are quite different from those used for evaporation of inorganic and low-molecular-weight organic materials, to deposit a composite film it is usually necessary to have at least two different evaporators. Our scheme for simultaneous thermal and electron beam evaporation is shown in Figure 44. This installation is equipped with two devices for crucible heating and vapor treatment by accelerated electrons (2). One boat or crucible for thermal heating (3) could be used. A tantalum boat or titanium crucible at a distance from 100 to 300 mm from the substrate was used. The following substrates (rotated and stationary) were used: glass, quartz, Si, Ge, KBr, etc. (7). Polymer film thickness was measured during growth by a quartz monitor (8). For composite films, the characteristics of the absorptive component were controlled using an optical system (9), which measured both transmission and reflectance at one chosen wavelength. An electric field to accelerate ions was imposed in some experiments. A power of 40.68 MHz up to 70 W could be applied to the gaseous products. Mass spectra were recorded by using an MX-7301 mass spectrometer (10).

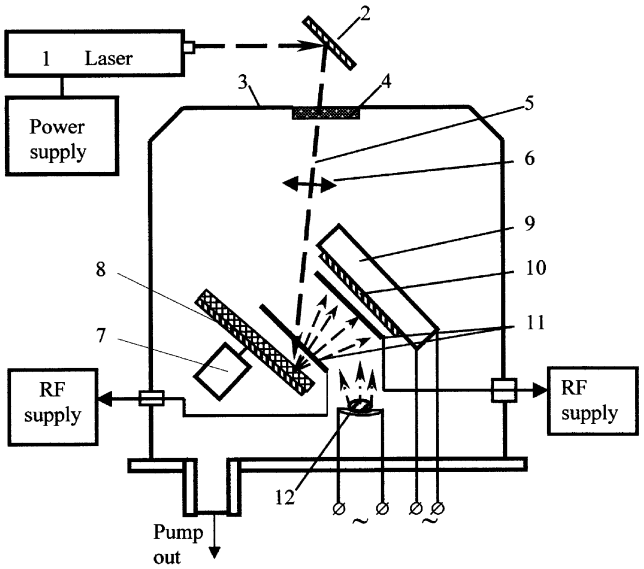

Figure 45. Scheme of deposition chamber for laser beam evaporation combined with thermal and plasma activation: (1) CO_2 laser, (2) mirror, (3) vacuum chamber, (4) KBr window, (5) laser beam, (6) spherical lens, (7) drive for target rotation, (8) target, (9) substrate holder, (10) substrate, (11) electrodes for RF discharge, (12) Ta boat.

Our installation for laser beam evaporation is presented in Figure 45. The installation was equipped with a target (8) for laser beam evaporation and a Ta boat (12) for thermal evaporation. A 40-W CO_2 laser was used (5). A spherical lens (6) was used for focusing the laser beam on the target surface. The diameter of the focused beam could be varied in the 6−10-mm range. The target, i.e., the polymer plate, was rotated at 1−10 rps. Varying the beam diameter and target rotation speed allowed us to obtain a variety of irradiation densities. The beam pulse length was modulated using a mechanical shutter. The distance between the target and substrate was 100 mm. A 40.68-MHz discharge of up to 30 W could be ignited in the chamber (11). The film thickness was measured by using a quartz crystal microbalance. For dye-filled film deposition, the dye could be spread onto a polymer or a KBr plate surface. The pressed mixture of polymer and dye powders at the desired composition also could be used as a target. The film growth rate varied up to 150 nm/s. But drops of liquid polymer can be emitted, so the parameters of the laser beam must be carefully maintained in a specific range.

Krasovsky and Belyi[112,119] established that the structure of films produced by co-deposition of metal and polymer is controlled by both the nature of the metal and the deposition conditions. The co-deposition of silver with any polymer formed a composite film with a particle size below 1 μm. Alkaline metals form homogeneous amorphous films with all polymers. PE formed composite films with Pb, Al, and Fe, whereas PCA, PTFE, and PA formed homogeneous amorphous films with these same three metals. The thermal stability of the Pb + PCA film was 200 K higher than that of PCA alone. Any aggregation of metal atoms at elevated temperature was negligible as a result of the presence of the second component, as well as by probable formation of

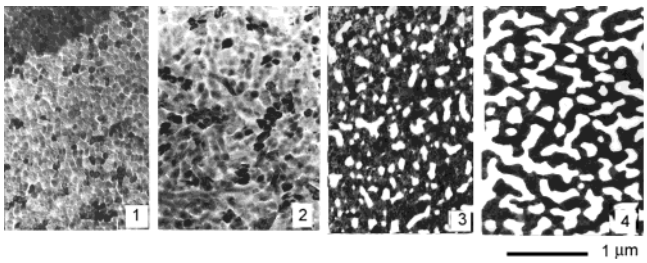

Figure 46. TEM images of Au and Te films: (1) Te on KBr, (2) Te on PTFE sublayer, (3) Au on KBr, and (4) Au on PTFE sublayer.

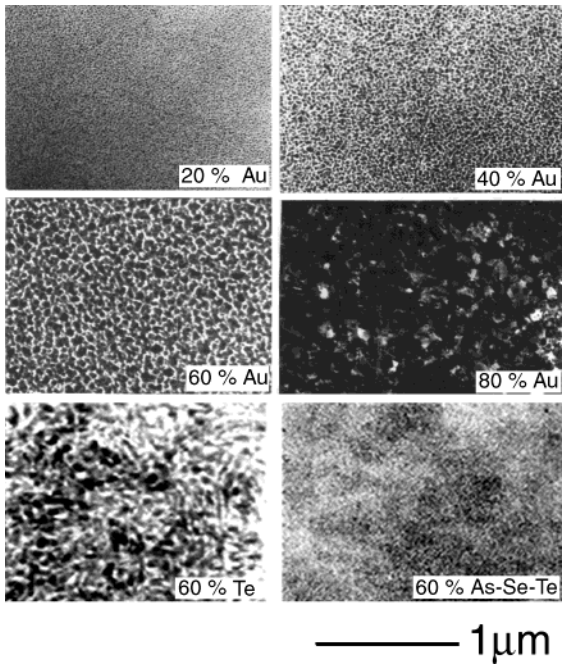

Figure 47. TEM images of Au- and Te-containing PTFE films.

chemical bonds between metal atoms and polymer. Later, Boonthanom and White[148] investigated the structure of films obtained by co-deposition of PE and PC with Cr, Al, Au, Ag, Cu, and Te. Their results correlate well with those obtained by Krasovsky.

Petrov et al.[149] studied films obtained by co-evaporation of PTFE with Au or Te. Au films deposited on KBr are more continuous than those deposited on KBr having been preliminarily coated with a 10-nm PTFE layer. The authors explain this by the influence of the low surface energy of PTFE, which sharply reduces the number of nucleation centers. Figure 46 depicts both Au and Te films on KBr and PTFE. Figure 47 shows images of Au- and Te-filled PTFE films. The size of both Au and Te particles grows as metal concentrations increase. Te crystals have some ordered orientation in the surface plane when a PTFE sublayer is used. The continuity of metal + polymer films is higher than that for pure metal ones. The authors attribute this effect to the stopping of crystallite growth due to the adsorption of PTFE particles on their faces and the increased amount of nucleation centers owing to a suppressed migration of adsorbed metal atoms. The structure of co-deposited films from these metals and PE, PCTFE, and PVDF is similar. The size of amorphous clusters of As−Se−Te alloy is smaller than the size of Te

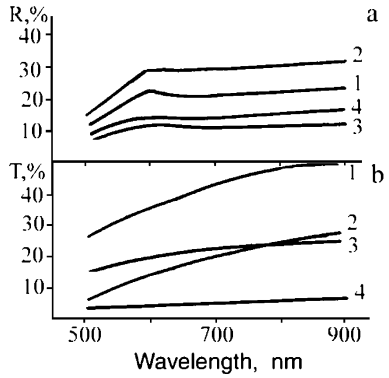

Figure 48. Optical spectra of Au-and Te-filled PTFE films: (a) reflection from substrate side; (b) transmittance. (1) 30% Te, (2) 60% Te, (3) 30% Au, and (4) 60% Au.

clusters.[107] Raman scattering spectra showed few metal−carbon bonds, so these films are two-phase composites. Figure 48 shows optical spectra of Au- and Te-filled PTFE films. The reflection peaks near 600 nm are stronger for Te-filled films. The reflection of Au-filled films from the substrate side is smaller than the reflection of Te-filled films, while reflection from the film side is more than 40% for 60% Au, and more than 20% for 30% Au films. This is evidence of nonlinear optical effects in particulate media, like those discovered for plasma-polymerized Au- and Pd-filled films.[150,151]

Films produced by laser beam evaporation of polymer pairs were investigated in earlier work.[44] Destruction products of PSF−PCTFE and PSF−PET pairs form films of a patchy structure, where each grain consists of only one polymer. When these films are heated, the grains grow in size. The PSF−PC pair is compatible only within certain compositional bounds. The IR spectra of these composite films is a superposition of the initial materials' IR spectra. A few polymer pairs formed homogeneous films over a wide range of compositions and evaporation conditions. A minor addition of a second component changes the process of structure formation in a polymer film. The annealing of a PC film at 380 K for 1.2 ks results in the growth of crystallization centers, whereas the addition of a few percent of PI evaporation products preserves the structure unchanged under the same conditions. This is the result of irregular block-copolymer formation or blocking of PC macromolecules' motion with those of PI. Homogeneous films are formed from all pairs if evaporation products are exposed to RF discharge. The film structure consists of transversely cross-linked macromolecular blocks of different components. These films neither melt nor dissolve in organic solvents.

Fujii et al.[152] deposited a PTFE film containing nanoclusters of inorganic semiconductors using both layer-by-layer and simultaneous co-evaporation by two UV lasers from two targets. A F_2 laser (157.6 nm) was used for PTFE deposition, while a KrF laser (248 nm) was used for CdTe deposition. Deposition was performed in an Ar gas medium at a pressure of 200 mTorr, which is favorable for the growth of CdTe nanoclusters. The CdTe cluster size was in the 4−7-nm range, decreasing in size as the Ar pressure decreases.

It was found that the co-deposition of dye and polymer in a vacuum can generate useful new films for nonlinear optics[153] and the optical recording of information.[154] Yang and his coauthors[153] evaporated a mixture of Teflon AF 1600 and 4-(dialkylamino)-4-nitrostilbene (DANS) powders from a single graphite crucible with a nozzle of 2−3-mm diameter. It was found that the DANS concentration in the film is about 5−10% lower than that in the source material. The film surface seems to be composed of lumps up to 1 μm in diameter. Films with a DANS concentration lower than 25% are amorphous. At higher DANS concentration, dye crystals appear in the film. XPS data showed that no covalent bonds between DANS and Teflon molecules were formed, so the film is a guest−host composite. Later, Fujii et al.[155] prepared perfluorinated cyclooxyaliphatic polymer (Cytop) doped with DANS by laser beam evaporation using the technique described in ref 152. At small DANS concentrations, the film was amorphous. With increasing DANS concentration, crystals appeared in the film distributed throughout the amorphous phase.

Gritsenko et al.[154,156−160] investigated phthalocyanine-filled polymer films, obtained either by dye co-evaporation with PTFE from dual sources or with PCTFE by a composite powder pellet. H_2Pc, VOPc, ZnPc, CoPc, and CuPc were used. TEM shows that the dye is condensed as a separate crystalline phase with a 5−30-nm particle size, dependent on dye concentration. The optical spectra of pure Pc films have a two-component Q-band structure. If the molecular planes are parallel to each other, i.e., if they form a stack, the blue component dominates. The red component is related to a less arranged structure. The spectrum of as-deposited H_2Pc + PTFE film consists of one broad peak at 610 nm, and the long-wavelength band is not resolved. The same effect was found in the case of other Pc's in polymer matrices. This is because the dye−dye interactions are stronger than the dye−polymer interaction. Pc molecules form stacks, but they are randomly oriented in the matrix and have a certain variation in size. After annealing at 473 K, there are minor direction-dependent variations in the film optical spectra, dependent also on the complexing metal. The long-wavelength band becomes more pronounced, but annealing does not change the bands in any noticeable manner. It should be noted that 1.8 ks is sufficient to complete the phase transformation of the pure VOPc film during annealing, while in a PTFE matrix the phase transformation does not finish even after 36 ks. Annealing leads to a higher order inside the dye clusters, but not to a cluster size increase. This is due to a restriction on molecular migration and on individual clusters growing larger in the PTFE matrix. Figure 49 presents optical spectra of H_2Pc + PTFE films after annealing at 200 °C for 2 h. These spectra show a gradual change as H_2Pc concentration decreases.[157,158] At a high dye concentration, the aggregates are formed. At lower dye concentration, the matrix prevents aggregation by "freezing" dye molecules at the deposition sites. So the kinetic factor results in a nonequilibrium film structure with an isolated monomer-like state of dye molecules. The

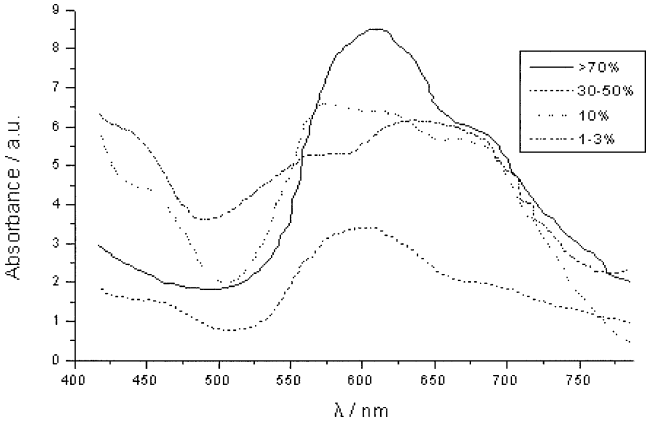

Figure 49. Optical absorption spectra of H_2Pc + PTFE films with the following H_2Pc concentrations: (1) >70%, (2) 30−50%, (3) 10−15%, (4) 1−3%. [Absorption of (3) and (4) multiplied by 3.]

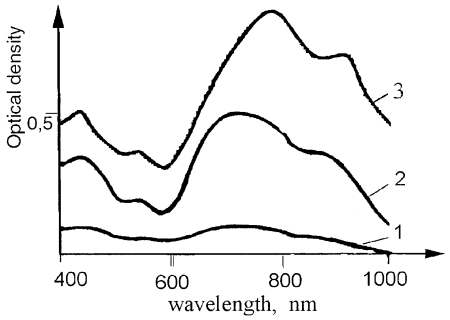

Figure 50. Optical absorption spectra of Mc + PCTFE films: (1) thickness 2000 nm, 0.2−0.5% Mc; (2) 500 nm, 25−30% Mc; (3) 300 nm of pure dye.

matrix influence is small due to its low surface energy. A 1% H_2Pc + PCTFE film, deposited by laser beam evaporation from a composite pellet, has the main band at 602 nm, which is shifted to shorter wavelength compared to that of pure dye film, but longer than for thermally deposited composite films with small H_2Pc concentration. The long-wavelength band is also not resolved. Film deposited by laser beam evaporation of PCTFE + VOPc powder contains VOPc clusters in the high-temperature crystal modification 2. RF discharge during VOPc laser beam evaporation results in the low-temperature phase 1 formation. Laser beam evaporation of a mixture of PCTFE or PS with Pc's or merocyanine (Mc) powders leads to composite film formation.[148,151] Spectra of Mc + polymer and Mc films are presented in Figure 50. The polymer matrix widens the long-wavelength maximum and shifts it to shorter wavelength. The PCTFE matrix shifts the maximum more strongly than the PS matrix. Perhaps it is due to a weaker interaction between Mc and PCTFE molecules than between Mc and PS. An especially strong effect was obtained with the spiropyran dye. The pure dye film aggregates within 1 day, while dye + polymer is still smooth after 1 year. Laser beam evaporation of composite targets of dihydroxyanthraquinone (Alizarin, Aq) and some other dyes with PCTFE, PS, etc. was performed.[157,158,161] The photoluminescence (PL) spectra of alizarin-based films are present in Figure 51. The spectrum of the pure dye film has its most intensive band in the blue region, which is characteristic for Aq. PL spectra of composite films contain also a red component. PL in this region can be assigned to contaminants with higher evaporation temperature. During thermal evaporation, contaminants remain in the evaporation source, while laser beam evaporation deposits all components of the pellet. After annealing, the dye concentration decreases, because the dye is the most volatile component of the film.

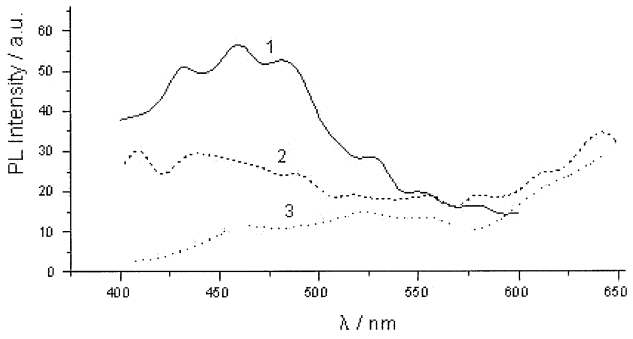

Figure 51. Photoluminescence spectra of alizarin and alizarin-filled polymer films: (1) alizarin, 100 nm thick, deposited by thermal evaporation; (2) 5 μm thick, deposited by laser beam evaporation of 1% Al + PCTFE as-deposited; and (3) annealed at 150 °C.

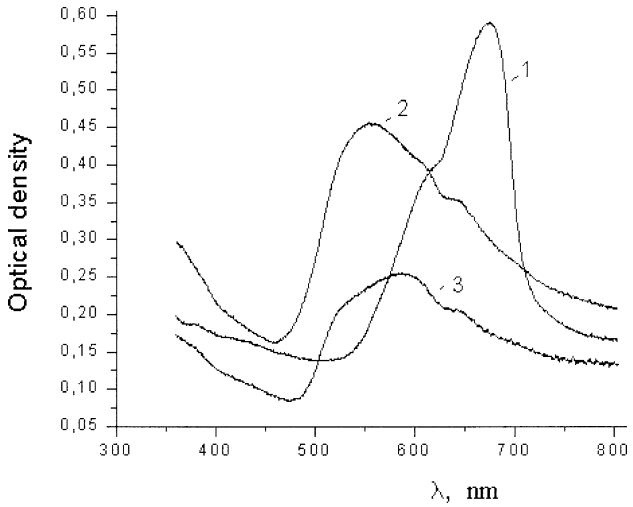

Figure 52. Absorption spectra of squarylium (Sq) and Sq-filled PCTFE films: (1) Sq film deposited by thermal evaporation; (2) Sq film deposited by laser beam evaporation; (3) Sq + PCTFE deposited by laser beam evaporation.

The thermal evaporation of squarylium (Sq) derivatives results in a film formation with a monomeric structural unit, while laser beam evaporation of the same dye results in the stack formation. RF discharge treatment of Sq vapor during laser beam evaporation resulted in a deposited film having a spectrum similar to that for thermally deposited film. Laser beam evaporation of a Sq + PCTFE powder mixture led to a film formation with its band maximum at a position intermediate between those of films deposited by thermal evaporation and laser beam evaporation.[161] These film spectra are shown in Figure 52. Thus, laser beam evaporation promotes cluster formation, while RF discharge and dilution in a polymer matrix works in the opposite direction.

Poctennyi and Misevich produced composite films by laser beam evaporation of mixtures of CuPc and

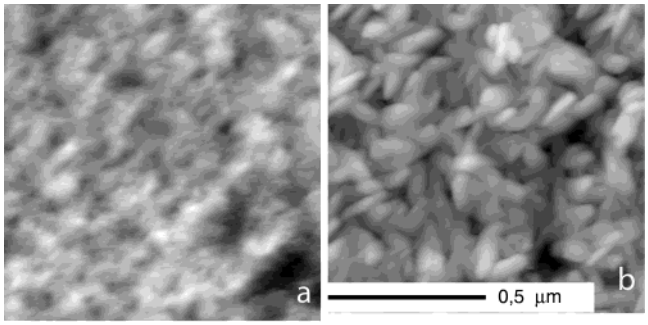

Figure 53. Surface relief of PS film filled with CuPc (a) as-deposited by CO_2 laser beam evaporation and (b) annealed. Scan size 165 × 165 nm. Reprinted from ref 215 with permission from the author.

PS powders.[162−165] Film thicknesses ranged from 100 to 1000 nm. The IR spectra of deposited PS films agree well with those of the original polymer. But after annealing, the intensity of the IR spectrum peaks decreases significantly. The authors attributed this effect to a partial evaporation of film material, which is due to a lower mass of the deposited film than that of the original polymer. The as-deposited PS film has a surface roughness of about 0.18 nm, while the CuPc film consists of crystallites ranging from 40 to 70 nm in size. The grain boundaries in as-deposited PS films containing 20% CuPc cannot be detected by AFM. Annealed at 200 °C, these 100-nm-thick films revealed irregularly oriented needle-like crystallites, typical for Pc's. AFM images of CuPc + PS films are shown in Figure 53. The authors explain that this is due to the presence of Pc crystallites on the film surface only. So the PS matrix allows aggregation and recrystallization instead of the PTFE matrix. The thin composite film (10 nm) was not recrystallized. The influence of different types of substrates on the recrystallization process was also mentioned.

The deposition of PANI with tetracyanoquinonedimethane (TCNQ) from a single crucible using a powder mixture reduced the grain size almost 10-fold.[145] The TCNQ concentration in the film was lower than that in the source. In some cases, a "seahorse"-like structure was formed in the composite film. An IR spectrum of the composite film revealed a new absorption band at 2179 cm^{-1}, which was assigned to the formation of a charge-transfer complex.

In summary, processes of film growth from polymer degradation products have features in common with those from inorganic vapor. They are based on physicochemical specifics of polymers:

(i) close values of chemical bond energies and the condensation energies of molecular fragments;
(ii) high potential of chemical activity, concentrated at distinct places within the molecular chain;
(iii) molecular chain flexibility which allows high mobility of chain ends with small displacements of the macromolecule center; and
(iv) comparatively long characteristic times of deposition processes that determine growth kinetics and the nonequilibrium thermodynamic state of the condensate.

These peculiarities determine the properties of deposits and provide us with the possibility of controlling them by varying the deposition conditions. During a composite film deposition, processes for the growth of both components are taking place simultaneously. The following peculiarities should be taken into special account:[166]

1. The high energy of condensing metal atoms can promote desorption of organic molecules.
2. The sticking probability of each compound can be different, so the film composition is not equal to that in the gas phase.
3. Growing particles of each phase prevent the growth of particles of the second phase.
4. Metal atoms and dye molecules can react with active organic fragments both in the gas phase and in the growing film. As a result, new chemical species are formed that can be useful or not.
5. In any multicomponent film, the physical interactions between molecules (atoms) of compounds exist. The relative importance of these interactions is responsible for the ultimate film structure, e.g., whether it is a one-phase solid solution or a composite two-phase material. But for large unsymmetrical organic molecules, it can mean the formation of other aggregation states or crystal structures.

A scheme generalizing all processes that take place during film deposition is presented in Figure 54.[166] Division of the all processes into physical and chemical processes was made for better understanding, but really there is no clear border between them. A comparison of thermal, laser, and electron beam evaporation methods from a technological viewpoint is presented in Table 9.

3.4. Conclusions

The processes that take place during polymer film or composite growth are rather complex and interrelated. An understanding of these processes presents us with the possibility of controlling deposited film structure and properties.

The introduction of a dye or metal into polymer matrices by co-deposition often results in nanocluster formation. Such nanoclusters exhibit unusual optical and electronic properties, while the polymer matrix provides the deposits with superior stability. Incorporation of delicate organic molecules into a polymer matrix by co-evaporation seems rather promising, while a plasma polymerization technique is not acceptable because it not only activates the monomer but also causes dye molecule degradation. Incorporating specially designed dye molecules which have a double bonds at the end into the polymerization process during polymer film growth is rather difficult, but it is a promising method for the stabilization of the film's optical and electronic properties. It can be predicted that further research will be focused on functional films with complex chemical and physical structures.

4. Properties of Thin Polymer Films

4.1. Film Strength and Adhesion

The strengths of adhesion of PCTFE, PC, PSF, P(TFE-E), and P(CTFE-E) films, deposited by laser

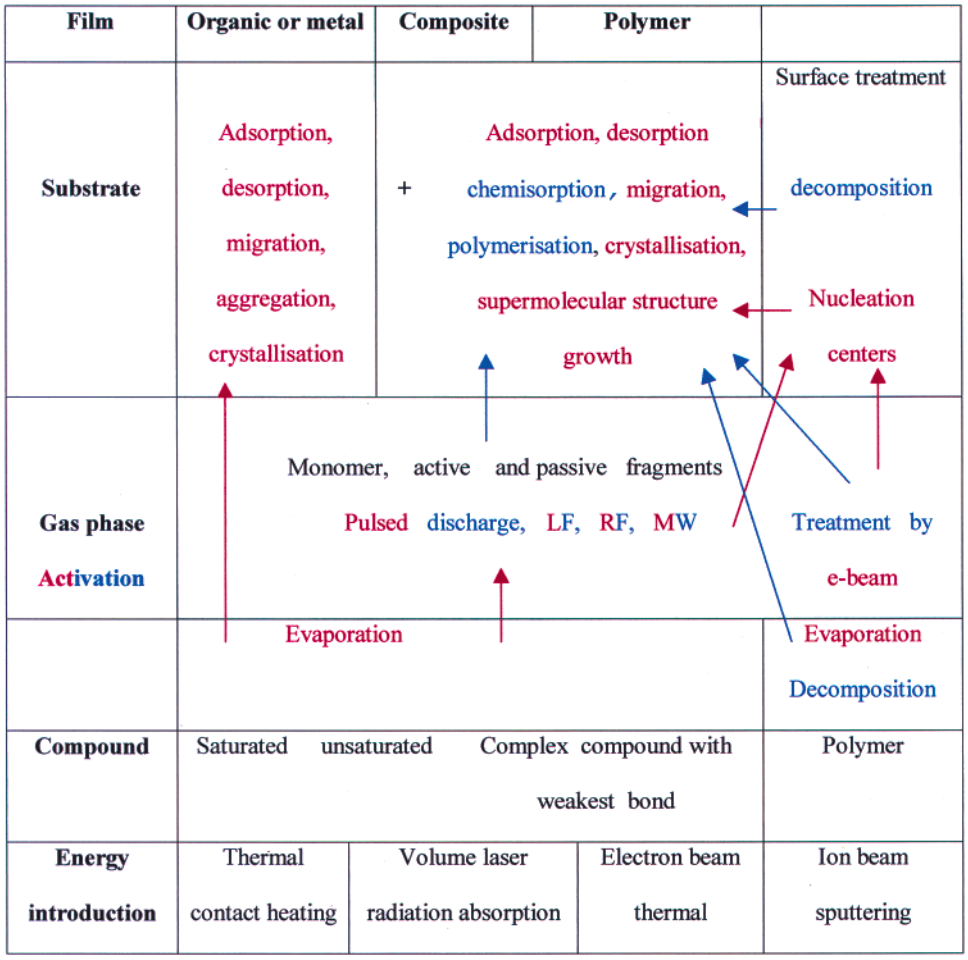

Figure 54. General scheme of processes taking place during film deposition. Red, physical processes; blue, chemical processes.

Table 9. Comparison of Polymer Film Deposition by Thermal, Laser, and Electron Beam Evaporation

	method		
	thermal evaporation	laser beam evaporation	electron beam evaporation
high evaporation rate	− evaporation rate is limited by heat supply from crucible to organic solid, which is limited by low thermal conductivity of organic matter	+ energy supply is directed to surface layers of solid; limited by free surface of evaporated material	+ electron beam is not applicable for polymer evaporation with few exceptions, because accelerated electrons decompose monomer also
fast control of evaporation rate	− limited by thermal inertion of crucible	+ limited by laser beam control mechanism	+ limited by electron beam control mechanism
co-evaportation of two or more materials	+	+ high-speed jumps from one evaporator to another	+ high-speed jumps from one evaporator to another
evaporation at high pressure with activation by plasma	+	+	− electrical breakthrough

beam evaporation, to their Al, Cu, Ti, and glass substrates was measured using a shear method and turned out to be higher than the films' cohesive strengths.[12] This was, in a sense, preordained by the films' generally low molecular weight and, consequently, their relatively low strength. Fluoropolymer films deposited on glass (heated to 370−450 K) by laser beam evaporation exhibited adhesive failure. Films 1−10 μm thick, produced by PTFE electron beam evaporation[33] on glass, Cu, and Ti substrates, failed similarly. Thinner coatings failed in a cohesive or an intermediate mode.

The dependence of failure mode on film thickness and substrate temperature is a window to the role of internal film stress. The material of most films deposited under typical conditions is in a highly plastic, low-modulus condition. Thus, the relaxation of internal film stress can occur at a stress level lower than the adhesive strength. Thicker films or films deposited at elevated temperature possess higher

modulus and can support higher internal stress. Films deposited by PTFE and PCTFE electron beam evaporation at a rate of 50 nm/s exhibit poor strength,[12] owing to the film's low molecular weight. Films 5 μm thick, produced by PCTFE electron beam evaporation on steel, achieved maximum adhesion when the substrates were annealed at 873 K and glow discharge treated prior to the deposition. Decontamination of the surface played the major role in improving adhesion. The increase in the film's molecular weight, as well as the presence of a larger number of chemical bonds between the film and the substrate, need also to be considered.

Krasovsky[167,168] studied the strength of films he obtained by thermal evaporation. The strength was estimated from the load at which an indenter punctures the film, making an electrical contact with the conducting substrate. With the indenter used, it was established that a 1−5-μm-thick film withstands up to 2 GPa of static load. This is due to plastic yield in the material under the indenter point, which produces a rim of displaced material. As the indenter approaches the substrate surface, the yield resistance in the narrowing gap rises. Films deposited by laser beam evaporation of PCTFE with RF discharge were twice as strong as those deposited without such activation.[44] This is attributable to the larger number of chemical bonds with the substrate, as well as cross-linking within the film.

It has been established[106] by the normal break-off method that the adhesion of PE films deposited by electron beam evaporation on glass or metal substrates exceeds 6 MN/m^2. Kabaev et al.[122,123] have shown that PE film adhesion to a PET substrate is higher than that of PET to a PE substrate. Gritsenko[107] measured the adhesion of 20−300-nm-thick films deposited on glass with activation by accelerated electrons using the method of normal break-off and found that the results depend on the nature of the material: for PE, PP, and PVDF, 0.5 MN/m^2; for PCA, 0.7 MN/m^2; for PTFE, more than 1 MN/m^2. PE and PP film adhesion is governed by hydrogen and dipolar bonds, while for PCA and PTFE films few chemical bonds with the substrate are formed. Using an RF discharge during deposition brings PTFE film adhesion as high as 5 MN/m^2. Pisanova et al.[169] found that a PTFE interlayer affects the adhesion of a glass fiber to a PC matrix considerably. Adhesion strength rises with interlayer thickness, maximizing at 80−100 nm. A thicker interlayer still reduces this adhesion to the characteristic shear strength of bulk PTFE. We can conclude that it is possible to vary film adhesion and strength considerably by changing the substrate temperature as well as the method of activation.

4.2. Frictional Properties

Controlling the slipperiness of plastic-coated surfaces has much practical importance, and has spurred on tribological investigations. Frictional characteristics of films obtained by PCA thermal evaporation have been described in refs 170 and 171. The test regime was as follows: test chamber pressure, 6.5 mPa; frictional pair configuration, 3-mm-diameter disk-on-sphere; indenter load, 1 N; and sliding velocity, 2 m/s. A 3−5-μm-thick film on steel had a 0.01−0.18 coefficient of friction (COF) over a time span of 3.6−10.6 ks (Figure 55). The uncoated sample seizes up at 0.3−0.6 ks into the run. The distance of the run is about 1 km, and the steady service friction path is about 5 km. Beginning with the sixth kilometer, COF increases, indicating film failure. Wear probably starts on the roughness peaks. The COF of film deposited by PCTFE laser beam evaporation onto an Al alloy was investigated in ref 12. The coated disk substrate was rotated at a linear velocity of 7−15 m/s in contact with a 3-mm-diameter steel ball, normally loaded at 0.15 N. The COF dependence on film thickness is similar to that of many other thin coatings, and in particular PTFE.[171] Its peculiarity is that COF grows as thickness decreases below 1 μm.[12,171] This was explained by a 2−3-fold increase in shear resistance in the thin interfacial layer over the bulk material. The bare tops of the steel substrate microasperities play a significant role, as do changes in polymer structure in the boundary layer.

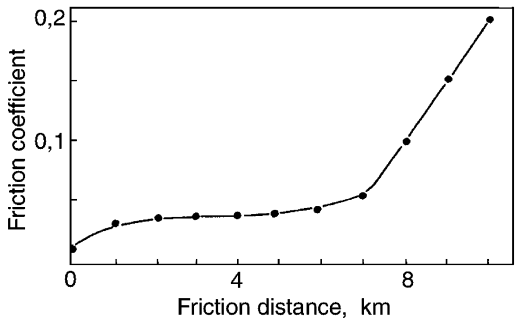

Figure 55. Dependence of friction coefficient of PCA film upon distance.

The COF values for films obtained by RF-activated laser beam evaporation of PCTFE, PC, and PI are lower than those for films without activation.[44] An explanation was not given, but the correlation between the COF data and the surface properties of the films, in particular the water contact angle, should be noted. The COFs measured in this work are some 1.5−2-fold higher than reference data for the original polymers. They are also 1.5−2 times higher than reference data on glass and commercial PI film. Hence, the differences in COF might be attributed to different test conditions. It should be noted, however, that the COF for films obtained by evaporation without activation corresponds to that of the original polymers.

Rogachev and his coauthors[171] estimated theoretically the contribution of adhesion to thin-film friction and found it to be very significant. Experimental COF data for thin films correlate with their water contact angles. The above experimental data, including those of Kamiljanov,[172] confirm that frictional data are as much dependent on test conditions as dielectric data.

4.3. Surface and Protective Properties

Surface properties of solids, which are the outward manifestations of the chemical structure of their surface layers, can be probed by specific free surface energy measurements. The surface properties of thin

polymer films, especially those of the first molecular layers involved in adhesive interaction, are different because the structures of these films can differ significantly from the structure of the bulk.[173] The surface characterizing water contact angle for films deposited by laser beam evaporation depends little on formation conditions, excluding of course activation by glow discharge.[44] The surface energy of the thinnest films depends on the substrate material, for certain atomic groups can have an ordered orientation near the surface. The effect of CF_3 end group orientation on free surface energy in PTFE was studied in earlier work.[174] These researchers found that the surface energy is much lower in cases where polymer chains are oriented normal to the surface, rather than parallel to it. Discharge activation of evaporated products has a considerable influence on surface properties. Though deposition from the activated molecular flow led to the formation of more polar films, the water contact angle increased.[44,175] This might be connected with the formation of oriented texture under the action of an electric field.

Protective properties depend on film continuity. Porosity can be examined by using optical or electron microscopy, as well as by exposure to substances which react in some noticeable fashion with substrate material: acids, alkalis, etc. It can also be evaluated by considering the electric conductance between a drop of electrolyte on the polymer coating surface and the underlying metal substrate. Defects within the films (pores, cracks) can exist or be formed by a variety of reasons: aggregation of macromolecular fragments and macromolecules themselves during condensation, internal stresses, particles of dust on the substrate surface, polymer melt drops, etc. Surface roughness affects film quality in cases where the deposition system has a molecular flow pattern which is unable to penetrate into a "geometrical shadow". When a sharp substrate asperity exceeds the film thickness, continuity at its peak is often inadequate. Treating substrates with surfactants or glow discharge noticeably reduces this type of film porosity. It has been noted[33] that the size of pores within films obtained by polymer evaporation is usually less than 1 μm, and their abundance is usually in the range of 10^4-10^7 m^{-2}. As the temperature of film deposition approaches 423 K, the porosity is reduced, but at higher temperatures it increases for PCTFE and is reduced further for PTFE. Protective properties of films were tested in aggressive solutions and vapors.[33,44,176] They were evaluated from the corrosion rates of a metal coated with a polymer film. This corrosion rate was estimated from electrical resistance. The onset of substrate corrosion in sulfur dioxide is observed after 126 and 259 ks of exposure for 5- and 10-μm PCTFE films, respectively. PTFE films 1 and 10 μm thick, deposited by electron beam evaporation, were stable under similar conditions for 36 and 162 ks, respectively.[171] The protective properties of films produced by laser beam evaporation of PC and PSF were evaluated in a 30% solution of sodium hydroxide.[44] Etching of the Al sublayer begins when the alkaline solution penetrates into micropores and progresses due to a wedging effect of the solution. An Al film covered with a 6-μm PSF film corroded in 30 ks. Protection of photovoltaic cells by electron beam evaporation of PTFE was also studied recently.[177]

4.4. Electro-physical Properties

Most early thin polymer film dielectric measurements borrowed methods developed for thicker films. As a result, some of the published data are inaccurate. Tolstopyatov[178,179] analyzed these errors by studying the passage of alternating current through a metal−dielectric−metal system. The main error was shown to arise from the relatively large distributed resistance of the thin-film capacitor plate, which particularly affected dielectric loss tangent results. This error grows with frequency and as the thickness of either the polymer film or the plate is reduced. Another source of error is any modification of the polymer surface which can occur during the vacuum deposition of the upper metal electrode. The high temperature of metal vapor can cause a partial degradation of the polymer surface. The effect of this modified layer on dielectric results depends on its relative thickness. One additional procedural peculiarity should be considered when determining the temperature dependence of the dielectric properties. Due to the considerable difference in coefficients of thermal expansion of metal and polymer, the thin metal electrode may crack as a result of thermal cycling stresses. When this happens, its resistivity rises abruptly, affecting loss tangent results.

For direct current measurements, the surface capacity of the thin-film capacitor needs to be taken into account, not neglected as with thicker specimens. This is especially important if the capacitor is fed by a current source having a high internal resistance. The use of a high-resistance bridge for determining volume resistivity of submicrometer films requires hundreds to thousands of seconds for attaining readings. Thus, the use of such a method is unacceptable. Devices that are fed from a voltage source are better. The time constant of measurements is to be estimated as well. A number of publications do not contain information on whether the above-noted procedural conditions have been adopted. This fact has hampered our analysis of results obtained by all investigators. The determination of thin-film dielectric strength has difficulties arising from the properties of deposited electrodes and the presence of pores. Through-film pores short-circuit electrodes, and blind pores reduce the effective thickness of the film, raising its apparent resistivity.

Current−voltage characteristics of films produced by laser beam evaporation of PCTFE, PC, and PSF[12] and thermal decomposition of PCA[167] are presented in Figures 56 and 57. The plots generally have three zones: a linear zone of high differential resistance at low voltage, a linear zone of low differential resistance at high voltage, and an intermediate transitional zone. The film material plays some role, although anomalous results seem to come from the sandwich system as a whole. The alternating current dielectric characteristics of PTFE and PCTFE films produced by electron beam evaporation were studied

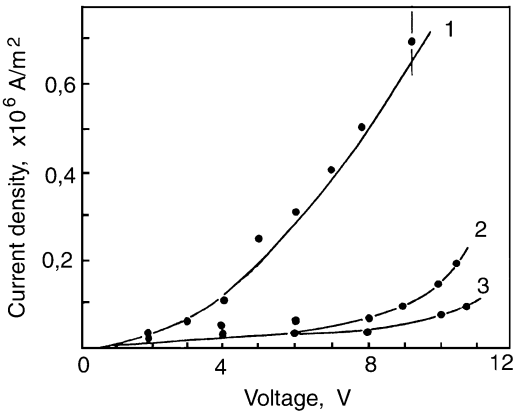

Figure 56. Volt−ampere characteristics of films deposited by laser beam evaporation of (1) PCTFE, (2) PC, and (3) PSF.

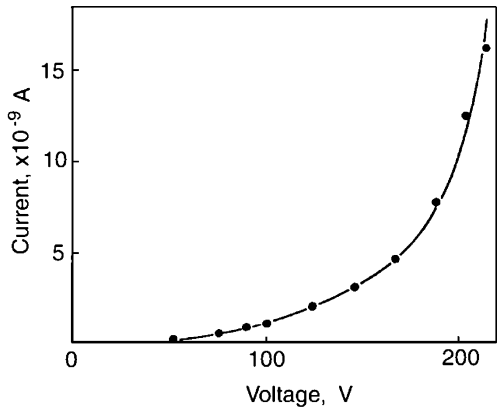

Figure 57. Volt−ampere characteristics of film deposited by thermal decomposition of PCA.

by Zadorozhny et al.[180−182] as a function of temperature (Figure 58). The authors[180] explain the improvement of dielectric properties, which approach those of the initial polymer at higher deposition temperature, by increasing molecular weight and reduced defect density. These results are unique but inexplicable. Films produced by PCTFE electron beam evaporation are characterized by a monotonic growth in dielectric permittivity with temperature, with a positive temperature coefficient of capacitance (TCC) of $+0.65 \times 10^{-3}$ K^{-1}. For the film obtained by laser beam evaporation of the same polymer, dielectric permittivity growth proceeds up to 350−360 K (Figure 59) at a TCC of $+10^{-3}$ K^{-1}. But at higher temperatures it declines, with a TCC of -1.2×10^{-3} K^{-1}. The cause of the permittivity increase was not explained. The apparent decrease in ϵ above 360 K was caused by thermal expansion of the film. Tolstopyatov[178,179] drew attention to the congruence of the maxima of $\epsilon(T)$ and tg $\delta(T)$, suggesting a phase transition. Zadorozhny and Polishchuk[180] observed a linear decline in dielectric permittivity with temperature from 285 to 500 K at a TCC of -3.6×10^{-4} K^{-1} on films obtained by electron beam evaporation of PTFE. This is close to the values obtained for a PTFE film deposited using electron beam evaporation by de Wilde[126] for temperatures from 240 to 330 K. The TCC below t_g was 3.8×10^{-4} K^{-1}; above this temperature it was 10.8×10^{-4} K^{-1}. Permittivity varied from

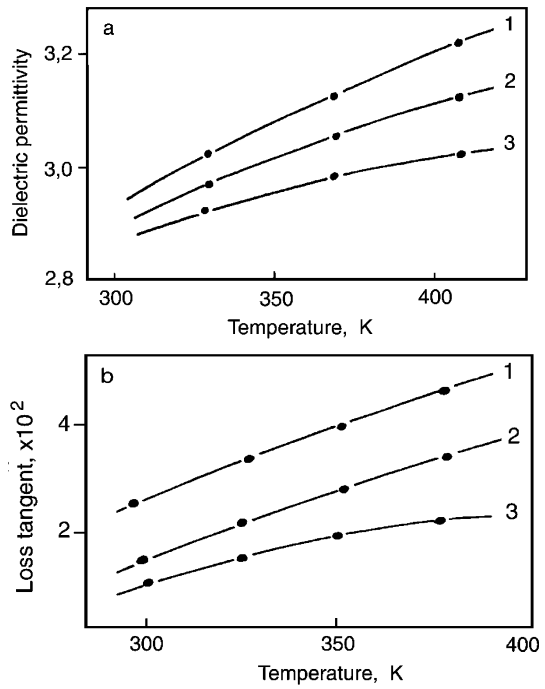

Figure 58. (a) Dielectric permittivity and (b) loss tangent vs temperature of film deposited by electron beam evaporation of PCTFE under the following substrate temperatures: (1) 313, (2) 373, and (3) 433 K.

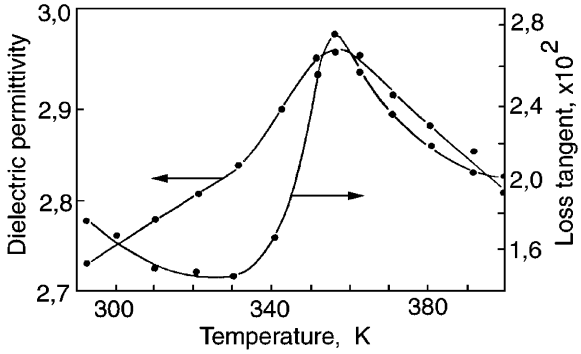

Figure 59. Dielectric permittivity and loss tangent vs temperature of films deposited by laser beam evaporation of PCTFE.

2 to 2.9, and the loss tangent varied from 0.22 to 0.62. The tg δ decreased after 1 day of storage to a few tenths of a percent. The author proposed further polymerization, which would be expected to improve structural order in the film. The resistivity of the film was estimated to be 2×10^{15} Ω-cm. The breakdown strength was 2×10^6 V/cm. Further studies of dielectric properties at various frequencies led to the conclusion that mobile ions were largely absent from the PTFE film. Zadorozhny and Polishchuk[180,181] investigated the substrate temperature effect on dielectric characteristics of films. The temperature dependence of the dielectric loss tangent of films deposited by electron beam evaporation of PTFE is presented in Figure 60. The films had better characteristics than commercial PTFE films. The authors did not give an explanation, but we consider that the reason is the above-mentioned procedural errors. All dielectric properties are improved considerably if the condensation temperature is increased from 300 to

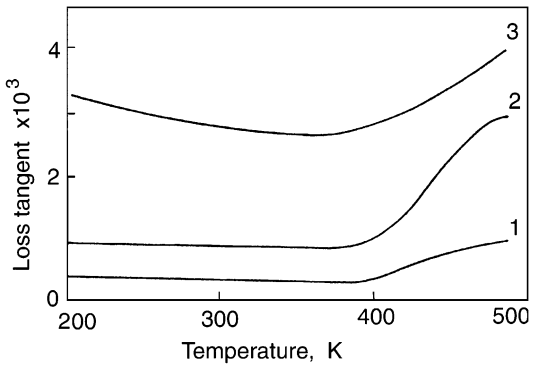

Figure 60. Loss tangent vs temperature of film deposited by electron beam evaporation of PTFE: (1) with substrate temperature 513 K and electron beam irradiation with density 2 A/m^2; (2) with substrate temperature 513 K; (3) commercial film.

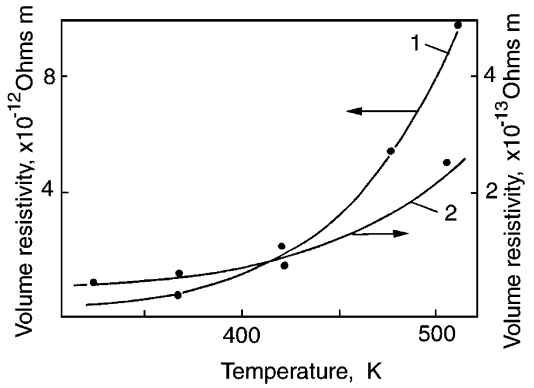

Figure 61. Volume resistivity vs condensation temperature of films deposited by electron beam evaporation of (1) PTFE and (2) PCTFE.

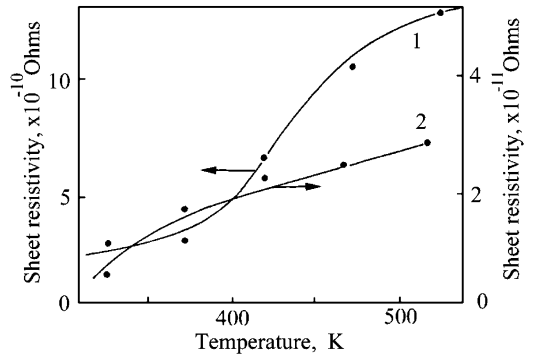

Figure 62. Sheet resistivity vs condensation temperature of films deposited by electron beam evaporation of (1) PTFE and (2) PCTFE.

500 K (Figures 61−63). This effect was attributed to increasing molecular weight and a decrease of defect concentration. Kruglyak and his coauthors[182] studied the temperature dependence of ϵ and tg δ of films produced by electron beam evaporation and thermal evaporation of PE. A positive TCC was observed over the 253−473 K range. The highest tg δ of (2−3) $\times$ 10^{-3} was achieved at a low temperature. Hogarth and Iqbal[129] found that annealing at 100 °C in a vacuum over 30 min led to an increase of the PP film resistivity from 3.4 $\times$ 10^{12} to 1.2 $\times$ 10^{13} Ω-cm. They attributed this to PP agglomeration. The permittivity was 1.75 and 1.81 before and after annealing, respectively.

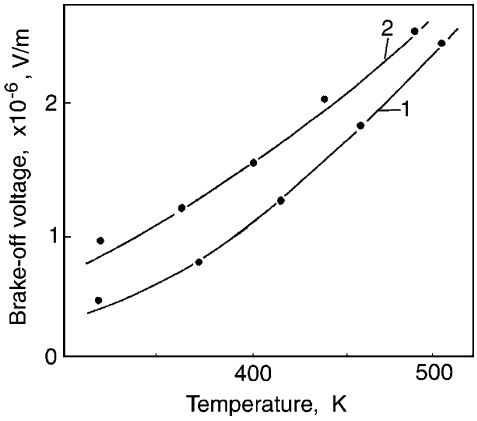

Figure 63. Breakdown voltage vs condensation temperature of films deposited by electron beam evaporation of (1) PTFE and (2) PCTFE.

The influence of film surface activation by electron irradiation on the dielectric characteristics was studied by several researchers. Polishchuk[106] found an optimum electron current density and electron energy under which PTFE films have perfect dielectric properties. Kruglyak et al.[182] found that electron irradiation of PE film during its growth raised its tg δ from (1−4) $\times$ 10^{-4} to 10^{-3}. On the other hand, in another paper[183] it was asserted that discharge activation of PTFE decomposition products improves film characteristics. This is a result which has no reliable explanation, since discharge activation increases the film polarity. Plasma activation increased the dielectric constant of films deposited by laser beam evaporation[44,179] (Table 10). Zadorozhny and Polishchuk[180] did not observe any changes in PTFE film dielectric permittivity when they used electron irradiation during the growth of the film. Tolstopyatov[44] established that RF activation of PC and PhN vapors during laser beam evaporation gave an improvement in the tg δ and dielectric strength. The activation probably caused a shift of relaxation loss peaks on the frequency scale. Therefore, the observed value of tg δ at a fixed frequency can be either higher or lower than that of films prepared without activation: it increases in PC, PhN, and PE films and is reduced in P(TFE-E) film. Figure 64 presents the frequency dependence of dielectric permittivity and the tg δ of films obtained by laser beam evaporation of PCTFE, PC, and PSF.[179,184] Dielectric permittivity monotonically declines over all frequencies. There are regions of positive and negative curvature on the tg δ vs frequency diagrams. This confirms the existence of different relaxation processes.

We can conclude that both types of activation under optimum conditions improve the dielectric strength of films. The tg δ improves for polar polymers. The tg δ is rarely less than 10^{-3}, because values near 10^{-4} are limited to nonpolar materials, whereas electron irradiation causes destruction and cross-linking of molecules, which results in an increase of their polarity. A mechanism for the positive effect of irradiation probably lies in removal of low-molecular-weight impurities. Thus, the use of electron irradiation or discharge treatment on nonpolar polymers (PE, PTFE) permits us to reach tg δ below 1 $\times$ 10^{-3} only if deposition conditions are optimal. The mech-

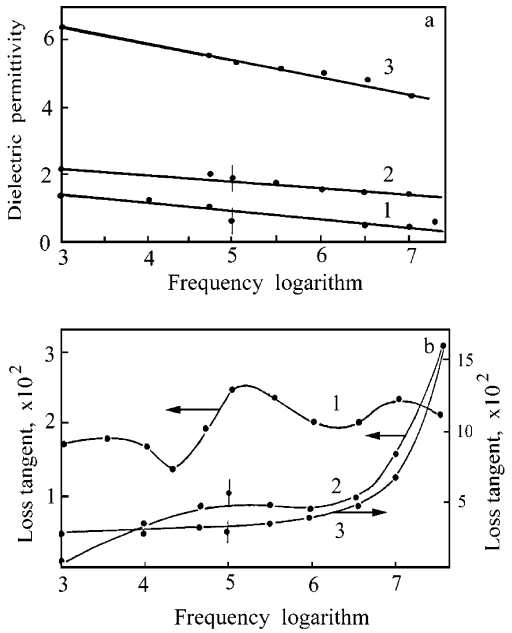

Figure 64. (a) Dielectric permittivity and (b) loss tangent as a function of frequency of films deposited by laser beam evaporation of (1) PCTFE, (2) PC, and (3) PSF.

anism for improvement in the tg δ of polar polymer films (PhN, PCTFE) is assumed to be the tying up of polar groups by cross-links. As a result, the tg δ of films deposited with activation from a variety of polymers ranged narrowly ($(1-3) \times 10^{-3}$), being nearly independent of the original polymer.

Table 10 summarizes electrical property data on a variety of films and sources. It indicates the scatter in the results, which is partly due to differing test conditions and procedural errors, and partly due to the unstable state of the films (i.e., aging). The dielectric permittivity of the PSF film is unusually low. Tolstopyatov[44] attributed this to a very loose film structure. The dielectric properties of films deposited by laser beam evaporation are unusually dependent on their thicknesses. Comparing results obtained with sprayed and plated (a drop of liquid Ga) electrodes leads us to presume that the main source of variation in dielectric properties may be surface layer doping with metal. The doped layer differs in characteristics, so the properties of the entire sandwich system are dependent on its relative thickness. Thicker films possess higher values of ϵ and tg δ. The dielectric strengths vary over a wide range. A high value of breakdown voltage of about 880 MV/m was recorded for films obtained by laser beam evaporation of PC with activation, while the values for PTFE and PCTFE were as low as 0.5 and 1 MV/m, respectively. It is interesting to note that a film obtained by RF sputtering was in an electret state.[185] As a result of free charge accumulation and the polarization of the film during deposition, a field of over 10 MV/m was formed, and the potential difference across the film reached tens of volts. PTFE films of $2-20$ μm were poled into electrets in air by a corona discharge. The electret produced initially had an effective charge density of $3-4$ mC/m^2. Upon ambient storage over 1.5 years, that was reduced to $0.2-0.3$ mC/m^2.

From the above, it follows that films can be divided into two groups on the basis of their dielectric properties. The first group includes films obtained from polymers of modest reputation in electrical applications. These essentially preserve their original dielectric properties. The second group contains films from high-quality, high-frequency dielectrics, whose characteristics are worse than those of their starting polymer. Activation of either the molecular flow region or the condensation surface with accelerated electrons or electrical discharge brings the properties of the two groups closer.

The room-temperature resistivities measured in a vacuum were respectively 10^{10}, 10^7, and 10^5 Ω·cm for PAN films annealed at 400, 450, and 500 °C, respectively.[120] Activation energies for the conducting and absorption edges were 0.4 and 1.4 eV, respectively, for films annealed at 500 °C. Conductivity was considered to be caused by carriers originating from impurities, or by carriers hopping between adjacent conjugated bonds. The PANI + TCNQ film was conductive, while the pure PANI film proved to be an insulator.[145]

4.5. Luminescent Properties of Polymer Films

PPP films, deposited by thermal evaporation, were evaluated for use in electroluminescent (EL) devices.[186−189] Kobayashi and Haga[186] studied the optical absorption, photoluminescence (PL), electrical, and EL properties of multilayer systems using PPP as a hole transport layer and 8-hydroxyquinoline aluminum (Alq_3) as the electron-transporting layer. Current increases nonlinearly with voltage. EL onset voltage decreases and luminance intensity increases in thinner PPP layers. Figure 65 shows luminescence intensity vs current density at various PPP and Alq_3 film thicknesses. Figure 66 shows luminance−distance characteristics of EL systems at optimal layer thicknesses. The optimum thickness of a PPP layer was 30 nm. The luminance decreases as the PPP layer withdraws from the indium−tin oxide (ITO) electrode. Figure 67 shows the variation of luminance−current density as substrate temperature is varied during the PPP deposition. Maximum luminance is achieved at a substrate temperature of 100−150 °C. The authors attributed this effect to the differing structures of PPP films produced. At low substrate temperature the film was amorphous, while above 100 °C it was crystalline. The degree of polymerization is expected to be higher at elevated temperature. Intermolecular interactions increase and traps decrease, both of which are favorable to carrier transport. Lee[187] and Song[188,189] with their coauthors reported a blue luminescence from PPP film. Figure 68 presents the absorption, PL, and EL spectra of PPP film. The absorption spectrum has a peak at 314 nm, corresponding to the expected $\pi-\pi^*$ interband transition. The PL spectrum of the PPP film, deposited by thermal evaporation, is sharper than that of the starting PPP powder, and the PL intensity of the film is stronger at shorter wavelengths. This result was attributed to a narrower distribution of shorter conjugation lengths in PPP film compared to the PPP starting powder. Figure 69 gives EL spectra for multilayer systems. All systems show an EL peak at 446 nm with well-

Table 10. Dielectric Characteristics of Thin Polymer Films

polymer	deposition method[a]	thickness, μm	dielectric constant	loss tangent, $\times 10^3$	resistivity, Ω·m	dielectric strength, MV/m	ref
PTFE	EBE	0.05−0.1	2.0−2.9	2.2−6.2	2×10^{15}	200	126
PTFE	EBE	0.5−4	2.0−2.2	0.25−0.6	10^{16}	0.5−2.5	12, 178
PTFE	EBE+RFa	4−10	2.0−2.2	1.2−1.7	$10^{10}-10^{13}$	50−75	12, 179
PCTFE	LBE	0.8−4	2.7−2.8	6−15	$10^{15}-10^{17}$	20−30	12, 44
PCTFE	EBE+EBs	0.5−4	2.7−2.9	8−30	$5 \times 10^{12}-10^{13}$	1−2.5	42
P(TFE-E)	LBE	0.3−08	2.5	5−7	10^{13}	150	12, 44
P(TFE-E)	LBE+RFa	0.3−2.2	2.7−2.9	3−4	10^{13}	200	12, 44
P(TFE-E)[b]	LBE	0.5		1.2	−	200	12, 44
PCA	TE	0.1−0.5	3−4	5−10	1.4×10^9	270	12, 15
PC	LBE	0.5	3.2	3.6	10^{14}	600	12
PC	LBE+RFa	0.5	6.3	5	−	500	12
PhN	LBE	0.7−1.4	4.0−4.4	7−9	$10^{13}-10^{14}$	150−240	12
PhN	LBE+RFa	0.2−0.3	5.5−5.7	17−19	−	300−340	12
PSF	LBE	0.6−3.2	1.3−9.4	60−90	10^{14}	100−140	12
PSF	LBE+RFa	0.8−1.5	3.5	14−17	−	150−300	12
PE	TE	1−2	2.2−2.4	0.1−0.4	−	−	23
PP	TE	0.01−0.26	1.83	−	$10^{12}-10^{13}$	−	129

[a] TE, thermal evaporation; EBE, electron beam evaporation; LBE, laser beam evaporation; RFa, activation by radio frequency discharge; EBs, electron beam irradiation of substrate. [b] Measurements with attached electrodes.

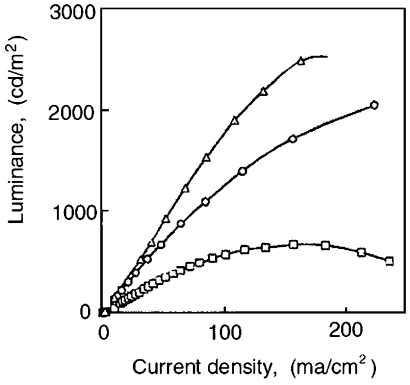

Figure 65. Current density−luminance characteristics for ITO/PPP/Alq_3/Mg vs thickness of PPP and Alq_3 layers: (□) PPP 70 nm, Alq_3 50 nm; (○) PPP and Alq_3, 50 nm; (△) PPP 30 nm, Alq_3 70 nm. Reprinted with permission from ref 186. Copyright 1997 Elsevier Science.

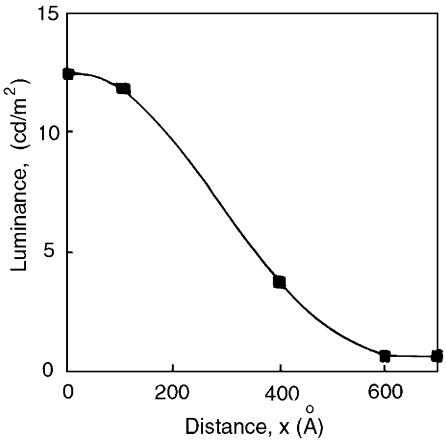

Figure 66. Luminance−distance characteristics for ITO/PPP(30 nm)/Alq_3(70 nm)/Mg devices at a current density of 1 mA/cm^2. *X* is the distance from the ITO layer to the PPP layer. Reprinted with permission from ref 186. Copyright 1997 Elsevier Science.

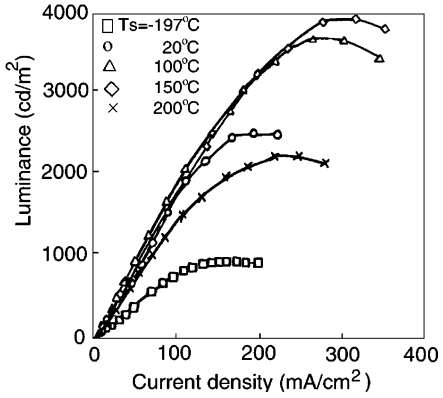

Figure 67. Dependence of luminance−current density vs substrate temperature during PPP deposition for ITO/PPP-(30 nm)/Alq_3/Mg devices. Reprinted with permission from ref 186. Copyright 1997 Elsevier Science.

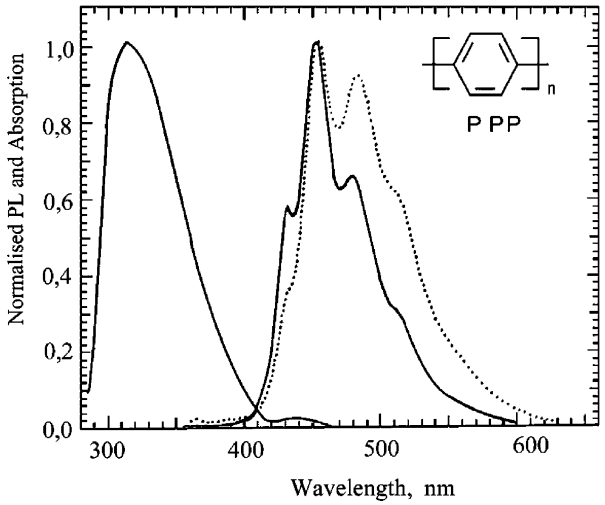

Figure 68. Absorption (thin solid line) and photoluminescence (thick solid line) spectra of PPP film and PL for PPP powder (dotted line). Reprinted with permission from ref 187. Copyright 2000 Elsevier Science.

resolved vibronic structure. This study of ITO/PPP/Al, ITO/PVK/PPP/Al, and ITO/TPD/PPP/Al included the dependence of quantum efficiency (QE) on deposition temperature. The first two systems are nearly temperature independent, implying that a tunneling mechanism plays an important role in carrier injection. But the QE of the third system increases as deposition temperature is lowered. This is charac-

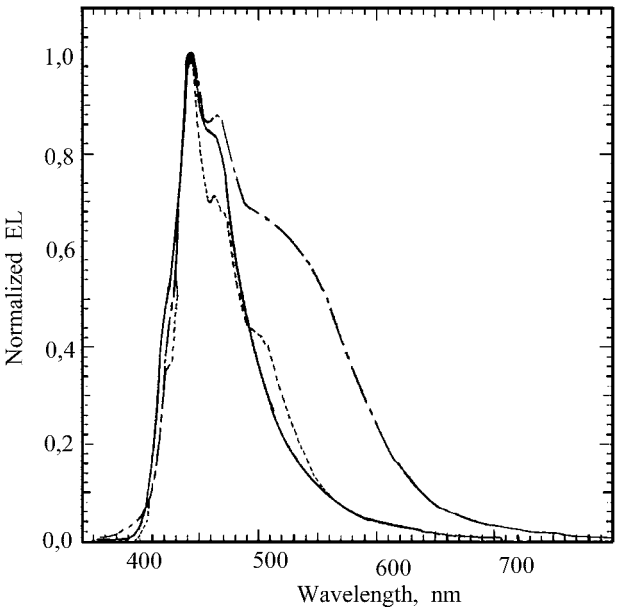

Figure 69. EL spectra of ITO/PPP/Al (solid line), ITO/TPD/PPP/Al (dotted line), and ITO/PVK/Al multilayer systems (dot−dashed line). Reprinted with permission from ref 187. Copyright 2000 Elsevier Science.

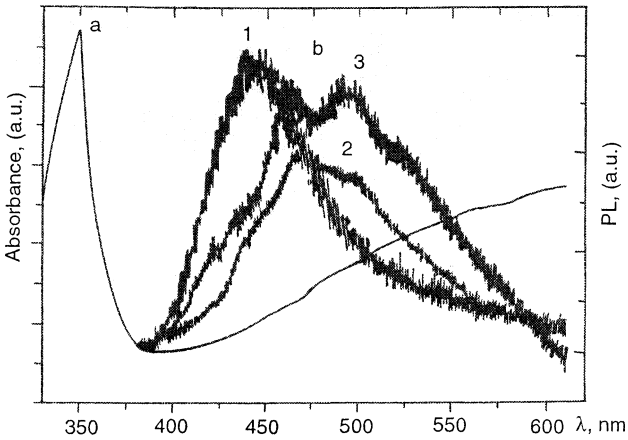

Figure 70. (a) Absorption and (b) emission spectra of (2) PVK film, (1) PVK powder, and (3) vinylcarbazole powder. Reprinted with permission from ref 191. Copyright 2001 Elsevier Science.

teristic of a space-charge-limited current in a trap-filled insulator. The hole mobility in the first system was estimated to be 4×10^{-6} cm^2/V. D'Almeida and Bernede with their coauthors[190−192] reported a blue EL in a PVK film deposited by thermal evaporation. Figure 70 presents the optical spectra of PVK and vinylcarbazole (VK). The emission spectrum of the PVK film differs from that of the PVK powder. The 450-nm maximum in the film spectrum corresponds to PVK, while 474 and 500 nm correspond to VK. This is evidence for a shorter chain length for macromolecules in TE PVK film than those in the powder. The spectrum of the ITO/PVK/Alq_3/Al structure has a PL peak at 550 nm. In this structure, the emission originates in the Alq_3 layer, while PVK serves as a hole-transport layer. Figure 71 compares PL spectra for PVK, Alq_3, and the PVK/Alq_3 bilayer. Figures 72 and 73 show EL characteristics of the ITO/PVK/Al and ITO/PVK/Alq_3/Al structures. The bilayer

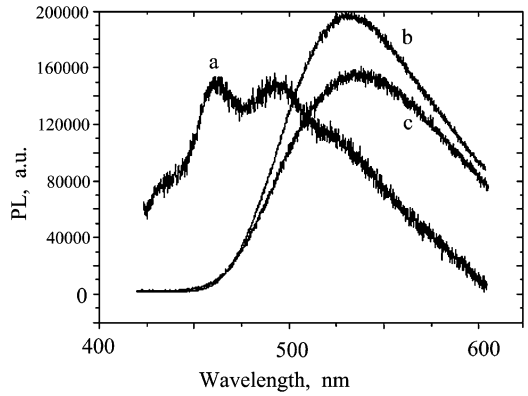

Figure 71. PL spectra of (a) PVK and (b) Alq_3 films and (c) PVK/Alq_3 bilayer. Reprinted with permission from ref 191. Copyright 2001 Elsevier Science.

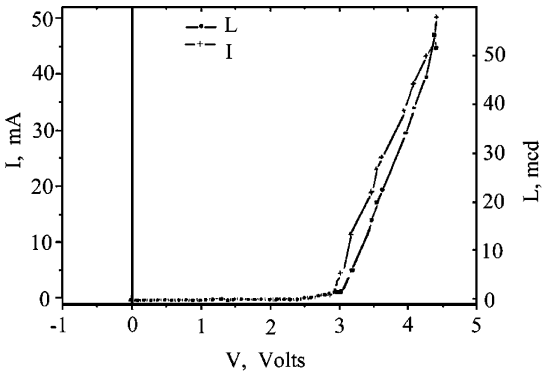

Figure 72. $I-V$ and EL characteristics of the SnO_2/PVK/Al structure. Reprinted with permission from ref 191. Copyright 2001 Elsevier Science.

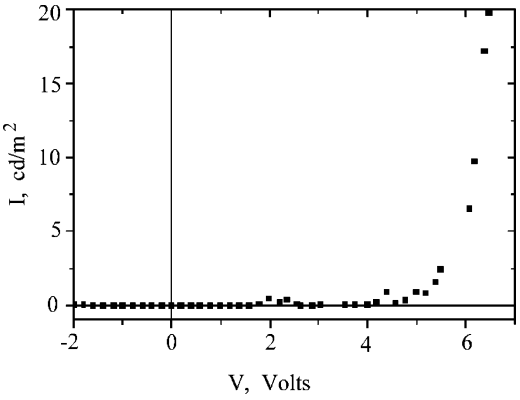

Figure 73. EL characteristics of the ITO/PVK/Alq_3/Al structure. Reprinted with permission from ref 191. Copyright 2001 Elsevier Science.

diode exhibits improved performance. The authors explained away these characteristics with the injection of both types of charge carriers from the electrodes. The holes are the majority carriers, while electron injection is effectively the limiting factor for EL. The same group studied poly(tetrabromo-*p*-phenylene diselenide) (PBrPDSe) TE deposited film in the following EL structure: ITO/PBrPDSe/CZ/Al.[192,193] Table 11 shows the turn-on voltage and field as compared with those of the structure without PBrPDSe. PBrPDSe is nearly insulating and serves as a hole-trapping layer. The authors consider that, due to hole trapping, the electron injection is made easier, and that enhances diode performance.

Table 11. Turn-on Voltages and Fields[a]

ITO/CZ/Al		ITO/PBrPDSe/CZ/Al		
CZ thickness, nm	turn-on voltage, V	CZ thickness, nm	turn-on voltage, V	turn-on field, V m^{-1}
200	3.7	200	2.4	1.2×10^7
450	2.8	210	2.7	1.28×10^7
600	2.6	250	3	1.2×10^7
		350	3.3	0.95×10^7

[a] CZ, carbazole monomer.

4.6 Appendix

It follows from data reported by many researchers that the relief, and consequently the structure, of almost all polymer films were lumpy. The films contain aggregates of various types, up to several micrometers in diameter. Undoubtedly, such morphological units must influence the electron and hole mobility-related properties strongly (for example, look at grain size-dependent mobility in oligothiophene films[194]). Unfortunately, no data on this topic are available for vacuum-deposited polymer films. Only one systematic investigation to produce a very smooth (at the nanometer level) polymer film was made by Gritsenko, but electrical properties were not evaluated. Certain other data, including those of synchrotron radiation deposition, UV laser beam evaporation, and CO_2 laser beam evaporation, using an elevated temperature of substrate in the latter case, allow us to deduce that very smooth films can be produced by using other polymers. Only these very smooth films can be used in photonics chips and integrated devices with micrometer-sized active elements.

5. Application of Thin Polymer Films

5.1. Dielectric Layers

Several authors[12,33,44,106] are optimistic that the dielectric properties of vacuum-deposited polymer films make them ideal for use in thin-film capacitors and microcircuits layers. Both existing production methods for thin-film capacitors — either using foil conductors, or a layer-by-layer formation of conductor and insulator films on an elastic polymer substrate — are acceptable. The rate of polymer film deposition by electron beam or laser beam evaporation is comparable with that of the metal. This parity makes for efficient capacitor production. It is important that the process for making microelectronics device polymer films proceeds without the potential for damage to other circuit components. PTFE was used as the dielectric layer in a metal−insulator−semiconductor integrated circuit.[195] It is desirable to use biologically inert polymer films to protect metal electrodes and sensors in vivo. Inayoshi and co-workers[85] used synchrotron radiation etching for the micromachining of a deposited PTFE film (Figure 74). They anticipated the future use of such processes for many types of microdevices.

5.2. Antifriction Layers

Slip layers show promise for use in magnetic information films, where a minimum clearance is needed between the magnetic head and the recording medium. Nikonov[196] found that films obtained by polymer evaporation have COFs comparable to those of diamond-like films. PTFE films were used for the modification of frictional properties of a polyurethane surface.[197] Thin antifriction polymer films are useful in precision friction joints with demanding requirements for contact clearance working under moderate loads, as well as for devices with limited life. Tests of both PTFE and PI films in supporting the elements of gas bearings showed them to be serviceable for several hours under severe operating conditions.[12]

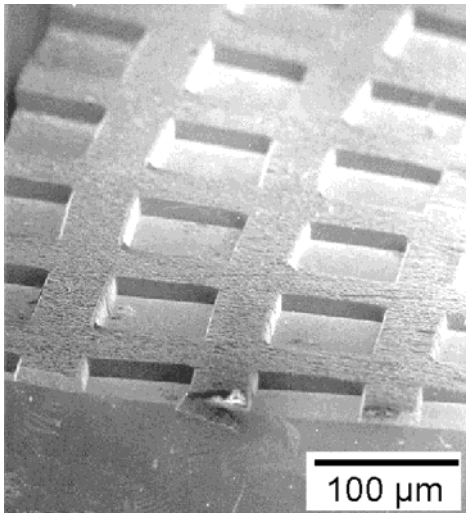

Figure 74. SEM image of synchrotron radiation etched pattern in PFEP film deposited by synchrotron radiation evaporation at substrate temperature 200 °C. Reprinted with permission from ref 86. Copyright 1999 American Vacuum Society.

5.3. Corrosion-Protective Layers

The use of a PTFE film results in a 2.5-fold lifetime increase for a hologram-recording MnBi layer.[33] Similar improvements were achieved for optical elements of KBr, NaCl, and other hygroscopic materials.[44] PC, PSF, PI, and PTFE films of 100−600 nm thickness can be used to render metal surfaces hydrophobic, for use in, e.g., heat exchangers.[44] A 3−4-μm PTFE film deposited on a car headlight reflector gave it good protection under high humidity and temperature.[167] A PET film was tried as a cover on the surface of a space satellite.[121] It is worth restating that only vacuum evaporation techniques can be used in the vacuum of space to deposit polymer coatings on the functional parts of satellites.

5.4. Films in Optics and Electronics

PE, PP, PVDF, and PTFE films were used as a thermal barrier for recording layers made of Te alloys, Ni + NiO_x, and Te + CH_x to improve their sensitivity to laser radiation.[96,107,128,198−204] A 30−50-nm sublayer permits the creation of a recording medium with a sensitivity equal to that on a thicker polymer and a stability for multiple read-outs similar to that on a glass substrate. It allows better control of laser mark's shape through adapting the polymer sublayer's physical and chemical properties to work

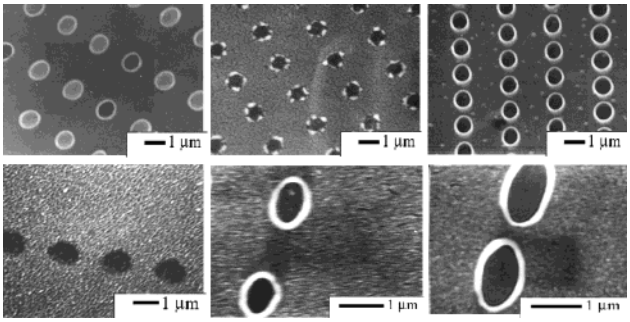

Figure 75. Holes recorded in (a) AsSeTe/PTFE bilayer, 830 nm, 5 mW, 150 ns; (b) AsSeTe + PTFE/PTFE, 830 nm, 5 mW, 150 ns; (c) AsSeTe/AsSeTe + PTFE/PTFE, 530 nm, 10 mW, 75 ns; (d) VOPc/glass, 530 nm, 15 mW, 75 ns; (e) VOPc/PTFE, 830 nm, 7 mW, 75 ns; (f) cyanine/PTFE, 830 nm, 7 mW, 75 ns.

well with the recording layer. PE and PTFE films were used as thermal barriers between metal oxide layers for servotracks recorded with a 530-nm wavelength laser and a dye layer for recording information by a semiconductor laser at 830 nm.[205] Films produced by the co-deposition of PE, PCTFE, and PTFE with Au and Te,[147,206−208] and of PTFE with a Pc dye,[204] were used as a recording layer. These recording media, with holes marked by the laser beam, are shown in Figure 75. The use of a PTFE layer in addition to an AsSeTe recording layer, an intermediate layer, and/or a sublayer allows us to control the shape of the laser marks. Some images were taken from the inner surface of the cylindrical optical carrier, 14 mm in diameter. Thin films of Teflon AF 1600, filled with DANS by TE, exhibited an appreciable electro-optic effect: 2.5 pm/V.[153] Later, Kannari et al.[155] deposited DANS-filled Cytop for the same purpose, using laser beam evaporation instead. Proper material choice is important in the active layer of an integrated optical device. Kannari et al.[152] found a third-order optical nonlinearity in CdTe + PTFE films. These films functioned as irradiance-dependent lenses, producing both focusing and defocusing in the far field. Metal and/or dye nanoclusters in a polymer matrix exhibited a variety of nonlinear optical and electrical properties.[209−213] Such films are intensively studied worldwide. Composite CuPc + PS films had a stronger sensing of, and a shorter recovery time for, NO_2 gas.[214−216] The kinetics of the composite film's response to NO_2 gas is shown in Figure 76. A nearly 5-fold increase in sensitivity was found. PANI + TCNQ films exhibited conductive behavior,[145] so they too can be considered for use in microelectronics.

PE and PTFE films that are vacuum-deposited and then unidirectionally rubbed by a cloth are used as a sublayer which allows the growth of an aligned dye (oligomer, polymer) film with a high dichroic ratio during the following cycle of vacuum evaporation.[217−221] Figure 77 presents polarized optical absorption spectra for two Sq films as a function of their thickness. It should be noted that vacuum-deposited PTFE film aligned two Sq dyes, while friction-transferred PTFE film aligned only one OH-Sq. Figure 78 presents an SEM image of OH-Sq onto vacuum-deposited PTFE film. Formation of aligned dye nanowires is clearly

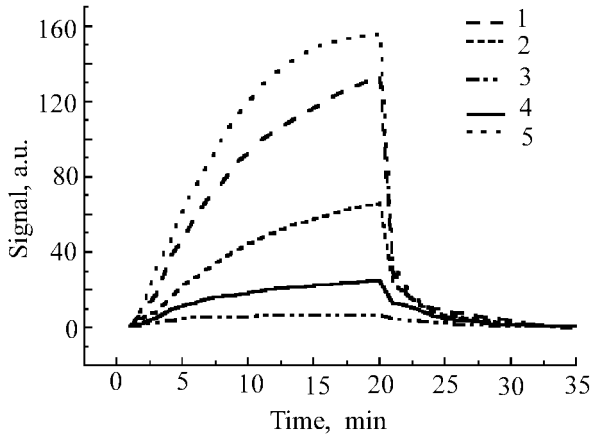

Figure 76. Response of 20% CuPc + PS films to 2 ppm of NO_2 gas. Films were annealed at (1) 120, (2,4,5) 150, and (3) 200 °C. Measurements were made at the following temperatures: (4) 100, (1,2,3) 120, and (5) 150 °C. Reprinted from ref 215 with permission from the author.

seen. Friction-transferred PTFE film aligned OH-Sq also, but structure was as smooth as invisible in SEM. A PDA film which was aligned and then irradiated through a mask was used as a polarizing beam-splitter for a magneto-optical system.[147]

Several groups have studied the application of vacuum-deposited polymer films for electroluminescent light-emitting diodes, flat panel displays, lasers, nonlinear optics, etc.[187−195,221,222] Poly(dimethylsilylene) films for use in EL diodes are deposited using thermal evaporation with activation by accelerated electrons.[222] So, there are good grounds to expect that further progress will be made in the development of thermoresistors, pressure gauges, radiation detectors, diodes, sensors, and other smart devices that will include thin polymer and composite films as an active layer. For such use, the polymers and dopants with complex chemical structure should be custom-synthesized.

5.5. Porous Films

In the high-power extreme, laser "evaporation" of PTFE results in formation of a fibrous−porous deposit on any substrate. The layer is formed from clusters and droplets of PTFE, up to several micrometers in size, that are ejected from PTFE by the gaseous degradation products.[223−226] It is a promising material for various industrial applications due to its outstanding thermal and chemical stability, as well as its biocompatibility. It has been tested for use in RF devices.[227] Various kinds of PTFE filters are being introduced into Russian industry.

It may be of interest to note the use of dye-filled polymer films transferred by laser ablation for high-speed printing.[228] It involves also not just the evaporation of a polymer decomposed into low-molecular-weight species, but it is similar to the process of polymer microcluster transfer from the target to the substrate by decomposition products. A further development along this line of thought is the new matrix-assisted pulsed laser evaporation (MAPLE).[229,230] This method employs another easily evaporatable solid material as the matrix in which

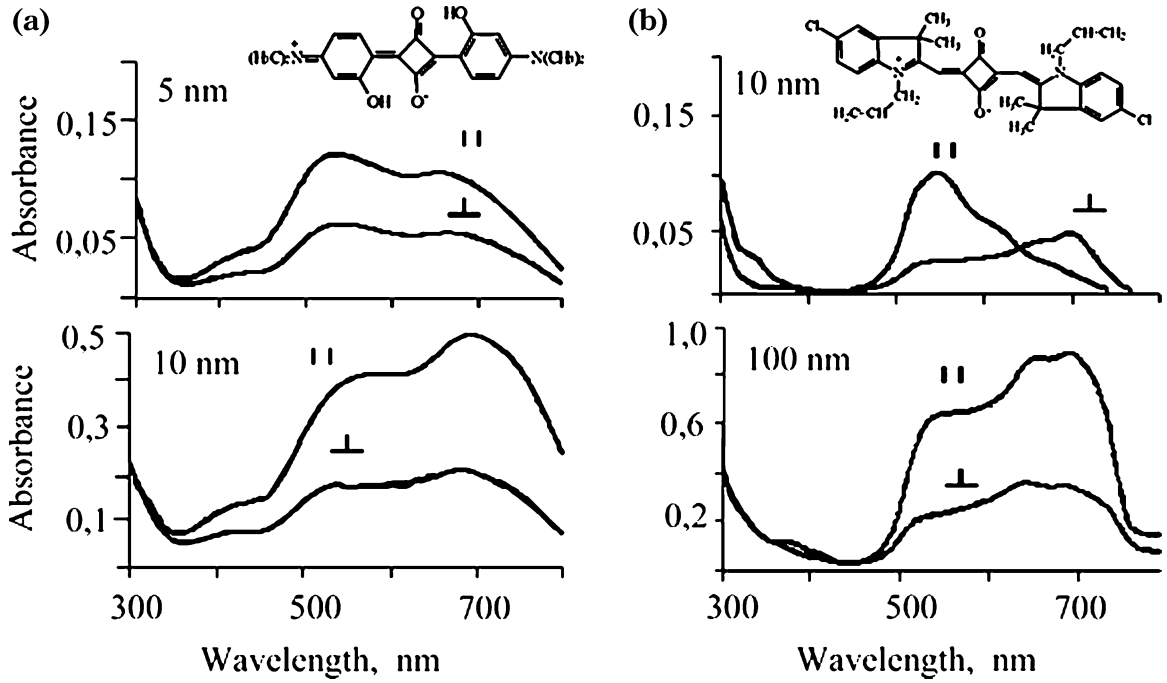

Figure 77. Polarized absorption spectra of films of (a) OH-Sq and (b) allyl-Sq dyes deposited on aligned PTFE sublayer vs film thickness.

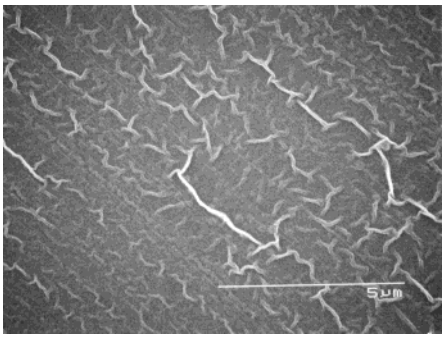

Figure 78. SEM image of oriented squarylium (OH-Sq) film deposited onto aligned PTFE sublayer.

higher molecular weight molecules are dissolved or dispersed. The laser irradiation pulse converts that matrix to a gas, which gives an impetus to free up and push out the larger molecules from the target to substrate. Films of poly(lactic-co-glycolic acid), poly(ethylene glycol)−carbon nanotube composites, and biomolecules were successfully deposited. These films may be useful in smart optoelectronics and bioelectronics devices. Use of resonant IR laser pulsed evaporation allows selective dissociation of chemical bonds, which can widen the range of polymer materials applicable for polymer film deposition, namely by destruction of the macrochain.[89,231] A more easily evaporated polymer (PS) can serve as the matrix, making possible delicate dye (target, 1% of allyl-Sq with PS) deposition using a conventional CO_2 laser beam.[232] Composite dye + PS film was formed, while pure allyl-Sq dye was decomposed under CO_2 laser beam action. Tsuboi and coauthors reported pulsed laser deposition of silk fibroin.[233] But films with structure more similar to the original fibroin were deposited when using an anthracene sensitizer for target doping to prevent direct photoexcitation of fibroin molecules.

6. Conclusions

The above survey confirms that the initial research, conducted in the 1950s and 1960s in the field of application of vacuum decomposition of polymers to the making of thin films, has developed into its own branch of technology. It has attracted researchers worldwide. In the near future these studies are expected to develop rapidly, owing to the promise they hold in chemistry, optoelectronics, and informatics. We expect an emphasis will be placed on the combined deposition methods for complex (nanocomposite, solid solution, etc.) films for use as both active and passive functional layers. For the manufacture of advanced devices, having a variety of deposition methods to make multilayer systems will be valuable, and polymer-based film deposition in a vacuum will find its place. The next step will be the controlled, oriented, and aligned growth of polymer films and multilayer systems, like the first advances mentioned in the review by Forrest.[234] Compared to "man-made" inorganic superlattices, the organic analogy extends our possibilities of controlling and organizing matter. The control begins by molecule active core design and chemical synthesis, followed by film structure construction during deposition. We are pleased to survey the lastest publications from the former Soviet Union that include both old and new research groups working on advanced and combined methods for polymer film deposition, in some cases together with Western researchers.[235−245]

7. List of Abbreviations

Cytop	perfluorinated cyclooxyaliphatic polymer
PA	polyarylate
PAN	poly(acrylonitrile)
PANI	polyaniline
PBrPDSe	poly(tetrabromo-*p*-phenylene diselenide)
PEG	poly(ethylene glycol)

PC	polycarbonate
PCA	polycaproamide
PCHD	polycyclohexadiene
PCTFE	poly(chlorotrifluoroethylyne)
P(CTFE-E)	chlorotrifluoroethylene and ethylene copolymer
PE	polyethylene
PET	poly(ethylene terephthalate)
PhN	phenylon
PI	polyimide
PMMA	poly(methyl methacrylate)
PP	polypropylene
PPP	poly(*p*-phenylene)
PPS	poly(*p*-phenylene sulfide)
PPX	poly(*p*-xylylene)
PS	polystyrene
PSF	polysulfone
PTFE	poly(tetrafluoroethylene)
P(TFE-E)	tetrafluoroethylene and ethylene copolymer
PFEP	poly(tetrafluoroethylene and hexafluoropropylene) copolymer
PVDF	poly(vinylidene fluoride)
PVK	poly(vinylcarbazole)
Pc	phthalocyanine
Sq	squarylium
EPR	electron paramagnetic resonance
ϵ	dielectric permittivity
tg δ	dielectric loss tangent
IR	infrared
RF	radio frequency
SEM	scanning electron microscopy
TEM	transmission electron microscopy
AFM	atomic force microscopy
UV	ultraviolet
XRD	X-ray diffraction

8. Acknowledgments

The authors would like to thank all their colleagues who sent their figures in electronic format, lightening the duties of review preparation. Special thanks to Dr. W. F. Beach for assisting with English. K.P.G. expresses thanks to the EU Scientific Directorate for support of complex organic film deposition direction in Ukraine by STCU Grant No. 2348 (www.stcu.kiev.ua).

9. References

(1) Cooper, A. C.; Keller, A.; Waring, J. R. *J. Polym. Sci.* **1953**, *11*, 215.
(2) Keller, A. *J. Polym. Sci.* **1959**, *36*, 361.
(3) Gorell, J. H. *Plast. Technol.* **1964**, *10*, 45.
(4) Tkachuk, B. V.; Kolotyrkin, V. M. *Osajdenie tonkix dielectricheskix plenok iz gasovoi fasi*; Khimia: Moscow, 1977.
(5) Yasuda, H. *Plasma polymerization*; Academic Press: New York, 1985.
(6) Biederman, H.; Osada, Y. *Plasma Polymerisation Processes*; Elsevier Science Publishers: Amsterdam, 1992.
(7) Bernede, J. C.; Taoudi, H.; Kodjo, E.; et al. *Recent Res. Dev. Polym. Sci.* **1987**, *1*, 205.
(8) Usui, H. *Thin Solid Films* **2000**, *365*, 22.
(9) Gritsenko, K. P. *Proc. SPIE* **2002**, *4833*, 493.
(10) Feng, Y.; Zhu, M.; Liu, F.; et al. *Thin Solid Films* **2001**, *395*, 213.
(11) Burrows, P. E.; Graff, G. L.; Gross, M. E.; et al. *Proc. SPIE* **2000**, *4105*, 75.
(12) Krasovsky, A. M.; Tolstopyatov, E. M. *Raspilenie polymerov u vacuume*; Nauka i Technika: Minsk, 1989.
(13) *Belarussian SSR short Enciklopedia 3*; Nauka i Technika: Minsk, 1980.
(14) Krasovsky, A. M. In *Metalopolymer. Materiali i izdelia*; Belyi, V. A., Ed.; Khimia: Moscow, 1979; p 312.
(15) Krasovsky, A. M. Diss. Cand. Techn. Sci., Moscow, 1979; p 130.
(16) Grassie, N. *Chemistry of Destructon Processes in Polymers*; Izd Inostr. Liter.: Moscow, 1959.
(17) Madorsky, S. *Thermal Degradation of Organic Polymers*; Interscience Publishers: New York, London, Sydney, 1964.
(18) Tolstopyatov, E. M.; Grakovich, P. N.; Ivanov, L. F. *Vestn. Akad. Nauk BSSR* **1989**, *4*, 23.
(19) Gritsenko, K. P.; Krasovsky, A. M.; Tolstopyatov, E. M. *Opt. Mem. Neural Networks* **2001**, *10* (3), 173.
(20) Kuzmina, R. P.; Zaev, N. E. *Trydy VNII Elektromekh. Electrotechn. Mater.* **1974**, *40*, 196.
(21) *Dissociation eneries of chemical bond cleavage. Potentials of ionization*; Kondratiev, V. N., Ed.; Nauka: Moscow, 1974; p 214.
(22) Rossini, F. D.; Pitzer, K. S.; Arnett, R. L.; et al. *Selected Values of Physical and Thermodynamical Properties of Hydrocarbons and Related Compounds*; American Petroleum Institute Research Project 44; Carnegie Press: Pittsburgh, PA, 1953; p 120.
(23) Kruglyak, Yu. A.; Kirov, I. M.; Zadorozhny, V. G. *Conf. Vacuum Pokrytia '87, Riga* **1987**, 140.
(24) Kruglyak, Yu. A.; Kirov, I. M.; Zadorozhny, V. G. *Deponent Ukr. NIINTI* **1987**, No. 1679-UK-87.
(25) Luff, P. P.; White, M. *Vacuum* **1968**, *18* (8), 437.
(26) Lantoukh, G. V.; Gritsenko, K. P.; Dyachenko, N. S. *Ukrain. Khim. J.* **1990**, *59*, 1221.
(27) Khimchenko, Yu. I.; Gritsenko, K. P.; Radkevich, L. S.; et al. *Ukr. Khim. Zh.* **1988**, *54*, 762.
(28) Gritsenko, K. P., unpublished.
(29) Gritsenko, K. P. *Ukr. Khim. Zh.* **1991**, *57*, 782.
(30) Belyi, V. A.; Gorbach, N. S.; Krasovsky, A. M. *Dokl. Akad. Nauk BSSR* **1972**, *16*, 223.
(31) Collins, R. D.; Fiveash, P.; Holland, L. *Vacuum* **1969**, *19* (3), 113.
(32) Murakami, Y.; Shintani, T. *Thin Solid Films* **1972**, *9*, 301.
(33) Zadorozhny, V. G. Diss. Dr. Chem. Sci. Kyiv, 1989; p 511.
(34) Royh, I. L.; Rafalovich, D. N.; Zadorozhny, V. G. *Prib. Tekh. Eksp.* **1976**, *4*, 110.
(35) Skripov, P. V.; Puchinskis, S. E.; Begishev, V. P.; et al., personal communication, 1997.
(36) Akashi, G.; Nahara, A.; Arai, Y. (Fuji Photo Film Co.). U.S. Patent 4,543,275, 1985.
(37) Gritsenko, K. P.; Petrov, V. V.; Antonov, A. A.; et al. U.S.S.R. Patent SU 1,753,733, 1992.
(38) Agabekov, V. E.; Chaplanova, G. D.; Kuznetsov, A. E.; Scharendo, E. V. Conf. Polymer. Kompoziti−1998, Gomel, September 29−30, 1998; p 143.
(39) Agabekov, V. E.; Chaplanova, G. D.; Kuznetsov, A. E.; Ivko, A. A. Conf. Polymer. Kompoziti−1998, Gomel, September 29−30, 1998; p 281.
(40) Rogachev, A. V.; Kharitonov, V. V. *Ingenerno-Fyzicheskii Zhurn.* **1983**, *44*, 105.
(41) Fainstein, A. I.; Silantiev A. I. *Visokomol Soed. A* **1988**, *30* (4), 834.
(42) Silantiev, A. I. Diss. Cand. Techn. Sci., Odessa, 1986; p 191.
(43) Krasovsky, A. M.; Tolstopyatov, E. M. *Lakokras. Mater.* **1981**, *2*, 26.
(44) Tolstopyatov, E. M. Diss. Cand. Phys.-Math. Sci., Moscow, 1985; p 163.
(45) Akishin, A. I.; Gujova, S. K.; Solovyov, G. G.; Isaev, L. N. *Khim. Vys. Energ.* **1976**, *10* (6), 494.
(46) Filatov, V. N.; Sysoev, A. A.; Morozov, O. V. *Prib. Tekh. Eksp.* **1981**, *1*, 179.
(47) Tolstopyatov, E. M., unpublished.
(48) Weissmantel, C. *Le Vide* **1976**, *31* (183), 107.
(49) Rost, M.; Reisse, G. *Beitr. Tag. Hochvac., 8th, Grenzflagen/Dunne Scichen* **1984**, 319.
(50) Ueno, Y.; Fuji, T.; Kannari, F. *Appl. Phys. Lett.* **1994**, *65* (11), 1370.
(51) Inoue, S.; Fuji, T.; Kannari, F. J. *Photopolym. Sci. Technol.* **1994**, *7*, 373.
(52) Jiang, W.; Norton, M. G.; Tsung, L.; Dickinson, J. T. *J. Mater. Res.* **1995**, *10* (4), 1038.
(53) Dickinson, J. T.; Shin, J. J.; Jiang, W.; Norton, M. G. *J. Appl. Phys.* **1993**, *74* (7), 4729.
(54) Tsunekawa, M.; Nishio, S.; Sato, H. *J. Appl. Phys.* **1994**, *76* (9), 5598.
(55) Nishio, S.; Chiba, T.; Matsuzaki, A.; Sato, H. *Appl. Surf. Sci.* **1996**, *106*, 132.
(56) Lu, Y. F.; Mai, Z. H.; Cheong, B. A.; et al. E-MRS Spring Meeting, June 1−4, Strasbourg, 1999; p B-38.
(57) Talrose, V. L.; Barashev, P. P. *Zhurn. VHO im. Mendeleeva* **1973**, *19*,15.
(58) Bunkin, F. V.; Kirichenko, N. A.; Lykianchuk, B. S. *Usp. Fiz. Nauk* **1982**, *138*, 45.
(59) Ilyasov, S. G.; Kalvina, I. N.; Kiulyan, G. A.; et al. *Kvantovaya Elektron.* **1974**, *1*, 2303.
(60) Parkhomenko, A. I.; Rautian, S. G.; Stokman, N. I. *Dokl. Akad. Nauk USSR* **1980**, *250*, 225.
(61) Nesterikhin, Yu. E.; Rautian, S. G.; Stokman, N. I. *Usp. Fiz. Nauk* **1982**, *138*, 321.
(62) Krasovsky, A. M.; Tolstopyatov, E. M.; Belyi, V. A. *Dokl. Akad. Nauk BSSR* **1984**, *28*, 1100.

(63) Mirkin, L. I.; Pilipetsky, N. F. *Mekhanika Polym.* **1966**, *4*, 624.
(64) Akimov, A. I.; Mirkin, L. I.; Pilipetsky, N. F. *Mekhanika Polym.* **1967**, *28*, 493.
(65) Ashkinazi, B. M.; Vladimirov, V. I.; Lihachev, V. A.; et al. *Zh. Eksp. Techn. Fiz.* **1966**, *50*, 1187.
(66) Sultanov, M. A. *Mekhanika Polym.* **1972**, *2*, 359.
(67) Novikov, N. P. *Struktura i svoistva polymer. Mater.*; Zinatne: Riga, 1979; p 160.
(68) Mikhailova, G. V.; Novikov, N. P.; Iudin, Yu. I. *Dokl. Akad. Nauk USSR* **1968**, *182*, 874.
(69) Babajan, E. I.; Kosachev, V. V.; Lohov, Yu. N. *Fiz.-Khim. Obrab. Mater.* **1979**, *4*, 37.
(70) Novikov, N. P.; Kholodilov, A. A. *Mekhanika Polym.* **1971**, *1*, 122.
(71) Tolstopyatov, E. M.; Barahvostov, A. A. Conf. Lucheva Obrab. Kompoz. Mater., Ternopol, Ukraine, 1990; p 30.
(72) Grakovich, P. N.; Ivanov, L. F.; Tolstoyatov, E. M.; Krasovsky, A. M. Conf. Resursosb. Ekolog. Chisty Technol., Grodno, Belarus, 1995; p 171.
(73) Bykovsky, Yu. A.; Bahirkin, Yu. A.; Oshurko, V. B.; Chistyakov, A. A. *Khim. Vys. Energ.* **1994**, *28*, 437.
(74) Said-Galiev, E. E.; Nikitin, L. N.; Dvorikova, R. A.; et al. *Khim. Vys. Energ.* **1994**, *28*, 444.
(75) Ivanov, L. F., personal communication.
(76) Tovstonog, V. A. *Teplofiz. Vys. Temp.* **1991**, *29*, 268.
(77) Garrison, B. J.; Srinivasan, R. *J. Appl. Phys.* **1985**, *57* (8), 2909.
(78) Hill, D. A.; Soong, D. S. *J. Appl. Phys.* **1987**, *61* (6), 2132.
(79) Lee, I. Y. S.; Wen, X.; Tolbert, W. A.; Dlott, D. D. *J. Appl. Phys.* **1992**, *72* (6), 2440.
(80) Wen, X.; Hare, D. H.; Dlott, D. D. *Appl. Phys. Lett.* **1994**, *64* (2), 184.
(81) Hare, D. H.; Dlott, D. D. *Appl. Phys. Lett.* **1994**, *64* (6), 715.
(82) Hare, D. H.; Franken, J.; Dlott, D. D. *J. Appl. Phys.* **1995**, *77* (11), 5950.
(83) Tsunekawa, M.; Nishio, S.; Sato, H. *Jpn. J. Appl. Phys.* **1995**, *34*, *1*, 218.
(84) Nishio, S.; Sato, H. *J. Photochem. Photobiol. C: Photochem. Rev.* **2001**, *18*, 1.
(85) Inayoshi, M.; Hori, M.; Goto, T.; et al. *J. Vac. Sci. Technol.* **1996**, *A14* (4), 1981.
(86) Inayoshi, M.; Ito, M.; Hori, M.; et al. *J. Vac. Sci. Technol.* **1999**, *B17* (3), 949.
(87) Katoh, T.; Zhang, Y. *Appl. Surf. Sci.* **1999**, *138*−*139*, 165.
(88) Zhang, Y.; Katoh, T.; Endo, A. *J. Electron Spectrosc. Relat. Phenom.* **2001**, *119*, 247.
(89) Bubb, D. M.; Horwitz, J. H.; Callahan J. H.; et al. *J. Vac. Sci. Technol.* **2001**, *A19* (5), 1.
(90) Itina, T. E.; Zhigilei, L. V.; Garrison, B. J. *Nucl. Instrum. Methods Phys. Res. B* **2001**, *180*, 238.
(91) Williams G. J.; Zhigilei L. V.; Garrison B. J. *Nucl. Instrrm. Methods Phys. Res. B* **2001**, *180*, 209.
(92) Lukyanchuk, B.; Bityurin, N.; Arnold, N.; et al. *Appl. Surf. Sci.* **1996**, *106*, 120.
(93) Lukyanchuk, B.; Himmelbauer, H.; Bityurin, N.; Arnold N. *Nucl. Instrum. Methods Phys. Res. B* **1997**, *122*, 347.
(94) Arnold, N.; Bityurin, N.; Bauerle, D. *Appl. Surf. Sci.* **1999**, *138*−*139*, 212.
(95) Perveev, A. F.; Muranova, G. A. *Prib. Tekh. Eksp.* **1969**, *4*, 200.
(96) Petrov, V. V.; Gritsenko, K. P.; Kriuchin, A. A. Conf. Vacuum. Pokryt.−87, Riga, 1987; p 138.
(97) Gritsenko, K. P.; Gritsenko, V. S. *Poroshk. Metall.* **1990**, *2*, 98.
(98) Luff, P. P.; White, M. *Thin Solid Films* **1970**, *6*, 175.
(99) White, M. *Thin Solid Films* **1973**, *18*, 157.
(100) Stephens,A. W.; Levine, A. W.; Fech, J.; et al. *Thin Solid Films* **1974**, *24* (2), 361.
(101) Winters, H. F. *J. Appl. Phys.* **1978**, *49* (10), 5165.
(102) Krasovsky, A. M.; Yurkevich, A. R. *Vestn. Akad. Nauk BSSR* **1973**, *2*, 110.
(103) Gritsenko, K. P.; Khimchenko, Yu. I.; Lantoukh, G. V. In *Optich. Zapis Inform.*; Petrov, V. V., Ed.; Naukova Dumka: Kyiv, 1987; p 85.
(104) Vinogradov, G. K. *Khim. Vysokih. Energ.* **1986**, *20*, 195.
(105) Wijesundara, M. B.; Ji, Y.; Ni, B., et al. *J. Appl. Phys.* **2000**, *88* (9), 5004.
(106) Polishchuk, S. G. Diss. Cand. Techn. Sci., Moscow, 1985; p 185.
(107) Gritsenko, K. P. Diss. Cand. Techn. Sci., Gomel, 1997; p 139.
(108) Gritsenko, K. P. Conf. Ionizing Radiation and Polymers−98, Weinbohla, 1998; p P10.
(109) Szwarc, M. *Discuss. Faraday Soc.* **1947**, *2*, 46.
(110) Krasovsky, A. M.; Tolstopyatov, E. M.; Grakovich, P. N. *Vysokomol. Soed.* **1988**, *30* (2), 448.
(111) Krasovsky, A. M.; Grakovich, P. N.; Gut, M. M.; et al. Conf. Resursosb. Ekolog. Chisty Technol., Grodno, Belarus, 1995; p 178.
(112) Krasovsky, A. M.; Belyi, V. A. *Dokl. Akad. Nauk BSSR* **1968**, *12*, 1097.
(113) Kazachenko, V. P.; Rogachev, A. V.; Barinov, V. Yu. *Dokl. Akad. Nauk BSSR* **1989**, *33* (5), 430.
(114) Rogachev, A. V.; Kazachenko, V. P. Conf. Teoret. Prikl. Plasmohim. Ivanovo, 1995; p 262.
(115) Kazachenko, V. P.; Rogachev, A. V.; Egorov, A. I. *Dokl. Akad. Nauk Belarusi* **1996**, *40* (6), 54.
(116) Usui, H.; Yamada, I.; Takagi, T. *J. Vac. Sci. Technol.* **1986**, *4*, 52.
(117) Usui, H.; Numata, K.; Dohmoto, H.; Yamada, I.; Takagi, T. *Mater. Res. Soc. Symp.* **1988**, *108*, 201.
(118) Usui, H.; Koshikawa, H.; Tanaka, T. *J. Vac. Sci. Technol.* **1995**, *A13*, 2318.
(119) Krasovsky, A. M. 1 Symp. Dispersed Metal Plenkah, Kanev, 1972; p130.
(120) Suzuki, M.; Takahashi, K.; Mitani, S. *Jpn. J. Appl. Phys.* **1975**, *9*, 741.
(121) Shrinet, V.; Chaturvedi, U.K.; Agraval, S. K.; et al. *J. Vac. Sci. Technol.* **1982**, *21* (1), 1040.
(122) Kabayev, M. M.; Libonas, Y. Y.; Pashkavichus, V. V.; Pyatkavichus, P. V. Conf. Vacuum. Pokryt.−87, Riga, 1987; p 124.
(123) Kabayev, M. M.; Lipin, Yu. B.; Pyatkavichus, P. V.; et al. Conf. Vacuum. Pokryt.−87, Riga, 1987; p 125
(124) Komakine, M.; Namikawa, T.; Yamazaki, Y. *Macromol. Chem.* **1986**, *7*, 139.
(125) Miyashita, K.; Kaneko, M. *Synth. Met.* **1995**, *68*, 161.
(126) De Wilde, W. *Thin Solid Films* **1974**, *24*, 101.
(127) Gritsenko, K. P.; Krasovsky, A. M.; Goncharenko, A. C. *Poverhnost* **1989**, *11*, 106.
(128) Gritsenko, K. P.; Krasovsky, A. M.; Kriuchin A. A.; et al. *Kompoz. Polim. Mater.* **1990**, *47*, 19.
(129) Hogarth, C. A.; Iqbal T. *Phys. Status Solidi* **1981**, *65*, 11.
(130) Kruglyak, Yu. A.; Kirov, I. M.; Zadorozhny, V.G. Conf. Vacuum Pokryt.−87, Riga, 1987; p 140.
(131) Gritsenko, K. P.; Schrader, S.; Brehmer L.; Jurga J. Conf. Nowe kierunki Modif. i zastosovan tworzyw sztuczych, Rydzyna, Poland, 2001; p 71.
(132) Fritz, T., personal communication, 2000.
(133) Nagayama, K.; Sei, M.; Mitsumoto, R.; et al. *J. Electron Spectrosc. Relat. Phenom.* **1996**, *78*, 375.
(134) Lantoukh, G. V.; Gritsenko, K. P. *Zh. Prikl. Spektrosk.* **1990**, *52*, 611.
(135) Painter, P.; Koulman, M.; Konig, D. *Theory of Vibrational Spectroscopy: Application to Polymer Materials*; Nauka: Moscow, 1986; p 220 (transl. from English).
(136) Zadorozhny, V. G. Conf. Vacuum. Pokryt.−87, Riga, 1987; p 114.
(137) Touihri, S.; Safoula, G.; Bernede, J. C.; et al. *Thin Solid Films* **1997**, *304*, 16.
(138) Das, A.; Bera S.; Dhara S.; Patnaik A. *Nucl. Instrum. Methods Phys. Res. B* **1998**, *134*, 377.
(139) Das, A.; Bera, S.; Patnaik, A.; et al. *Appl. Surf. Sci.* **1998**, *135*, 37.
(140) Tolstopyatov, E. M.; Grakovich, P. N.; Gritsenko, K. P.; et al. Conf. Nowe kierunki Modif. i zastosovan tworzyw sztuczych, Rydzyna, Poland, 1998; p 352.
(141) Nishio, S.; Kato, S.; Matsuzaki, A.; et al. *Synth. Met.* **1996**, *83*, 67.
(142) Nishio, S.; Chiba, T.; Matsuzaki, A.; Sato, H. J. *Appl. Phys.* **1996**, *79* (9), 7198.
(143) Nishio, S.; Narisada, Y.; Kuriki, S.; et al. *Synth. Met.* **1999**, *101*, 80.
(144) Lee, K. K.; Vohs J. M.; DiNardo, N. G. *Surf. Sci.* **1999**, *420*, L115.
(145) Li, J. C.; Xue, Z. Q.; Zeng, Y.; et al. *Thin Solid Films* **2000**, *374*, 59.
(146) Fujii, T.; Yokoi, T.; Hiramatsu, M.; et al. *J. Vac. Sci. Technol. A* **1996**, *14* (5), 2849.
(147) Nakao, S.; Suzuki, T.; Takeda, T.; et al. *Jpn. J. Appl. Phys.* **1996**, *35*, 508.
(148) Boonthanom, N.; White, M. *Thin Solid Films* **1974**, *24*, 295.
(149) Petrov, V. V.; Kriuchin, A. A.; Gritsenko, K. P. *Dokl. Akad. Nauk Ukr. SSR* **1989**, *12*, 64.
(150) Fejfar, A.; Martinu, L.; Ostadal, L. *Vacuum* **1989**, *39*, 19.
(151) Gritsenko, K. P. *J. Appl. Sci. Photogr.* **1998**, *39* (5), 419.
(152) Fujii, T.; Inoue, S.; Kannari, F. *Appl. Surf. Sci.* **1996**, *96*−*98*, 621.
(153) Yang, G. R.; Ma, X. F.; Chen, W. X.; You, L.; et al. *Appl. Phys. Lett.* **1994**, *64* (5), 533.
(154) Gritsenko, K. P. Conf. Kompos. Mater., Soligorsk, Belarus, 1995; p 65.
(155) Fujii, T.; Shima, H.; Matsumoto, N.; Kannari, F. *Appl. Surf. Sci.* **1996**, *96*−*98*, 625.
(156) Gritsenko, K. P.; Slominsky, Yu. L.; Fedotov, K. *Proc. SPIE* **1997**, *3359*, 479.
(157) Gritsenko, K. P.; Dimitriev, O. P.; Kislyk, V. V.; et al. 9 Conf. Organised Molecul. Films, Potsdam, 1, 2000; p 190.
(158) Gritsenko, K. P.; Dimitriev, O. P.; Kislyk, V. V.; et al. *Colloids Surf. A: Physicochem. Eng. Aspects* **2002**, *198*−*200*, 625.
(159) Gritsenko, K. P.; Ivanov, L. F.; Grakovich, P. N.; et al. *Proc. SPIE* **1999**, *3738*, 461.
(160) Gritsenko, K. P.; Ivanov, L. F.; Grakovich, P. N. *J. Appl. Sci. Photogr.* **2001**, *46* (3), 65.

(161) Gritsenko, K. P.; Dimitriev, O. P.; Glasirin, N. P.; et al. Conf. ECOER, Potsdam, 2001; p 210.
(162) Pochtennyi, A. E.; Shishkin, N. Ya.; Misevich, A. V.; et al. Conf. Ecologich. chisty i resursosb. Technol., Grodno, Belarus, 1996; p 243.
(163) Pochtennyi, A. E.; Sagaidak, D. I.; Misevich, A. V.; et al. Conf. Datchik−96, Gurzuf, 1996; p 249.
(164) Stukalov, O. M.; Pochtennyi, A. E.; Misevich, A. V.; et al. Sovesch. Zond microscopia, Nizny Nowgorod, Russia, 2000; p 102.
(165) Stukalov, O. M.; Misevich, A. V.; Pochtenny, A. E. *Phys. Low-Dim. Struct.* **2001**, *3/4*, 205.
(166) Gritsenko, K. P. *Polymer and Composite Film Deposition from Gas Phase*; Chemnitz and Dresden Technical University: Potsdam, 1999.
(167) Krasovsky, A. M. Diss. Doct. Techn. Sci., Moscow, 1983; p 230.
(168) Krasovsky, A. M.; Nikonov, B. I. *Trenie Iznos* **1986**, *7*, 965.
(169) Pisanova, E. V.; Zhandarov, S. F.; Dovgyalo, V. A. Ninth Conf. on Mechanics of Composite Mater., Riga, 1995; p 125.
(170) Harrop, R.; Harrop, P. J. *Thin Solid Films* **1969**, *3*, 1209.
(171) Rogachev, A. V.; Luchnikov, A. P.; Kamiljanov, B. I.; Byi, M. V. *Trenie Iznos* **1988**, *9*, 891.
(172) Kamiljanov, B. I. Conf. Tribol. Povys. Resurs. Dvig. Kishinev, Moldova, 1990; p 126.
(173) Lipatov, Yu. S. *Mezcfaznii yavlenia v polymerah*; Naukova Dumka: Kyiv, 1980; p 260.
(174) Anderson, H. R., Jr.; Fowkes, F. M.; Hielscher, F. H. *J. Polym. Sci., Polym. Phys. Ed.* **1976**, *14*, 879.
(175) Ivanov, L. F. Conf. Fis. Mehan. Kompoz. Mater. na Osnove Polymer., Gomel, 1985; p 35.
(176) Zadorozhny, V. G.; Rafalovich, D. M. *Lakokras. Mater. Ikh. Primen.* **1977**, *3*, 38.
(177) Yablokov, M.; Kazachenko, V.; Kuznetsov, A.; Yakushenko, I. E-MRS Spring Meeting, Strasbourg, 2001; p 33.
(178) Tolstopyatov, E. M. *Izmer. Tekh.* **1984**, *4*, 44.
(179) Tolstopyatov, E. M. *Izmer. Tekh.* **1987**, *10*, 47.
(180) Zadorozhny, V. G.; Polishchuk, V. G. *Elektron. Tekh., Ser. 6* **1979**, *10*, 106.
(181) Zadorozhny, V. G.; Polishchuk, S. G. *Plast. Massy* **1981**, *4*, 27.
(182) Kruglyak, Yu. A.; Zadorozhny, V. G.; Kirov, I. M.; et al., Conf. Konstruir. I Issledov. Radioelectr. Uzlov na Osnove Mash. Proekt. Moscow, 1987; p 166.
(183) Zadorozhny, V. G.; Silantiev, A. I.; Pribbe, S. A. *Primen. Lakokras. Mater.* **1985**, *6*, 38.
(184) Tolstopyatov, E. M.; Krasovsky, A. M. Dep. SIF CNII Elektronika No R4810, Moscow, 1988.
(185) Osipov, K. A.; Klassov, V. N.; Folmanis, G. E. *Fiz. Khim. Obrab. Mater.* **1982**, *3*, 134.
(186) Kobayashi, S.; Haga, Y. *Synth. Met.* **1997**, *87*, 31.
(187) Lee, C. H.; Kang, G. W.; Jeon, J. W.; et al. *Thin Solid Films* **2000**, *363*, 306.
(188) Song, W. J.; Seoul, C.; Kang, G. W.; Lee, C. H. *Synth. Met.* **2000**, *114*, 155.
(189) Kang, G. W.; Lee, C. H.; Song, W. J.; Seoul, C. *Proc. SPIE* **2001**, *4105*, 362.
(190) D'Almeida, K.; Bernede, J. C.; Marsillac, S.; et al. *Synth. Met.* **2001**, *122*, 127.
(191) Djobo, S. O.; Bernede, J. C.; Marsillac, S. *Synth Met.* **2001**, *122*, 131.
(192) D'Almeida, K.; Bernede, J. C.; Ragot, F.; et al. *J. Appl. Polym. Sci.* **2001**, *82*, 2042.
(193) D'Almeida, K.; Bernede, J. C.; Godoy, A.; et al. *Eur. Polym. J.* **2002**, *38* (3), 451.
(194) Horowitz, G.; Hajalaoui, M. E. *Synth. Met.* **2001**, *122*, 185.
(195) De Vois, A. *Solid State Electron.* **1975**, *18*, 895.
(196) Nikonov, B. I. Diss. Cand. Techn. Sci., Gomel, 1989; p 139.
(197) Tereshko, Yu. D. Abstr. Conf. Polymer. Kompos.−95, Soligorsk, Belarus, 1995; p 82.
(198) Gritsenko, K. P.; Petrov, V. V.; Kriuchin, A. A.; Iudin, G. Yu. 5 USSR Conf. Probl. Optich. Pamyati, Kyiv, 1984; p 225.
(199) Petrov, V. V.; Kriuchin, A. A.; Gritsenko, K. P. Conf. Vichisl. Optoelectron. Erevan, 1987, p 71.
(200) Grinko, D. A.; Teologov, V. V. In *Optich. Zapis Inform.*; Petrov, V. V., Ed.; Nauk Dumka: Kyiv, 1991; p 138.
(201) Gritsenko, K. P. *Thin Solid Films* **1993**, *227*, 1.
(202) Gritsenko, K. P.; Teologov V. V. In *Optich. Zapis Inform.*; Petrov, V. V., Ed.; Nauk Dumka: Kyiv, 1991; p 76.
(203) Gritsenko, K. P. In *Problemi Optich. Zapisi Inform.*; Petrov, V. V., Ed.; Nauk Dumka: Kyiv, 1990; pp 42−48.
(204) Gritsenko, K. P.; Glazirin, N. P.; Ionov, V. V.; Krasovsky, A. M. Conf. Polymer. Komposit.−95, Soligorsk, 1995; p 30.
(205) Grinko, D. A.; Gritsenko, K. P.; Kriuchin, A. A.; et al. U.S.S.R. Patent SU 1,586,433, 1990.
(206) Petrov, V. V.; Kriuchin, A. A.; Gritsenko, K. P. Conf. Probl. Optich. Pamyaty, Moscow, 1990; p 65.
(207) Gritsenko, K. P. *Proc. SPIE* **1997**, *3347*, 165.
(208) Gritsenko, K. P. *Proc. SPIE* **1998**, *3417*, 268.
(209) Giro, A. M.; Goncharova, O. B.; Kurmaschev B. I.; et al. Novi mater. dla tonkoplenocnix funktsion. elementov electron. texniki; Nauka i Techn.: Minsk, 1994; p 206.
(210) Homilius, F.; Heilmann, A.; Rempel, U.; von Borczyskowski, C. *Vacuum* **1998**, *49* (3), 205.
(211) Shabatina, T. Conf. Organised Molecul. Films, Potsdam, 1, 2000; p 109.
(212) Pochtennyi, A. E.; Sagaidak, D. I.; Fedoruk, G. G.; et al. *Fiz. Tverd. Tela* **1998**, *40* (4), 773.
(213) Akamatsu, K.; Tsuboi, N.; Hatakenaka, Y.; Deki, S. *J. Phys. Chem. B* **2000**, *104*, 10168.
(214) Fedoruk, G. G.; Sagaidak, D. I.; Musevich, A. V.; Pochtennyi A. E. *Sens. Actuators B* **1998**, *48*, 351.
(215) Misevich, A. V. Diss. Cand. Techn. Nauk, Minsk, 2001; p 152.
(216) Misevich, A. V.; Pochtennyi, A. E. *Vesti Natl. Acad. Belarus* **1999**, *2*, 14.
(217) Sporer, A. H. *Appl. Opt.* **1984**, *23*, *16*, 2738.
(218) Tanigaki, N.; Kyotani, H.; Wada, M.; et al. *Thin Solid Films* **1998**, *331*, 229.
(219) Tanaka, T.; Honda, Y.; Ishitobi M. *Langmuir* **2001**, *17*, 2192.
(220) Gritsenko, K. P.; Tolmachev, A. I.; Tanaka, T.; et al. Conf. ECOER, Potsdam, November 17−21, 2001; p 208.
(221) Gritsenko, K. P.; Tolmachev, A. I.; Schrader, S.; et al. *Proc. SPIE* **2002**, *4833*, 482.
(222) Salyk, O.; Kuritka, I.; Weiter, M.; Schauer, F., www.fch.vutbr.cz/mol/sbornik00/oriented.pdf
(223) Ivanov, L. F. Diss. Cand. Techn. Nauk, Gomel, 1998; p 198.
(224) Ivanov, L. F.; Grakovich, P. N.; Ryabchenko, I. L. Sympos. New Khim. Materiali i Technol., Minsk, 1997; p 105.
(225) Krasovsky, A. M.; Tolstopyatov, E. M.; Grakovich, P. N. *Proc. SPIE* **1998**, *3343*, 1010.
(226) Krasovsky, A. M.; Tolstopyatov, E. M.; Grakovich, P. N.; Ivanov, L. F. Conf. Ionizing Radiation and Polymers−98, Weinbohla, 1998; p 12.
(227) Pekhota, V. V. Conf. Polymer. Komposit.−95, Soligorsk, Belarus, 1995; p 67.
(228) Tolbert, W. A.; Lee, I. Y. S.; Wen, X.; et al. *J. Imaging Sci. Technol.* **1993**, *37* (5), 485.
(229) Chrisey, D. B.; Pique, A.; Modi, R.; et al. *Appl. Surf. Sci.* **2000**, *168*, 345.
(230) Pique, A.; Wu, P.; Ringeisen, B. R.; et al. E-MRS Spring Meeting, Strasbourg, 2001; L26.
(231) Bubb, D. M.; Papantonakis, M. R.; Horwitz, J. H.; et al. *Chem. Phys. Lett.* **2002**, *352*, 135.
(232) Gritsenko, K. P.; Getsko, O. M.; Pochtennyi, A. E.; Misevich, A. V. Conf. SPIE, Kyiv, May, 24−26, 2002 (not published).
(233) Tsuboi, Y.; Goto, M.; Itaya, A. *J. Appl. Phys.* **2001**, *89* (12), 7917.
(234) Forrest, S. R. *Chem. Rev.* **1997**, *97*, 1793.
(235) Savenkov, G. N.; Nesterov, M. A.; Yanchivenko, K. N.; et al. *Khim. Vysokih. Energ.* **1996**, *30*, *3*, 214.
(236) Baydarovtsev, Yu. P.; Savenkov, G. N.; Yanchivenko K. N.; et al. Conf. Fundam. Probl. nauki o polymer., Moskow, 1999; p 2.
(237) Egorov, A. I. Diss. Cand. Techn. Sci., Gomel, 1999; p 130.
(238) Khomenkov, V. G. Abstr. of Conf. "Polycom-2000", Gomel, September 12−13, 2000; p 3.
(239) Kiselevsky, O. S. Abstr. of Conf. "Polycom-2000", Gomel, September 12−13, 2000; p 5.
(240) Agabekov, V. E. Abstr. of Conf. "Polycom-2000", Gomel, September 12−13, 2000; p 2.
(241) Gritsenko, K. P. *Polymer and Composite Film Deposition from Gas Phase for nonlinear optics*; Potsdam and Chemnitz Techn. Univ., 2001.
(242) Gritsenko, K. P. *Polymer film deposition from a gas phase;* OTB Engineering, Eindhoven, Laval University, Quebec, Sheffield Hallam University, June, 2002.
(243) Gritsenko, K. P.; Dimitriev, O. P.; Schrader, S.; et al. *Proc. SPIE* **2002**, *4833*, 487.
(244) Gritsenko, K. P.; Tolmachev, A. I.; Ray, A. K.; et al. Abstract accepted to E-MRS Spring Meeting, Strasbourg, June, 2003.
(245) Gritsenko, K. P.; Schrader, S.; Wittmann, J. C.; et al. Abstract accepted to E-MRS Spring Meeting, Strasbourg, June, 2003.

CR010449Q